8-18-2017

The Margination and Transport of Particles in Blood Flow

Erik James Carboni
University of Connecticut - Storrs, erik.carboni@uconn.edu

The Margination and Transport of Particles in Blood Flow, Erik Carboni, PhD,

University of Connecticut, 2017

Abstract

In blood flow in smaller blood vessels, red blood cells form a central core of flow and gives rise to a phenomenon known as margination. Margination is defined as the movement of a particle towards the periphery of blood vessels in blood flow. The margination of drug carriers, in particular, is desirable for the treatment of diseases because particles that exhibit marginating behavior are easier to diffuse into and/or target disease sites and deliver their drug payload. Experimentally, almost all existing studies of particle margination use particle adhesion as a mechanism for quantifying the margination propensity of particles. However, particle adhesion does not necessarily translate to margination and is affected by a number of other factors, limiting the conclusions that can be drawn from the results of these studies. This research investigates the margination of particles under various conditions via the use of direct particle tracking and without the limitations of an adhesion mechanism. Particle size, flow rate and margination distance were first investigated, finding that margination tends to increase with increasing particle size and with increasing flow rate. Furthermore, it was observed that smaller particles appear to require less channel length in the flow direction before significant margination was observed. Lastly, experimental evidence of larger margination velocities in blood were found, supporting modeling studies that suggest that particle-red blood cell interactions are largely responsible for margination. An interesting observation during this study was that the particle distribution after the channel constricted to its normal length from the inlet reservoir seemed to affect the margination of particles. A follow-up study of the effects of

constrictions on margination was begun, with applications to the treatment of arteriolosclerosis. In this study, the percent occlusion, length and eccentricity of a constriction and expansion region were all varied. Increasing percent occlusion and constriction length were each found to increase margination. A decreasing eccentricity, signifying a more gradual constriction entrance, was found to lead to decreasing margination except for the case of a sudden constriction/expansion geometry which also exhibited low margination. The presence of a constriction led to enhanced margination with the presence of an expansion resulting in the opposite. In the final part of this work, pulsatile flow was investigated. Margination in both steady and pulsatile flow was compared and no significant difference was found. Further, the wait time between pulses was varied and no difference in margination was observed. However, the variation of the amplitude of the pulsatile flow did display increasing margination with increasing amplitude, in line with the flow rate observations from the first experimental study.

The Margination and Transport of Particles in Blood Flow

Erik Carboni

M.S. University of Connecticut, United States, 2017

B.S. University of Rhode Island, United States, 2011

A Dissertation
Submitted in Partial Fulfillment of the
Requirements for the Degree of
Doctor of Philosophy
at the
University of Connecticut

2017

Approval Page

Doctor of Philosophy Dissertation

The Margination and Transport of Particles in Blood Flow

Presented by

Erik Carboni, B.S., M.S.

Major Advisor

_____

Dr. Anson W.K. Ma

Associate Advisor

_____

Dr. Leslie Shor

Associate Advisor

_____

Dr. Jeffrey McCutcheon

Associate Advisor

_____

Dr. Xiuling Lu

Associate Advisor

_____

Dr. Suzy Torti

University of Connecticut

2014

ACKNOWLEDGEMENTS

I would like to acknowledge financial support from the Department of Defense Mentor-Predoctoral Fellow Research Award Program, grant #W81XWH-10-1-0434, the National Science Foundation Graduate Research Fellowship Program, grant #DGE-1247393, National Science Foundation Grant #1250661 and the Graduate Assistance in Areas of National Need (GAANN) fellowship, grant #P200A150330.

I would first like to thank Dr. Anson Ma for his support and guidance for the past six years. He went out of his way during my first semester to begin work on an interdisciplinary project with a professor of the University of Connecticut Pharmacy department, Dr. Xiuling Lu. Dr. Lu was extremely helpful in our initial efforts to begin investigation into drug delivery to cancerous tumors and helped to set the groundwork for my PhD. Dr. Ma further supported me as I set up our new lab for my specific studies and guided me in research and had a large contribution in the evolution of our research into a study of margination. As we all know, many things can go wrong during experimentation or during a PhD in general. Dr. Ma kept me together when experiments failed, when results made little sense and when our initial ideas for a paper were "scooped" by another group. He has been incredibly supportive and I never would have completed the program if not for him.

I would also like to thank Dr. Leslie Shor. Her microfluidics course was the start of what would become the groundwork for the experimental methods I used. She not only provided a wealth of advice but also allowed me access to her lab and knowledge. I would

also like to thank her graduate students, Andrea Kadilak and Grant Bouchillon, who were an enormous help as I learned to make microfluidic masters, fabricate microfluidic devices and plasma bond. Were it not for Dr. Shor, Andrea and Grant, learning the entire processes involved in microfluidics would have been extremely difficult and would have likely taken many months of work. They were the catalyst that made this work possible.

Next, I want to thank Dr. Suzy Torti for her support with her Department of Defense grant when she came to UConn and for her general friendliness and helpfulness. Even though a collaboration did not work out, her support and her research did allow me to learn a lot about the potential of carbon nanotubes in a clinical setting and illuminated a link between the pharmaceutical sciences and the focus of Dr. Ma's lab, which was on carbon nanotubes early on.

I would also like to thank Dr. Jeffrey McCutcheon. His note-taking during my dissertation proposal was incredibly detailed and extremely helpful and I very much appreciate the attention that he showed. I learned a lot about the weaknesses and strengths of my presentation and how to improve it. Especially helpful was the information about where more detail would have been helpful and desirable, which is advice that I have incorporated into my future presentations.

Dr. Brice Bognet, who was a postdoctoral student of Dr. Ma's for a time, has my sincerest thanks as well. Dr. Bognet was one of the most vital people in the success of our studies since he developed, tested and tweaked the MATLAB particle tracking code that we used to analyze our results. This tracking code saved thousands upon thousands of hours of manual tracking and the improvements that he made resulted in code that was very

accurate and that took into account everything that would have resulted in large amounts of experimental error from less-developed or more general code.

My labmates were always very helpful and deserve a special mention as well. Sahil Vora, Yang Guo and Husseini Patanwala were all with me since our first day. While our projects were very different, I appreciated having others in the same lab to talk to and discuss ideas and sympathize regarding experimental difficulties and other challenges.

I am also thankful for all of the undergraduates that I worked with. In particular, I would like to thank Michael Ward and David Cowles, both of whom went above and beyond the call of duty and made significant contributions to studies at the expense of their own personal time. Their work and their effort was very helpful. Also, I would like to thank Kate Tschudi, who worked with us for a summer and was a huge help as well.

Next, I would like to thank Dr. Carol Norris. Carol was an absolutely invaluable part of my microscopy work and her knowledge and talent helped me through an enormous number of issues and confusing results. Carol helped me design an experimental protocol and also with the initial setup of the experimental apparatus so that it worked with the microscope. Further, she was always available for discussions of results and for the troubleshooting of any issues I ran into which was very helpful as I learned to use the microscope.

In the same vein, I thank Dr. Chris O'Connel who took over for Carol when she retired. Chris was, like Carol, extremely helpful. While I was fairly well versed in microscopy by this point, he helped me troubleshoot a number of tricky, specific issues and also to acquire software that I could use to get results that were consistent.

Next, I want to sincerely thank Leah Winterberger. Leah was an enormous help from day one, helping me with everything from scheduling my defenses to paperwork to general information on the graduate school. She ensured I never missed a deadline or forgot a form and always knew the answer whenever I had a question about the program or anything else.

I also wish to thank Susan Soucy, Nancy Kellerann and Shari Masinda who put up with my constant ordering of bovine blood and other experimental materials and always ensured that the blood arrived to my specifications and on the correct day, without fail.

Lastly, I would like to thank my parents, Curtis and Ursula Carboni, and my sister, Alyssa Carboni, for their love and constant support. Also, I would like to sincerely thank each and every one of my friends for their help in keeping me sane throughout grad school. There are too many of you to list here but you know who you are and I doubt I could have made it through without you all!

Table of Contents

List of Figures

List of Tables

1 Background

1.1 Circulatory System

The circulatory system of the body is made up of arteries and veins. These blood vessels have walls that are generally made up of endothelial cells and have diameters ranging from 1.5 cm for the aorta of the heart down to approximately 8 μm for a small capillary (Charm and Kurland 1974). The circulatory system is responsible for transporting blood and, by extension, oxygen, to each cell that makes up the body.

1.2 Properties of Blood

Blood is a biological fluid and is made up of a number of components. First are the erythrocytes, or red blood cells (RBCs). The volume fraction or percentage of RBCs in blood is known as the hematocrit and can vary from about 36% to 53% in humans (Kratz , Ferraro *et al.* 2004, Zhao, Shaqfeh *et al.* 2012). RBCs are typically shaped as biconcave discs approximately 8 μm in diameter and 2 μm in thickness and are also very elastic, or "floppy" (Pries, Secomb *et al.* 1996, AlMomani, Udaykumar *et al.* 2008, Sun and Munn 2008, Kumar and Graham 2011). Next, approximately 1% of blood volume is made up of leukocytes, or white blood cells (WBCs), which are spherical cells of approximately 8.5-μm in diameter and defend the body against infection (Schmid-Schonbein, Sung *et al.* 1981, Pries, Secomb et al. 1996, Yang, Forouzan *et al.* 2011). Finally, platelets make up a blood volume of approximately 0.7% and are responsible for blood clotting in the case of an open wound (Tokarev, Butylin *et al.* 2011). Thrombocytes, or platelets, have a discoidal shape; they are approximately 2-4 μm in diameter and 1 μm in thickness and are also much stiffer than RBCs (AlMomani, Udaykumar et al. 2008, Zhao, Shaqfeh et al. 2012). All of the components of blood are suspended in plasma, a liquid that makes up approximately

55% of total blood volume (Baele 2010). Blood plasma is mostly water but also contains hormones, nutrients, the end-products of cellular metabolism, clotting factors, immunoglobulins and proteins such as albumin (Baele 2010).

Because blood is a complex, multicomponent fluid, the modeling and analytical prediction of its flow behavior is challenging as it has shear-thinning properties due to being a cellular suspension. Its non-Newtonian nature combined with the various suspended cells and their interactions makes blood a very difficult fluid to predict accurately. Indeed, the presence of cells can have an effect on the flow behavior of blood beyond it being non-Newtonian. In smaller blood vessels, typically with diameters less than approximately 300 to 500 μm, RBCs have been found to move toward the center of the vessel and to tend to push other particles towards the walls of the blood vessel (Pries, Secomb et al. 1996, Lim, Ober *et al.* 2012, Carugo, Capretto *et al.* 2013). This phenomenon is termed margination.

1.3 Margination

Margination is currently defined as the movement or migration of a particle or cell in blood flow towards the periphery of the blood vessel. This movement towards the wall of a blood vessel was first observed as a naturally occurring phenomenon but it was soon discovered that other particles, including drug-carrying particles, are also capable of marginating.

1.3.1 History

In physiology, margination refers to the migration of WBCs toward the endothelium during blood flow and is relevant to the process of inflammation. Margination and the subsequent adhesion of WBCs to the endothelium allows the WBCs to transmigrate

across the endothelial wall and enter an inflamed area of tissue. The margination of WBCs was first observed in the blood vessels of tadpole tails by Dutrochet in 1824 (Dutrochet 1824). It was again observed by Gert Vejlens in 1938 and the margination of WBCs was correlated with the aggregation of RBCs *in vivo* (Vejlens 1938). WBC margination is often followed by: 1) their adhesion to blood vessel walls, 2) the movement of the WBCs into the space between the endothelial cells, 3) the transport of WBCs through tissue, and 4) the treatment of inflammation by the WBCs. The steps following the margination of WBCs are fairly well understood, but the exact origin and detailed mechanisms that lead to margination remain somewhat unclear (Langer and Chavakis 2009). While WBCs were the first "particles" that were observed to display the propensity to marginate, other particles, such as platelets and nanoparticles, have also been observed to exhibit margination in blood flow (Charoenphol, Onyskiw *et al.* 2012, Lim, Ober et al. 2012, Namdee, Thompson *et al.* 2013). One of the first mentions of particle margination is by Segré and Silberberg in 1962 during their studies of rigid spheres suspended in a mixture of glycerol, 1-3 butanediol, and water (Segré and Silberberg 1962). The authors observed that polymethylmethacrylate (PMMA) spheres, with radii ranging from 0.32 mm to 1.71 mm, migrated away from the center of the tube and moved closer to the wall of the tube in Poiseuille flow (Segré and Silberberg 1962).

1.3.2 Applications

The margination of particles in blood has applications in microfluidic devices for the removal of pathogens and also for the separation of cells (Munn and Dupin 2008, Hou, Bhagat *et al.* 2010, Jain and Munn 2011, Hou, Gan *et al.* 2012). Margination is especially relevant to cancer diagnostics and therapy wherein it can bring sensing, imaging, and/or

therapeutic nanoparticles closer to capillary entrances, which are located near the periphery of the larger blood vessels, thereby allowing these nanoparticles to enter the microcirculation more readily (Gentile, Chiappini *et al.* 2008). Margination also allows the particles to come close to the endothelium and, by attaching biorecognition molecules such as antibodies to nanoparticles, the nanoparticles can then be used to sense the increased amount of integrins and receptors of tumor endothelial cells (Godin, Serda *et al.* 2010).

In terms of therapeutics, margination enhances the diffusion of drug-carrying nanoparticles into the tumor sites through the Enhanced Permeability and Retention (EPR) effect that results from the characteristic leaky vasculature and lack of lymphatic vessels near tumor (Decuzzi, Pasqualini *et al.* 2009). For some bioimaging applications, low or no margination propensity may be desirable so that the nanoparticles will circulate in the blood stream for an extended period of time (Godin, Serda et al. 2010). An understanding of the fundamentals of margination is important to the engineering of particles for more effective drug delivery (Carboni, Tschudi *et al.* 2014). It is, therefore, vital to understand the mechanisms that are responsible for margination, including the physics of blood flow that leads to it and also the effects that different particle properties, suspending media and flow properties can have on the magnitude of margination in a system.

1.4 Mechanisms of Margination

While the reasons for the occurrence of margination are not completely understood, it is thought that blood flow and the resultant forces and interactions that arise from the unique properties of blood are responsible. As such, it is important to first understand the physics of blood flow and the forces that can result from it. Brownian motion may play a

role in the margination phenomena as well and several studies have found that heterogeneous particle collisions, or collisions between an elastic RBC and stiffer particles, may be the major cause of margination.

1.4.1 Physics of Blood Flow

Blood flow in the body is generally considered as laminar flow, although the flow can become turbulent under certain conditions, such as in the ascending aorta (Gulan, Luthi *et al.* 2012). In laminar flow, a simple Newtonian fluid exhibits a parabolic velocity profile and the flow is comprised of a multitude of fluid layers, oriented parallel to one another in the flow direction, that travel smoothly without disruption alongside one another. Unlike turbulent flow, wherein fluid naturally experiences irregular disruptions and, as a result, lateral mixing, in laminar flow there is no occurrence of lateral mixing from fluid convection. Laminar flow and turbulent flow are described by the dimensionless Reynolds number, which is a ratio between the inertial and viscous forces acting on a flowing fluid. The Reynolds number is given by:

$$Re = \frac{inertial\ forces}{viscous\ forces} = \frac{\rho u L}{\mu} \tag{1-1}$$

where ρ is the density of the fluid, u is the velocity of the fluid, L is the characteristic length (e.g., the diameter or width of a blood vessel or channel), and μ is the dynamic viscosity of the fluid. Turbulent flow occurs at high Reynolds numbers while laminar flow takes place at low Reynolds numbers. Given the small diameter of many blood vessels in the human body, blood flow is usually classified as being laminar, although blood is a non-Newtonian fluid due to the presence of RBCs and other blood constituents. A generalized Reynolds

number for a power law fluid, applicable here, was defined by Metzner and Reed (Metzner and Reed 1955) as well as Madlener, Frey and Ciezki (Madlener, Frey *et al.* 2009) as:

$$\mathrm{Re}_{genPL} = \frac{\rho D^n \bar{u}^{(2-n)}}{K((3n+1)/(4n))^n 8^{(n-1)}} \tag{1-2}$$

where n is the power law index of the fluid and K is the flow consistency index of the fluid. Unlike most fluids, the fact that blood is a cellular suspension means that unique effects can occur even at extremely low Reynolds numbers due to the interactions between the cells.

1.4.2 Cell-Free Layer

It was first observed by Goldsmith et al. that RBCs formed an RBC-rich core region in the center of the flow in the vessel, which resulted in the formation of a cell-free layer (CFL) near the endothelium that was free of RBCs (Goldsmith and Spain 1984). The authors also found that WBCs added into glass tubes containing blood that was free of RBCs did not exhibit margination (Goldsmith and Spain 1984). The CFL is thin, approximately 3 μm thick for blood flow in a 40 μm diameter vessel, but its thickness varies with the vessel diameter and geometry (Fedosov, Caswell *et al.* 2010). The geometric change near bifurcations, for example, changes the trajectory of RBCs and this geometry has been demonstrated to change the thickness of the CFL as a result of the non-uniform flow pattern (Fedosov, Caswell et al. 2010). Furthermore, higher flow rates tend to break up RBC aggregates, thereby expanding the RBC-rich core and subsequently decreasing the thickness of the CFL (Fedosov, Caswell et al. 2010). The reason for this RBC-rich core region can be partially explained by the existence of lift forces.

An asymmetric pressure field may be developed beneath or above the blood cells as a result of the lubricating flow between the wall and a blood cell, resulting in a "wall lift force" that pushes WBCs and RBCs away from the wall during fluid flow (Abkarian, Lartigue *et al.* 2002, Abkarian and Viallat 2005). This lift force can be calculated by:

$$F_l = \mu\dot{\gamma}\frac{r^3}{h}f(1-V) \tag{1-3}$$

where μ is the viscosity of the medium, $\dot{\gamma}$ is the shear rate, r is the radius of the particle, h is the particle's distance from the wall and $f(1-V)$ is a dimensionless function (Abkarian, Lartigue et al. 2002, Abkarian and Viallat 2005). V is the reduced particle volume and is given by:

$$V = \frac{\mathcal{V}}{\frac{4}{3}\pi\left(\frac{S}{4\pi}\right)^{3/2}} \tag{1-4}$$

where $\mathcal{V}$ is the enclosed volume and S is the surface area of the particle (Abkarian, Lartigue et al. 2002, Abkarian and Viallat 2005). Generally, WBCs are stiffer than RBCs and maintain a roughly spherical shape even in high shear flow. The lift forces acting on WBCs are weak compared those acting on RBCs, allowing WBCs to maintain their position in the CFL and remain close to the endothelium (Schmid-Schönbein, Usami *et al.* 1980, Mohandas and Chasis 1993, Ferri, Lombardini *et al.* 1994, Abkarian and Viallat 2005). Conversely, the discoidal shape of RBCs, combined with their elasticity and membrane fluidity, results in strong lift forces that push RBCs toward the center of the channel and lead to the formation of a CFL close to the endothelium (Schmid-Schönbein, Usami et al. 1980, Abkarian and Viallat 2005). This movement, termed the "axial migration" or focusing of RBCs, has been observed in multiple studies and is typically found in channel diameters less than approximately 300 to 500 μm (Bayliss 1959, Goldsmith and Mason

1961, Pries, Secomb et al. 1996, Lim, Ober et al. 2012, Carugo, Capretto et al. 2013). The formation of the CFL further leads to a decrease in the hydrodynamic resistance, which allows the WBCs to marginate more easily and reach the vessel wall (Bishop, Popel *et al.* 2001, Fedosov, Fornleitner *et al.* 2012). The deformability of the RBCs is crucial to their accumulation in the center of the vessel. In malaria patients, RBCs are significantly stiffer and these infected RBCs have been shown to exhibit margination (Hou, Bhagat et al. 2010). Lift forces are generally thought to be responsible for the formation of a RBC-rich core region in the center of the blood vessels and for the margination of WBCs to the wall. However, according to equation 1-3 , the actual lift forces acting on RBCs and WBCs also strongly depend on the actual cell size to the third-power (Abkarian, Lartigue et al. 2002). The authors of this paper noted that in reference (Abkarian and Viallat 2005) WBCs were calculated to have a slightly larger lift force (46 pN – 230 pN) than the RBCs (31 pN – 155 pN) based on the blood cell sizes assumed.

1.4.3 Brownian Motion

The Péclet number is a dimensionless quantity that describes the mass transport by taking the ratio of the convective transport by the fluid motion, and the diffusive transport by the chemical potential difference, mainly due to a concentration gradient (Kirby 2010). The Péclet number is given by (Kirby 2010):

$$Pe = \frac{convective\ transport\ rate}{diffusive\ transport\ rate} = \frac{Lu}{D_{trans}} \tag{1-5}$$

where L is the characteristic length, u is the average velocity of the fluid and D_{trans} is the translational diffusion coefficient (Kirby 2010). Higher Péclet numbers indicate a larger hydrodynamic contribution to mixing whereas low Péclet numbers indicate a larger

diffusional contribution. For a dilute suspension and a small Re number, the translational diffusion coefficient of a spherical particle can be calculated using the Stokes-Einstein-Sutherland equation (Kirby 2010):

$$D_{trans} = \frac{k_B T}{6\pi\eta R} \tag{1-6}$$

where k_B is the Boltzmann constant, T is the temperature, μ is the viscosity of the suspending medium and *r* is the radius of the spherical particle. According to equations 1-5 and 1-6, small particles have a higher diffusion coefficient and the corresponding Péclet number is smaller. This implies that diffusive transport becomes more significant in the case of nanoparticles. The end result is the random Brownian motion of nanoparticles, wherein the particles fluctuate across streamlines (Einstein and Fürth 1956).

1.4.4 Heterogeneous Collisions

Particle dynamics simulations by Graham and co-workers revealed that collisions between "stiff" and "floppy" particles in a suspension resulted in the eventual movement of stiff particles towards the wall (Kumar and Graham 2011, Kumar, Henríquez Rivera *et al.* 2014). Collisions in the near-wall region between stiff and floppy particles resulted in a greater displacement of the stiff particles towards the wall, and margination did not occur in cases where only one particle type was present (Kumar and Graham 2011, Kumar, Henríquez Rivera et al. 2014). It follows that once a stiff particle reaches the near-wall CFL, it tends to remain there (Kumar and Graham 2011, Kumar, Henríquez Rivera et al. 2014). This phenomenon in combination with the CFL, which arises from lift forces, is thought to be responsible for the margination of particles in blood flow (Narsimhan, Zhao *et al.* 2013). Further, the migration velocities and collision tendencies of particles were

linked with margination behavior (Henríquez Rivera, Sinha *et al.* 2015). Despite the discovered importance of these interactions, however, particle properties can also have a very large impact on the margination propensity of particles, presumably by altering the magnitude or frequency of particle-RBC interactions (Kumar and Graham 2011, Kumar and Graham 2012, Carboni, Tschudi et al. 2014).

1.5 Effects of Particle Properties on Margination

Margination propensity is dependent on parameters such as the particle size, shape, density, stiffness, and concentration and aggregation state of red blood cells. The following is an overview of the experimentally observed effects of varying each of these properties on the margination of smaller particles (<~5 μm diameter).

1.5.1 Particle Size

The size of a particle is an important parameter. Particles larger than 200 nm are at risk of being filtered out of the blood or destroyed by the liver, spleen, and bone marrow, whereas particles less than approximately 10 nm will leave the blood stream through the kidney or via extravasation from a tumor (Liu, Tan *et al.* 2012). For margination to occur, the particles need to escape the fluid-flow streamlines and move laterally as a result of gravity, buoyancy, hydrodynamic forces, van der Waals forces, and/or Brownian motion (Toy, Hayden *et al.* 2011). In the case of nanoparticles, gravitational forces are usually neglected given the small size of the particles (Lee, Ferrari *et al.* 2009). However, as particle size increases, gravitational forces become increasingly important. Gentile et al. studied spherical particles with diameters of 50, 100, and 200, 500, 750 nm and 1, 6, and 10 μm (Gentile, Curcio *et al.* 2008). They found that gravity facilitated the margination of the larger (> 500 nm) particles in the direction of the gravitational force (Gentile, Curcio

et al. 2008). A modeling study by Lee et al. confirmed these results and found that for smaller particles (< 500 nm), gravity has a negligible effect compared to Brownian motion (Lee, Ferrari *et al.* 2009). Toy et al. measured the margination of spherical nanoparticles ranging from 60 to 130 nm diameter in a bloodless solution via their adhesion to the walls of a microfluidic channel (Toy, Hayden et al. 2011). They observed a faster margination time for smaller particles and attributed it to their higher diffusivity, as explained in Section 3.2 (Toy, Hayden et al. 2011).

According to a modeling study by Decuzzi et al., gravitational forces dominate far from the endothelium, whereas van der Waals forces dominate close to the endothelium (Decuzzi, Lee *et al.* 2005). The van der Waals forces cause a "jump into contact" behavior where the particle is suddenly attracted to the endothelium. The authors also found that the competition between electrostatic, van der Waal, steric and buoyancy forces leads to a critical radius where the margination time is the longest, as shown in (Decuzzi, Lee et al. 2005). Below and above this radius, the nanoparticles marginate more readily (Decuzzi, Lee et al. 2005). The calculated critical radius varies from 50 to 250 nm, depending on a number of factors, such as the particle density, blood ionic concentration, and endothelial cell electrostatic properties (Decuzzi, Lee et al. 2005). It should, however, be noted that the analytical model developed by Decuzzi et al. considered the interactions between nanoparticles and endothelial cells only; no interactions between nanoparticles or between blood cells and nanoparticles were included in the model (Decuzzi, Lee et al. 2005). Gentile et al. found experimentally, for the discrete bead sizes that they used, that there were two distinct margination mechanisms, based on the particle diameter (Gentile, Curcio et al. 2008). The 500 nm to 10 μm particles were found to be largely affected by gravity, whereas

the 50 to 200 nm particles were found to be largely affected by collodial forces, such as van der Waals forces (Gentile, Curcio et al. 2008). However, because particles of discrete sizes were used, the exact critical diameter is unknown and the gravitational effect between 200 to 500 nm is unclear.

Charoenphol et al. examined the particle size effect experimentally using spheres with a diameter ranging from 0.5 to 10 μm suspended in blood (Charoenphol, Huang *et al.* 2010). They observed that the margination propensity of particles increased with increasing particle size, as shown in (Charoenphol, Huang et al. 2010). Namdee et al. observed that micron-sized spheres (2 and 5 μm diameter) marginated much more effectively than spherical nanoparticles (200 and 500 nm diameter) in a suspension of RBCs (Namdee, Thompson et al. 2013). They further attributed the reduced margination of nanoparticles to the trapping of nanoparticles within the spaces between the RBCs (Namdee, Thompson et al. 2013). A similar observation was made by Lee et al. in a combined experimental and modeling study (Lee, Choi *et al.* 2013). In the experimental portion, fluorescent nanoparticles were tracked in the microvasculature of a mouse via intravital video microscopy and 1 μm particles were found to exhibit margination whereas 200 nm particles were found to distribute randomly in the blood vessel, with no apparent tendency to marginate (Lee, Choi et al. 2013). In the modeling part of the study, the model showed that nanoparticles (<100 nm) moved along with the RBCs in the core of flow whereas the larger particles(0.5 to 1μm) exhibited margination (Lee, Choi et al. 2013).

D'apolito et al. studied particle size effects in a direct tracking study and found that 3 μm particles showed enhanced margination compared to 1 μm particles (D'Apolito,

Tomaiuolo *et al.* 2015). However, it should be noted that a manual tracking procedure was employed and a very limited number of particles was likely observed as a result of this.

1.5.2 Particle Shape

Many experiments use only spherical nanoparticles in their study of margination (Segré and Silberberg 1962, Decuzzi, Lee et al. 2005, Gentile, Curcio et al. 2008, Charoenphol, Huang et al. 2010, Lee, Choi et al. 2013, Namdee, Thompson et al. 2013). For non-spherical particles, the physics is more complicated. The velocity gradient in fluid flow results in a non-uniform distribution of forces along the axis of symmetry of the particles, leading to particle rotation. Toy et al. studied the margination of gold nanospheres versus that of gold nanorods with a width-to-length ratio of 0.45 suspended in water (Toy, Hayden et al. 2011). The gold nanorods were shown to exhibit a much higher margination propensity when compared to the gold nanospheres (Toy, Hayden et al. 2011). Likewise, Gentile et al. observed that disc-shaped and hemispherical nanoparticles marginated more compared to spherical nanoparticles (Gentile, Chiappini et al. 2008). However, this study focused on the sedimentation of particles and so the differently shaped nanoparticles also had different densities (Gentile, Chiappini et al. 2008). Doshi et al. studied how the shape and size of particles influence margination in a bifurcating microfluidic device (Doshi, Prabhakarpandian *et al.* 2010). Particles investigated included spheres of 1, 3 and 6 μm diameter, which were then stretched to form elliptical discs, circular discs, and rod-like particles. Higher aspect ratio particles tended to exhibit greater particle adhesion overall, with the difference becoming more pronounced with larger particle size (Doshi, Prabhakarpandian et al. 2010). This could be attributed to the greater contact surface area between the bovine serum albumin (BSA) antibody-conjugated

particle and the BSA-coated wall, making the higher aspect ratio particles more likely to bind and "stick" to the vessel walls. Lee et al. found that higher rotational inertia leads to more pronounced lateral drifting and, thus, a larger margination propensity (Lee, Ferrari et al. 2009).

For non-spherical particles, margination does not show a clear trend as a function of shear rate. High shear rates can pull the nanoparticles off from the endothelium when particle adhesion is used for the measurement of margination propensity, as previously discussed (Section 3.2). Tan et al. simulated spheres with varying particle densities, rods with an aspect ratio of three, and rods with an aspect ratio of five (Tan, Shah *et al.* 2013). They found that, similar to the results obtained by Gentile et al. and Toy et al. (Gentile, Chiappini et al. 2008, Toy, Hayden et al. 2011), the spheres and the rods exhibited decreasing margination with increasing shear rates (Tan, Shah et al. 2013). They postulated that the trend comes from the competition between the adhesion to the walls and drag forces (Tan, Shah et al. 2013). At low shear rates, the adhesion forces are larger than the drag forces, regardless of the particle orientation. At higher shear rates, these forces depend on the orientation of the particle. If there is only a point contact, then the drag force is stronger than the adhesion force whereas if a particle's long axis is adhered to the endothelium, then the adhesion force can overcome the drag force (Tan, Shah et al. 2013).

1.5.3 Particle Density

In an experimental study by Toy et al., 65 nm particles with different densities were studied (Toy, Hayden et al. 2011). It was found that nanoparticles with a higher density adhered less than those with a lower density (Toy, Hayden et al. 2011). Toy et al. explained that the higher-density particles carried more momentum and, as a result, hydrodynamic

forces dominated, whereas the low-density particles were dominated by diffusive motion, allowing them to escape streamlines (Toy, Hayden et al. 2011). However, when the effects of gravity are included, such as for larger particles, the effect reverses. In Gentile et al.'s study, differently shaped particles with sizes of approximately 1 μm had drastically different margination propensities (Gentile, Chiappini et al. 2008). The discoidal particles were 20% heavier and the number of particles marginated was five times larger relative to the spherical particles (Gentile, Chiappini et al. 2008). Likewise, the margination of hemispherical particles that were 60% heavier was three times larger than that of the spherical particles (Gentile, Chiappini et al. 2008). Both Toy et al. and Gentile et al. studied particles in an aqueous medium with no blood cells. Toy et al. used sub-100 nm particles whereas Gentile et al. used particles ranging in size from 1 – 3 μm and focused only on their sedimentation to the bottom surface of the flow chamber – not their margination to any wall. This may explain the discrepancy in results between the two studies.

1.5.4 Particle Stiffness

There are two different views on the effect of RBC stiffness on WBC margination. Freund modeled the interactions between RBCs and WBCs and the subsequent effect on WBC margination (Freund 2007). He increased the stiffness of RBCs by a factor of 10, but the WBCs exhibited only slightly decreased margination (Freund 2007). The author concluded that the margination of WBCs does not have a strong dependence on the deformability of RBCs and is likely more dependent on the mismatched size or shape of RBCs and WBCs (Freund 2007). Kumar and Graham mathematically modeled a system comprised of a dilute suspension of neo-Hookean capsules between infinite parallel walls, subjected to simple shear flow (Kumar and Graham 2011). Contradicting the results of

Freund, they found that stiff particles, such as WBCs, tend to marginate whereas more elastic ("floppy") particles, such as RBCs, undergo the opposite phenomenon and accumulate at or near the center of the channel (Kumar and Graham 2011). The study first modeled systems comprised entirely of stiff particles or entirely of elastic particles, and no margination was observed (Kumar and Graham 2011). However, upon modeling a system comprised of both types of particles, the stiffer particles were observed to migrate nearer to the wall of the channel and the elastic particles were observed to remain in the center of the channel (Kumar and Graham 2011). Kumar and Graham proposed that heterogenous collisions — collisions between stiff and elastic particles — were responsible for the margination of the stiffer particles (Kumar and Graham 2011). This accurately describes the phenomenon of RBC aggregation in the center of a blood vessel and WBC margination to the walls of the blood vessels. Interestingly, Kumar and Graham also found that the heterogenous collisions had a much larger displacement effect on the stiffer particles towards the wall than on the elastic particles (Kumar and Graham 2011, Kumar and Graham 2012).

1.5.5 Shear Rate

Shear rate affects the shape of the WBCs or particles, which will in turn modify the adhesion and lift forces acting on those particles. A number of studies showed that WBC margination increases significantly as a function of decreasing shear rate (Goldsmith and Spain 1984, Nobis, Pries *et al.* 1985, Firrell and Lipowsky 1989, Abbitt and Nash 2001, Freund 2007). Similar trends have been reported for particles. Toy et al. coated the channel walls with fibronectin to capture nanoparticles that marginated and, therefore, came close to the wall (Toy, Hayden et al. 2011). They reported that increasing shear rate decreased

the margination and further attribued this to the detachment of nanoparticles at high shear rates (Toy, Hayden et al. 2011). Namdee et al. came to a similar conclusion when using 2 and 5 μm spherical particles in an adhesion-based assay (Namdee, Thompson et al. 2013). Charoenphol et al. seeded endothelial cells onto glass and inserted the glass substrate into a flow chamber (Charoenphol, Huang et al. 2010). Particles were bound with ligands, which in turn bound to receptors on the endothelial cells. They observed that particle binding initially increases as a function of shear rate because, for the same particle concentration, the number of particles passing through the channel increases and thus the chance for particles to bind onto the wall increases (Charoenphol, Huang et al. 2010). However, as the shear rate exceeded a certain critical value, the number of particles bound to the wall decreased as a function of shear rate (Charoenphol, Huang et al. 2010). Gentile et al. found that the number of particles that marginated via sedimentation has a empirical power-law relationship with the shear rate (Gentile, Chiappini et al. 2008). The exponent varied for differently shaped particles: $\dot{\gamma}^{-0.63}$ for spherical particles, $\dot{\gamma}^{-0.85}$ for discoidal particles, and $\dot{\gamma}^{-1}$ for quasihemispherical particles, respectively (Gentile, Chiappini et al. 2008).

1.5.6 Hematocrit and RBC Aggregation

Margination is affected by the interactions between particles and RBCs. Tan et al. modeled particle margination with and without RBCs and showed that margination was almost doubled in the case with RBCs (Tan, Thomas *et al.* 2012). The enhanced margination in the presence of RBCs was more pronounced at higher shear rates, where the RBCs tumbled faster. A number of studies investigated the effect of hematocrit — the volume percentage of RBCs in blood — on WBC margination. Fedosov, Fornleitner and

Gompper found in their modeling study that the margination of WBCs was highest at hematocrits of 25% and 35% (Fedosov, Fornleitner et al. 2012). For a hematocrit of 55%, the authors found that RBCs caused a "lift-off" mechanism, wherein the RBCs entered the gap between the WBC and the wall and lifted the WBCs off the wall (Fedosov, Fornleitner et al. 2012). It should be noted that this "lift-off" mechanism is completely different from the lift force. No explanation was, however, given for why margination of WBCs at 45% hematocrit was lower than that of WBCs at hematocrits of 25% and 35%.

In studies where particle adhesion was used to quantify margination, there is a disagreement over whether hematocrit affects particle margination. Charoenphol et al. reported changes in hematocrit did not affect the margination of spherical particles ranging from 100 nm to 10 μm (Charoenphol, Huang et al. 2010). However, another study by Namdee et al. reported that increasing the hematocrit from 30% to 50% increased the adhesion of nanoparticles, but reduced the adhesion of micron-sized particles (Namdee, Thompson et al. 2013). The decrease in adhesion for the micron-sized particles could be explained by the comparable size of the CFL to the size of the particles, causing RBCs to collide with the particles and knock the particles off of the wall (Namdee, Thompson et al. 2013). The discrepancy between the Charoenphol and Namdee studies could be a result of the difference in the size of the flow chamber used in each study and thus the thickness of the CFL.

One direct-tracking study exists that explores the effects of hematocrit variation. Fitzgibbon et al. investigated margination in a 300 μm width and 30 μm height channel with varying hematocrit from 10 to 30% via the use of direct, manual tracking. They found an increase in rate of particle margination when they increased the hematocrit from 10%

to a value to 20% but were unable to evaluate the effects of 30% due to clotting issues and a potentially poor blood sample. The 30% hematocrit experiment was, unfortunately, not repeated after the initial issues arose and so no results could be gleaned from the experimental portion of the study despite the simulation portion indicating that 30% hematocrit should show the most rapid margination.

Lastly, there are also conflicting views on whether the aggregation of RBCs affects margination. Jain and Munn perfused a device with dextran solutions and a plasma-free culture medium, respectively (Jain and Munn 2009). The highest margination propensity of WBCs was observed in the presence of dextran, which induced RBC aggregation at a similar level to that of RBCs in plasma (Jain and Munn 2009). Likewise, Pearson and Lipowsky demonstrated in their in-vivo experiments that the addition of dextran 500 (Dx500), a high molecular weight dextran known to increase the aggregation of RBCs, increased margination fourfold whereas the addition of dextran 40 (Dx40), a known disaggregating agent, decreased the margination of WBCs by half in the post-capillary venules of rats (Pearson and Lipowsky 2000). Furthermore, Fedosov, Fornleitner and Gompper found that the aggregation between RBCs at higher hematrocrits led to a tighter RBC packing and supressed the "lift-off" mechanism (Fedosov, Fornleitner et al. 2012). However, Freund found in his modeling study that WBCs marginated without RBC aggregation, suggesting that WBC margination does not depend on RBC aggregation (Freund 2007).

1.6 Research Objectives

The overarching purpose of this research was to experimentally investigate the effects of various parameters on the margination ratio in order to elucidate the mechanisms behind

it and to find the ideal conditions or particle properties for margination to take place, for drug delivery applications. The major research objectives and the associated specific aims were as follows:

(1) Measure margination of model polystyrene particles in varying circumstances via the use of an in-house developed, automated direct particle tracking methodology (Chapter 2), with the specific aims:

- Develop an in-vitro system that mimics the conditions in an arteriole in the human body with the help of microfluidics and utilizing either a syringe pump or a pressure-driven pumping system to generate flow
- Aid in the development of MATLAB™ particle tracking code for the direct tracking of moving particles
- Compare the effects of suspending media and if any margination is present in water vs blood
- Using direct tracking, find the migration velocities of particles in water and blood and compare the extent of y-movement between the fluids
- Study differing discrete particle sizes and discern the relationship between particle size and margination propensity
- Investigate the effects of margination distance on the extent of particle margination
- Examine different flow rates and the impacts of varying flow rate on particle margination

(2) Explore the effects of constricted channels on the margination of particles in blood flow (Chapter 3), with the specific aims:

- Design and fabricate microfluidic devices with controlled geometrical variations
- Check water as a suspending medium and if any basic geometric effects are observed in a simple fluid without the presence of RBC-particle interactions
- Investigate the effects of varying channel occlusion percentage, constriction length and eccentricity of the constriction on particle margination
- Quantify particle margination just before and just after a constriction and just before and just after an expansion to find the individual contributions to margination of each geometric change

(3) Examine the effects of pulsatile flow on particle margination in small blood vessels (Chapter 4), with the specific aims:

- Develop scripts for the pump and flow controller that replicate a physiologically relevant pulsatile flow
- Fit data to a sine curve to ensure a good fit, which indicates that the pump is capable of reproducing physiological pulsatile flow
- Compare margination in steady vs pulsatile flow and explore the possible mechanics if there are differences
- Vary the wait time between pulses and the amplitude of each pulse and investigate the effects of variations in each quality of the pulsatile flow

2 Direct Tracking of Particles and Quantification of Margination in Blood Flow

2.1 Introduction

The current understanding of margination is that two driving forces contribute to it, namely, wall-induced lift forces and heterogeneous collisions between red blood cells (RBCs), WBCs, and particles. As a brief summary, lift forces arise from an asymmetric pressure field developed as the particle deforms near the wall, which consequently pushes cells or particles away from the wall (Abkarian, Lartigue *et al.* 2002, Abkarian and Viallat 2005). The magnitude of the lift force depends on the deformability of the cells or particles. RBCs are less stiff than WBCs and, as a result, the lift forces experienced by RBCs are larger, leading to the formation of a layer free of RBCs, known as the cell-free layer (CFL) as shown in Figure 2-1(a) (Goldsmith and Spain 1984, Lim, Ober et al. 2012, Narsimhan, Zhao et al. 2013). Further, particle dynamics simulations by Graham and co-workers revealed that collisions between "stiff" and "floppy" particles in a suspension resulted in the eventual movement of stiff particles towards the wall (Kumar and Graham 2011, Kumar, Henríquez Rivera et al. 2014). Collisions in the near-wall region between stiff and floppy particles resulted in a greater displacement of the stiff particles towards the wall, and margination did not occur in cases where only one particle type was present (Kumar and Graham 2011, Kumar, Henríquez Rivera et al. 2014). It follows that once a stiff particle reaches the near-wall CFL, it tends to remain there (Kumar and Graham 2011, Kumar, Henríquez Rivera et al. 2014). This phenomenon in combination with the CFL, which arises from lift forces, is thought to be responsible for the margination of particles in blood flow (Narsimhan, Zhao et al. 2013). Further, the migration velocities and collision

tendencies of particles were linked with margination behavior (Henríquez Rivera, Sinha et al. 2015).

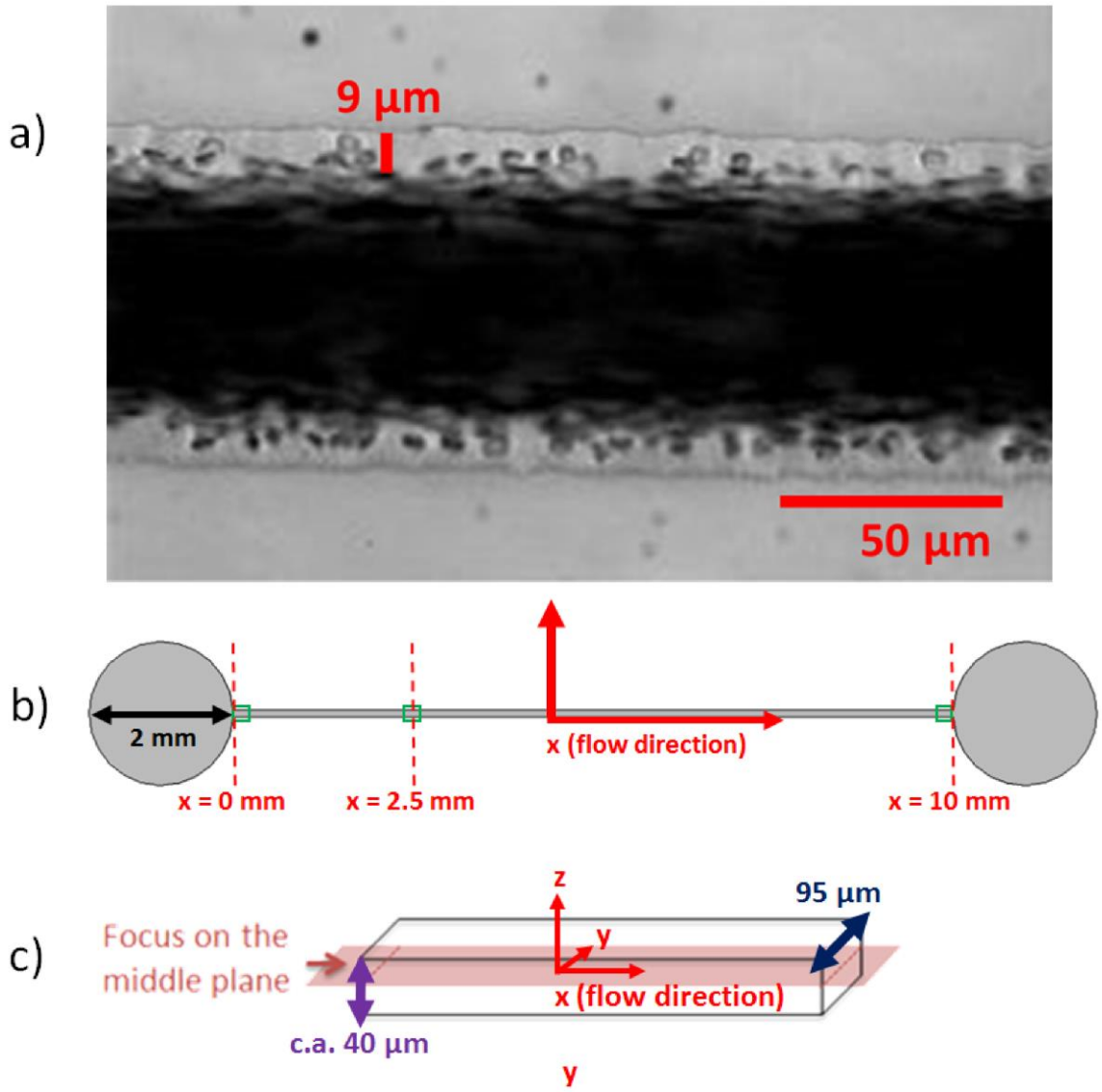

Figure 2-1: (a) Blood flow showing the formation of CFL within a microchannel. (b) Plane of focus for particle tracking with labeled imaging positions. (c) Schematic diagram of the microfluidic channel used in this study with the plane of focus for particle tracking.

A number of experimental (Decuzzi, Gentile *et al.* 2007, Gentile, Chiappini et al. 2008, Gentile, Curcio *et al.* 2008, Charoenphol, Huang et al. 2010, Doshi, Prabhakarpandian et al. 2010, Toy, Hayden *et al.* 2011, Lee, Choi *et al.* 2013, Namdee, Thompson et al. 2013, D'Apolito, Tomaiuolo et al. 2015) and theoretical (Decuzzi, Lee et al. 2005, Lee, Ferrari *et al.* 2009, Müller, Fedosov *et al.* 2014, Müller, Fedosov *et al.* 2015) studies have explored the effect of varying particle size on the margination propensity of particles. Several studies suggested that larger particles marginate much more readily than smaller particles and that there exists an optimal particle size for margination (Decuzzi, Lee et al. 2005, Gentile, Curcio et al. 2008, Lee, Ferrari et al. 2009, Charoenphol, Huang et al. 2010, Lee, Choi et al. 2013, Namdee, Thompson et al. 2013, Müller, Fedosov et al. 2015). There is, however, no consensus as to the exact particle size that results in optimal margination. In terms of the effect of flow rate, Charoenphol *et al*. (Charoenphol, Huang et al. 2010) reported that margination increased with increasing flow rate experimentally. However, for a given particle concentration and duration, a larger total number of particles would perfuse through the device at higher flow rates and this may explain the trend observed. Interestingly, a later independent experimental study by Namdee *et al*. (Namdee, Thompson et al. 2013) suggested that margination decreased with increasing flow rate, contradicting the study by Charoenphol *et al*. (Charoenphol, Huang et al. 2010). Namdee *et* al. attributed this to their measurement method, which involves perfusing a suspension of fluorescent particles through a microfluidic channel, followed by buffer solution flushing and measuring the fluorescence intensity emitted by particles that remained adhered to the wall (Namdee, Thompson et al. 2013). Particles may have detached from

the wall at higher flow rates due to increasing hydrodynamic drag and/or collision with red blood cells (Namdee, Thompson et al. 2013).

Many studies in addition to the Namdee study use particle adhesion as a method of measurement for the magnitude of margination. These studies conjugated particles with a ligand and coated channels with a receptor or chose to model such a system in order to measure the margination of various particles (Decuzzi, Gentile et al. 2007, Gentile, Chiappini et al. 2008, Gentile, Curcio et al. 2008, Decuzzi, Pasqualini et al. 2009, Charoenphol, Huang et al. 2010, Toy, Hayden et al. 2011, Tan, Thomas et al. 2012, Namdee, Thompson et al. 2013, Tan, Shah et al. 2013). The conjugated particles became bound to the walls of the channels upon coming into contact via margination. In this way, margination was measurable based on the number of particles adhered to the walls. Particle adhesion and margination are closely related. However, particle adhesion is also affected by other factors such as hydrodynamic forces, the number of ligands and receptors, the contact density, the characteristic length of the bond between the ligand and the receptor, the temperature of the medium, and particle deformability (Decuzzi, Gentile et al. 2007, Toy, Hayden et al. 2011).

Intuitively, the contact area of a spherical particle with the adhesion layer is proportional to the particle radius, *R*, and the thickness of the adhesion layer. However, the drag force experienced by the larger particle also increases. For a spherical particle, the drag force is given as:

$$F_D = \frac{1}{2}\pi\rho u_{pf}^2 C_d r^2 \tag{2-1}$$

where u_{pf} is the velocity of the spherical particle relative to the fluid, r is the particle radius, ρ is the density of the fluid and C_d is the drag coefficient. The value of C_d depends on the flow regimes. For small Reynolds numbers (calculated using the particle diameter as the characteristic length), the flow is in the Stokes regime wherein C_d scales with r^{-1}. As a result, the ratio of the adhesion to the drag forces would be independent of the size of the particle ($F_A/F_D \propto r/r$). For large Reynolds numbers, the flow is considered to be in the Newtonian regime, where C_d is a constant. Consequently, the ratio of the adhesion to the drag forces would scale with r^{-1}, implying that larger particles will detach from the adhesion layer eventually due to larger hydrodynamic drag. Such a simple scaling argument does not consider the collision between the RBCs and the adhered particles, which may also lead to the dislodgement of particles from the adhered surface. For non-spherical particles, adhesion also depends on the particle orientation, which determines the contact area between the particle and the endothelium and, therefore, the magnitude of the adhesive force.

All existing experimental studies, with only two exceptions (D'Apolito, Tomaiuolo et al. 2015, Fitzgibbon, Spann *et al.* 2015), assessed margination propensity based on the number density, or more precisely the fluorescence intensity, of fluorescent particles adhered to the channel wall after passing a particle suspension and subsequently a buffer solution through the channel (Decuzzi, Gentile et al. 2007, Gentile, Chiappini et al. 2008, Gentile, Curcio et al. 2008, Charoenphol, Huang et al. 2010, Doshi, Prabhakarpandian et al. 2010, Toy, Hayden et al. 2011, Tan, Thomas et al. 2012, Namdee, Thompson et al. 2013, Tan, Shah et al. 2013). In this study, margination propensity is quantified based on the direct tracking of individual particles. Direct tracking is less susceptible to the

aforementioned factors involved in using adhesion as a method of margination measurement, which could complicate the interpretation of experimental results.

Recently, direct tracking of particles has gained momentum as a result of the limitations of the adhesion mechanism for the measurement of margination (D'Apolito, Tomaiuolo et al. 2015, Fitzgibbon, Spann et al. 2015). In this method of margination measurement, a section of a channel is imaged and all particles are tracked. Particle velocities can be used to normalize the results and all particles in the CFL can be tracked and recorded as marginating particles. These direct tracking studies paint a better picture of the margination of particles in blood flow and suffer from none of the drawbacks of adhesion studies in terms of result reliability. A direct tracking study by D'Apolito *et al*. that was recently published focuses on different shapes of particles (D'Apolito, Tomaiuolo et al. 2015). In this study, however, two spherical particle sizes were used and it was found that the larger (3 μm) particles exhibited better margination when compared to the smaller (1 μm) particles. However, since this study focused on particle shape as opposed to size, these results are not conclusive and obviously do not cover smaller particle sizes that are of interest. Smaller particle size is advantageous for diffusive drug delivery, specifically to cancerous tumors due to the enhanced endothelial cell spacing in the walls of blood vessels near a tumor site, and should not be ignored. This is especially true since prior adhesion study results may not be reliable for particle size. Furthermore, this study manually tracked particles and, as such, only analyzed a limited number of particles. This small sample size could, in turn, lead to large errors in results.

Instead of manually tracking a limited number of particles, in this study a numerical code was developed to track thousands of particles to ensure that the experimental results

reported herein are statistically significant. Individual particles were experimentally tracked to calculate velocities both in the flow direction and in the margination direction. Mean square displacement data were further used to estimate the effective particle diffusivities in water and blood, respectively. Third, the degrees of margination at different travel distances from the inlet were assessed experimentally and analyzed for the first time.

2.2 Methodology

Defibrinated bovine blood (Lampire Biological Laboratories, Inc., Pipersville, PA) was washed and adjusted to 35% hematocrit. This hematocrit was chosen because, for channel diameters under 300 μm, the ratio of the hematocrit in the channel to that in the feed reservoir decreases with decreasing channel width (Fåhraeus 1929, Barbee and Cokelet 1971). As such, it is expected that a feed hematocrit of 35% will result in an effective channel hematocrit of approximately 85% of the inlet hematocrit for a 100 μm width channel (Barbee and Cokelet 1971), which works out to a hematocrit of 30%.

The bovine blood was washed to reduce particle adhesion to the channel walls and substrate surface during experiments. The bovine blood was first centrifuged at 500x g and the plasma was then decanted. Phosphate-buffered saline (Thermo Fisher Scientific Inc., Waltham, MA) was added to the blood to adjust it to a physiologically relevant 35% hematocrit (Barbee and Cokelet 1971, Brizel, Klitzman *et al.* 1993). This process was repeated twice more to ensure a thorough washing. While this process may have removed bovine serum albumin and other proteins that are naturally present in blood plasma, it served to minimize particle adhesion in the channel. In unwashed blood, this particle adhesion to the bottom of the channel was found to make particle tracking difficult or impossible. The degree of adhesion in unwashed blood could be a result of plasma proteins

in blood, which have been known to cause dispersed RBCs to adhere to each other and may have caused particles in this study to adhere to the channel sides or to the glass substrate (Pries, Secomb et al. 1996). The difference between unwashed and washed blood is shown in Figure 2-2. Furthermore, the washing of bovine blood and its resuspension in phosphate-buffered saline resulted in bovine RBCs that have similar elasticities to those of human RBCs (Amin and Sirs 1985).

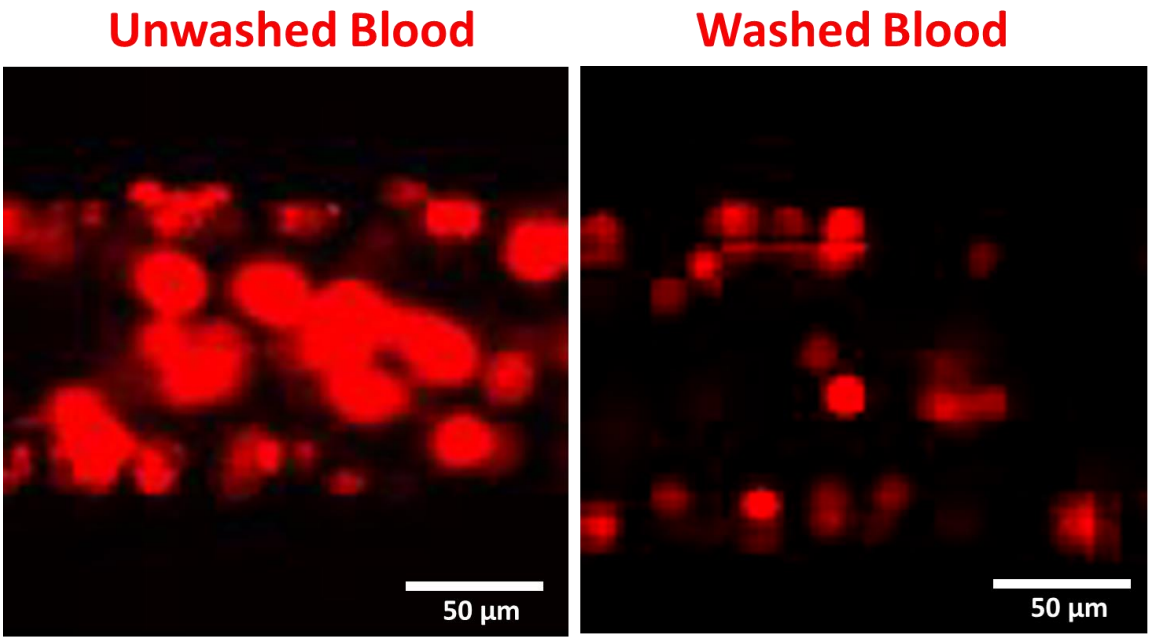

Figure 2-2: Fluorescent particle adhesion in unwashed vs washed blood

Spherical, fluorescent polystyrene particles (0.53, 0.84 and 2.11 µm diameter) were used as model particles in the experimental system (Spherotech Inc., Lake Forest, IL). These particle sizes were chosen because the endothelial cell spacing of leaky vasculature near tumor sites typically varies from 0.2 µm to 2 µm (MacEwan, Callahan *et al.* 2010). 2.11 µm was chosen as the largest particle size. A smaller particle size (0.25 µm) was tested initially, but accurate tracking of particle positions at the mid-plane was impossible due to

limited fluorescence signal and the obstruction of red blood cells. As such, 0.53-µm particles were chosen as the smallest particle size in this study. The original number concentrations of particles were 1.22×10^{11}, 3.07×10^{10} and 1.94×10^{9} particles per mL for the 0.53-, 0.84- and 2.11-µm particles, respectively. Polydimethylsiloxane (PDMS) pre-polymer and curing agent were used for the fabrication of microfluidic devices (Silgard 184 Silicone Elastomer Kit, Krayden Inc., Denver, CO).

2.2.1 Microfluidic Device Fabrication

A conventional soft lithography technique using SU-8 photoresist (Thermo Fisher Scientific Inc., Waltham, MA) was used to fabricate a silicon master. Briefly, SU-8 2025 photoresist (MicroChem Corp, Newton, MA) was spin-coated onto a 3" silicon wafer (NOVA Electronic Materials, LLC., Flower Mound, TX), exposed to UV light through a transparency photomask (Advanced Reproductions Corporation, North Andover, MA), which was designed using AutoCAD software, and submerged in developer solution (MicroChem Corp, Newton, MA). Upon drying, microfluidic devices were fabricated from the silicon master using PDMS (Silgard 184 Silicone Elastomer Kit, Krayden Inc., Denver, CO). Elastomer base and curing agent were mixed in a 10:1 ratio and degassed for 10 minutes. Next, the PDMS was poured over the master and degassed for an additional 10 minutes. The master was placed in an oven and the PDMS was allowed to cure for 2 hours at 60 °C. The device was cut out with a scalpel and an inlet and outlet were created using a 2-mm biopsy punch (Miltex Inc., York, PA) and punching vertically through the PDMS, into the 2-mm landing pad area of the device (Figure 2-1(b)). Lastly, the PDMS device was plasma bonded (Basic Plasma Cleaner PDC-32G, Harrick Plasma, Ithaca, NY) to a glass

coverslip slide (#1.5, Thermo Fisher Scientific Inc., Waltham, MA) to form a completed microfluidic device.

Of note during the step were several modifications to the general plasma-bonding procedure. Instead of cleaning the PDMS device with isopropyl alcohol, tape was used and dabbed onto the device repeatedly. This was found to effectively remove dust particles and yield a far cleaner device than isopropyl alcohol and a fiber wipe. Additionally, using tape removed the need for a drying step which removed a source of dust and other contamination on the device. The next modification was that the device was plasma bound for approximately 2 minutes instead of the recommended 45 seconds. This seemed to yield a stronger, more consistent bond to the glass coverslip. Finally, there existed a requirement to plasma bond and then put fluid into the device within 15 minutes in order to preserve hydrophilicity. However, due to the nature of the experiments in this study, not only was this impractical but it was also almost impossible to begin an experiment 15 minutes after bonding a device. It was, however, found that both water and blood could be successfully flowed through even a microfluidic device that had been plasma bound days or even weeks beforehand. Furthermore, interestingly, the bond in older devices was much more effective than in freshly-bound devices. To expand, many freshly bound devices had a corner or side that could be partially peeled away immediately after plasma bonding, sometimes peeling to the channel itself and rendering the device useless. Initially, this was considered a poor bond. However, it was found that this occurs fairly frequently and that if a device is allowed to rest for a while then the bond becomes extremely strong and the device can no longer be peeled from the cover slip substrate (it is thought ~1 hour minimum, though a day or more is best).

With the previous additional findings related to effective plasma bonding, plasma bonding very rarely failed and so these techniques were employed for every device once they were discovered.

2.2.2 Experimental Apparatus

Spherical, fluorescent polystyrene particles (0.53, 0.84 and 2.11 μm diameter, Spherotech, Inc., Lake Forest, IL) were diluted in the washed bovine blood and in water such that the final number concentration was calculated to be 4.073×10^6 particles per mL. A pressure-driven pump system with flow controller (Fluigent Inc., Villejuif, France) was used to pump each of the solutions through the microfluidic device. The pressure-driven pump system was chosen because it provides for superior flow rate control compared to the syringe pump that was initially used in this study, as shown in Figure 2-3. This figure shows individual particle velocities over the course of a typical experiment. As can be seen, there are large fluctuations in the flow patterns of the syringe pump, with some vaguely pulsatile tendencies being visible, whereas the pressure-driven pump shows a remarkably constant flow. While syringe pumps are useful for larger volumetric flow rates, the very tiny flow rate used in this study was an issue because the screw of the syringe pump could only turn so slowly and ended up yielding a somewhat pulsatile but chaotic flow.

Fluid was pumped using the pressure-driven pump through the microfluidic device at a physiologically relevant average velocity of 1 mm/s (Pries, Secomb *et al.* 1995, Kubota, Tamura *et al.* 1996, Cai, Fan *et al.* 2012). This velocity corresponds to a volumetric flow rate of 0.24 μL/min, an apparent shear rate of 61 s^{-1} and a wall shear rate of 67 s^{-1} for the channel dimensions. Apparent wall shear rates depend on the volumetric flow rates as well as the channel dimensions, but do not account for the non-Newtonian nature of blood

or the formation of the CFL. For a rectangular channel with a width *W* and a height *H*, the apparent shear rate is calculated as:

$$\dot{\gamma}_a = \left(\frac{6Q}{WH^2}\right)\left(1+\frac{H}{W}\right) f^*\left(\frac{H}{W}\right) \tag{2-2a}$$

where *H* is the channel height, *W* is the channel width, *Q* is the volumetric flow rate and *f** is a geometric constant based on the ratio of *H* and *W* (Son 2007). The wall shear rate is calculated as:

$$\dot{\gamma}_w = \dot{\gamma}_a\left(\frac{2}{3}\right)\left(\frac{b^*}{f^*}+\frac{a^*}{f^*}\frac{1}{n}\right) \tag{2-2b}$$

Where *n* is the power law index of the fluid and a* and b* are also geometric constants based on the ratio of *H* and *W* (Son 2007).

A number of 60,000-frame (~7.5 minutes) time-lapse videos of the flowing suspensions were acquired at the middle plane of the microfluidic device, as shown in Figure 2-1(c), using a dry objective lens (40x) with a high-speed camera (Andor iXon Ultra 897 iX0897 EMCCD, 130 frames/s, Andor Technology Ltd., Belfast, UK) and an inverted fluorescence microscope (Nikon Eclipse Ti-E, Nikon Instruments Inc., Melville, NY) with an Epifluorescence source (Intensilight C-HGFIE, Nikon Instruments Inc., Melville, NY). After each time-lapse video was collected, the reservoir of blood was gently shaken to keep the solution well mixed and the device was perfused at a high flow rate (~ 8 μL/min) for approximately 2 minutes. After every four time-lapses, the entire system was flushed for 10 minutes before taking the next time lapse.

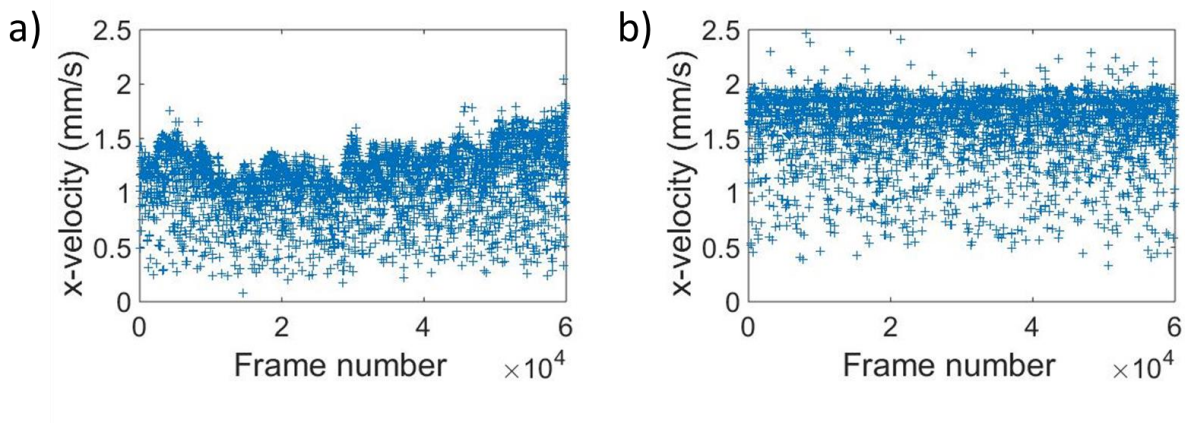

Figure 2-3: Individual particle x-velocities vs. the first frame number that the particle was tracked. 2.11-µm particles in water at a flow rate of 0.24 µL/minute, achieved using (a) a syringe pump and (b) a pressure-driven pump. Frame rate: 130 frames per second.

2.2.3 Image Analysis and Particle Tracking

The collected time-lapse videos were analyzed using MATLAB® code developed in-house. The particle tracking procedure consists of three major steps: (1) Background Correction: each time lapse video was split into 60,000 separate images and a background correction was performed to remove any bright pixels associated with particles adhered to the bottom of the channel (2) Particle Identification and Tracking: image-by-image, the position and size of all particles were calculated using a gradient-based method. The calculated particle size was used to eliminate out-of-focus particles based on their apparent larger size and the positions of all remaining particles were tracked as a function of time to calculate their displacements and velocities (3) Post-Processing: the results were cleaned of particles that were low-quality (i.e. only tracked for a few frames) or otherwise questionable and the cleaned, final results of the tracking were saved.

2.2.3.1 Background Correction

Despite the blood washing procedure, some particles adhered to the channel wall when suspended in blood, obscuring the tracking of moving particles through the channel. This was found to be especially significant for the case of the 2.11-µm particles, which are prone to sedimentation. For this reason, a background correction method was developed to remove the non-moving, fluorescent-light-emitting adhered particles and allowing the moving particles to be clearly and precisely tracked, without the interference of background noise from the adhered particles. However, since the number of adhered particles tended to change over time, the background noise from adhered particles constantly changed in both location and magnitude. To correct for this, a dynamic background correction method was applied to all frames. This correction method involves removing the dynamically computed background from each frame. For each frame, the computed background consists of the average of the *n* previous and *n* subsequent frames. For these experiments, *n* was arbitrarily set to 5 frames, which was enough to remove most noise from the background. Figure 2-4 shows both a raw (a) and background-corrected (b) image, for reference.

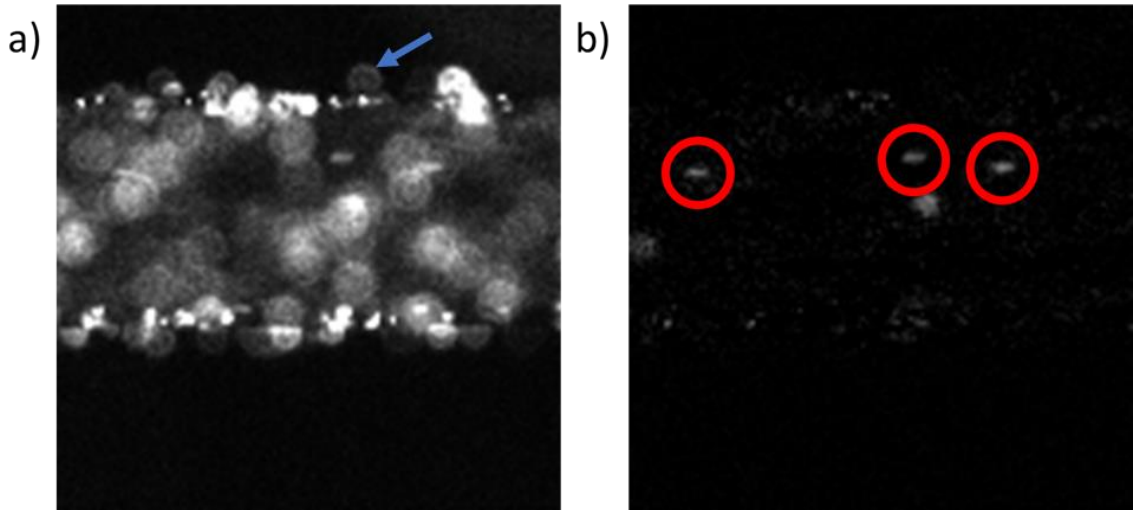

Figure 2-4: Fluorescent images of the microfluidic channel containing 2.11-µm particles suspended in blood: (a) before background correction, featuring adhered particles that are considered to be out-of-focus. The blue arrow points at an example out-of-focus particle and (b) after background correction, where the moving particles have become clearly visible. Moving particles are circled in red.

2.2.3.2 Particle Identification and Tracking

For all frames, a binary image was first generated based on the gradient of brightness in the grayscale, background-corrected images. The contours of all particles were detected based on a combination of the particle brightness and brightness gradient. These closed contours were then filled, resulting in a binary image where the background is black and the detected particles are white. For each individual particle detected on each frame, its cross-sectional area and center of brightness were computed from the binary image. Despite the shortest possible exposure time for the camera being used, many of the tracked particles that are in-focus appear elongated in the collected time lapse videos as a result of their high velocity. To ensure accuracy of particle positions as a result of this

problem of motion blur, the particle position was calculated by taking the center of mass of the particle based on the brightness (regardless of the apparent particle shape, elongated or not), which corresponds to the particle position at half of the exposure time if a constant particle velocity is assumed. This methodology ensures that the results were accurate and consistent.

Some out-of-focus particles were tracked, but they appeared larger on the binary image because of the "halo" generated around them. It is therefore easy to remove them from the results, using a simple threshold on the value of the previously computed cross-sectional area. Out-of-focus particles can be seen in Figure 2-4(a), adhered to the sides or bottom of the channel. A particle adhered to the wall is pointed at with a blue arrow.

The result file from the particle detection constitutes a table containing time (t), x- and y-position and cross-sectional area for all detected particles. The data required further treatment. The result table contains a cloud of points in the (t, x, y, particle size) space, where all particles are unrelated, except for being in order of appearance in the raw video file. This section briefly describes how the particles were finally grouped together to generate the time evolution of all tracked positions.

The sorting procedure is divided into three main steps: (1) detection and creation of a new active particle, (2) updating of an active particle and (3) the deactivation of a particle.

1. **Detection and creation of an "active" particle:** Particles that are detected but have not been previously identified as an active particle are identified as new "active particles". These active particles are assigned a unique identifying number and subsequently tracked.

2. **Tracking an active particle:** The trajectory of a particle, say, *Particle A*, is tracked by defining a bin around this particle. A particle that appears at a later frame within this bin will be treated as the same *Particle A* at its new position. If there is more than one particle, the particle with the closest position to the predicted position (based on previous displacement) will be treated as *Particle A*, and the corresponding displacement will be recorded.
3. **Deactivation of a particle:** A particle is "deactivated" if it has not been updated for a given number of time steps. This allows the tracking code to lose track of a single particle for a few frames as long as that particle is found and tracked again in subsequent frames. This deactivation procedure is included because particles may become obscured by the blood cells or adhered particles.

The tracking of a particle from its first frame to its last frame in the imaging window can be seen in Figure 2-5 (Particle #60).

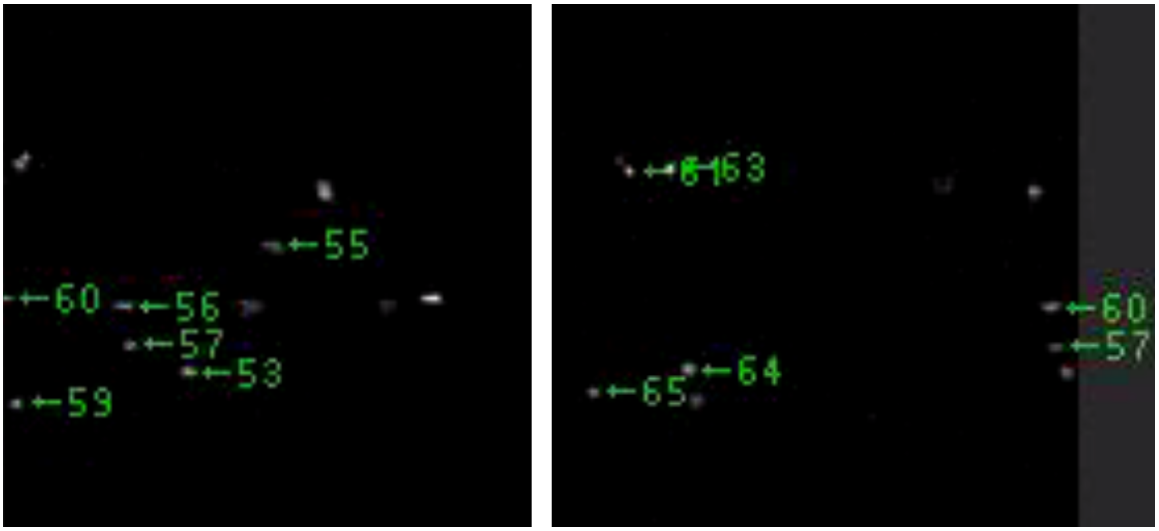

Figure 2-5: Sample images showing the successful tracking of particles from the first to the last frame for particle #60.

2.2.3.3 Post-Processing

Occasionally, the identification numbers of two particles may be switched if they are in close proximity or if they temporarily enter a region where the pixel brightness is over-saturated. Particle switching is associated with a sudden change in velocity, and all data points after that frame are removed. This procedure does not decrease the number of tracked particles; it only reduces the number of tracked points for a given particle. Each tracked particle's identification number, size, and position at a given time were stored in individual data cells. The minimum, maximum, and average y-position as well as the average x- and y-velocity for each particle can be easily accessed and calculations based on these values can be made whenever necessary.

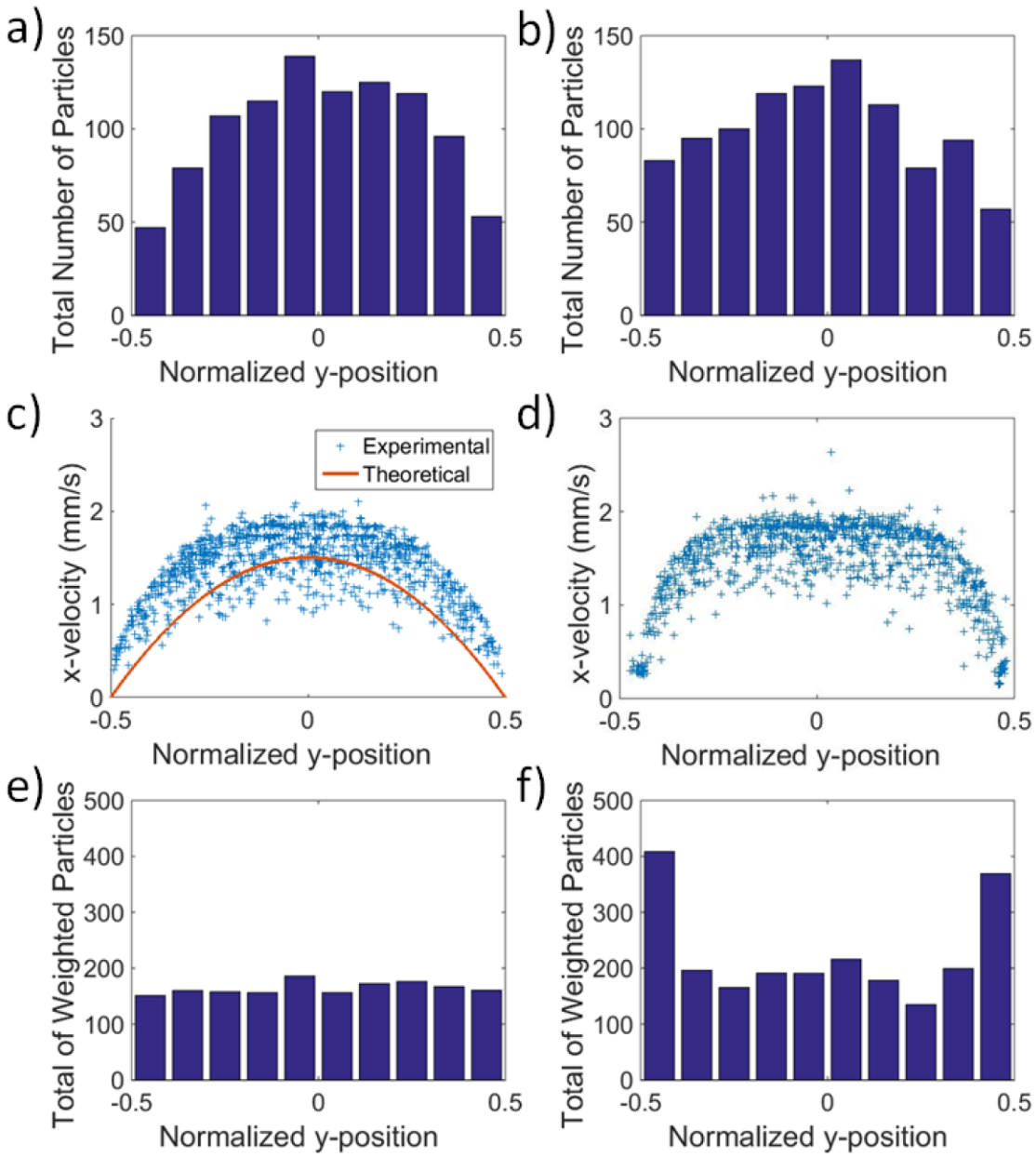

Figure 2-6: (a and b) Particle count per segment as a function of the normalized y-position for 2.11-mm particles suspended in (a) water and (b) blood. Volumetric flow rate: 0.24 mL/min; apparent wall shear rate: 61 s^{-1}. (c and d) Velocity profiles of 2.11-mm particles suspended in (c) water and (d) blood. (e and f) Total weighted particle count per segment $P_{ithsegment}$ as a function of the normalized y-position for (e) water and (f) blood.

2.2.4 Defining Margination

Figures 2-6(a) and 2-6(b) show the number of particles tracked as a function of the normalized y-position in both water and blood, respectively. The Reynolds number is calculated to be approximately 0.018, suggesting that viscous forces are dominant in relation to inertial forces and that the flow is laminar. In each case, a higher particle count was recorded close to the centerline. This can be explained by the velocity profile for pressure-driven flow through the channel, where the velocity is higher closer to the centerline. Figures 2-6(c) and 2-6(d) show the actual velocity profiles (x-direction) obtained by tracking the velocity of individual particles in water and blood, respectively. A parabolic velocity profile was recorded in the water case, as expected for a simple Newtonian fluid, whereas the blood case showed a profile closer to that of a plug-flow. The formation of a CFL and the higher concentration of RBCs near the centerline likely contributed to this profile. Such a blunted, plug-flow velocity profile for the blood experiment was first reported by Goldsmith and Spain experimentally (Goldsmith and Spain 1984). Higher velocities near the centerline will naturally lead to higher particle count since more particles are transported through the channel in a given time and for a uniform dispersion. To correct for the actual velocity profiles, the particle count has been weighted according to the particle velocities:

$$P_{i^{th}\,segment\,\in[1,10]} = \sum_{j\in[1,n]} \frac{v_{x,\max}}{v_{x,j}} \tag{2-3}$$

where $P_{i^{th}\text{-}segment}$ is the total weighted particle count for the ith segment, $u_{x,\max}$ is the maximum particle velocity across the channel, $u_{x,j}$ is the velocity of the jth particle within

the i^{th} segment, and n is the total number of particles within the i^{th} segment. Effectively, each particle in a given segment is assigned a weighted value. Equation 2-1 is set up to correct for the intrinsic velocity profile, where particles found closer to the wall always move at a lower velocity and consequently fewer particles are recorded closer to the wall relative to the center. Using Equation 2-3, particles moving at a slower speed will carry larger weights than fast-moving particles. For instance, for a $v_{x,\max}$ of 1 mm/s, a particle moving at 0.1 mm/s near the wall will have a weighted value of 10 whereas a particle moving at 0.9 mm/s near the center will have a weighted value of 1.11. Further, this method also corrects for any difference in actual velocity profile under different experimental conditions, such as suspending medium and wall shear rates. The use of this method is further supported by Figures 2-6(e) and 2-6(f), which show the weighted particle counts for different segments across the channel for water and blood, respectively. In the case of water, no preferential accumulation in the near-wall segments was observed, whereas the blood case clearly showed higher weighted particle counts in the segments nearest to the walls. Such trends are not so apparent in the original particle counts before velocity profile correction (i.e. Figures 2-6(a) and 2-6(b)).

In the literature, several definitions for margination propensity exist. In adhesion studies, the fluorescence intensity of adhered particles was directly correlated to the number of particles marginated. The higher the fluorescence intensity, the higher the margination propensity. In simulation studies, where the exact center of mass of particles is known, margination is conveniently defined as the number of particles at a given characteristic distance from the wall (e.g., the cell-free layer thickness or adhesion distance) (Kumar and Graham 2012, Reasor, Mehrabadi *et al.* 2012, Lee, Choi et al. 2013,

Müller, Fedosov et al. 2014, Müller, Fedosov et al. 2015, Vahidkhah and Bagchi 2015). In this study, each segment width is ~9.5 μm, which is close to the cell-free layer thickness as shown in Figure 2-1(a). Thus, we define the "margination parameter" as:

$$M = \frac{P_{1^{st}\ segment} + P_{10^{th}\ segment}}{\sum_{i^{th}\ segment\ \in [1,10]} P_i} \tag{2-4}$$

with a total of 10 segments and the fact that two of the segments are close to the wall, if there is no margination and an even distribution of particles then *M* should be equal to 0.2, as 20% of the total number of particles should be found near the channel sidewalls. *M* is, fundamentally, the percentage of particles that are in the CFL, after weighting, and that, therefore, have marginated (as defined by this study). An *M* value of 0.2 or 20% is equivalent to an even distribution of particles and is expected for the control experiments using water. Figure 2-6(e) shows a typical plot for a water experiment. Each segment has an approximately equal total weighted particle count and the *M* value of this plot is ~0.20, as expected for a water experiment. Values that are larger than this indicate marginating behavior. As shown in Figure 2-6(f) with blood as the suspending medium, segments 1 and 10 have higher total weighted particle counts compared to the rest of the channel. In fact, this particular plot has an *M* value of ~0.33, suggesting margination.

All near-wall particles (particles in segments 1 and 10) were manually checked in order to ensure the accuracy of the final results. While the automated tracking code greatly speeds up particle tracking and saves many hours of manual work, it is nevertheless important to ensure that no out-of-focus or false particles exist in the near-wall regions, by width. Particles in the regions nearest to the wall are considered to be marginating particles.

Because there are far fewer particles near the walls as a result of the velocity profile of the fluid, each particle in these regions has a very large impact on the results based on the chosen analysis methodology. Mistracked particles here can have large impacts on the *M* value by nature of their high weighting due to their low velocity as a result of being close to the wall. Particles in or nearer to the center of flow are, in contrast, very numerous and the manual checking of all of these particles would take much longer for little effect since these particles each have a very low weight. As such, only particles in segments 1 and 10 were manually checked.

For each experimental condition, a total of 3000 particles were analyzed to ensure the results are statistically significant. The average and standard deviation of the margination parameter, *M*, was calculated based on every 1000 particles tracked. This large number of particles was important because there existed significant standard deviations when only 100 particles were tracked whereas the tracking of 1000 particles was shown to reduce the standard deviations by anywhere from 289 to 692%. These standard deviation values for the 100 and 1000 particle cases are shown in Table 2-1 and correspond to the typical *M* values at the device outlet for each particle size/suspending medium in Figure 2-7(c).

Table 2-1: Average standard deviations of the margination parameter (*M*) calculated based on 100 and 1000 particles in water and blood and for different particle sizes.

	Standard deviation of the margination parameter (*M*)			
	Water		Blood	
Diameter (μm)	100 particles	1000 particles	100 particles	1000 particles
0.53	0.0483	0.0111	0.0511	0.0112
0.84	0.0434	0.00627	0.0504	0.0133
2.11	0.0458	0.00684	0.0567	0.0196

2.3 Results and Discussion

2.3.1 Effect of Suspending Medium: Water vs. Blood

Figure 2-7(a) shows the margination parameter, or *M*, as a function of x (see Figure 2-1(b)), the distance from the inlet, for three different sizes (0.53 μm, 0.84 μm, and 2.11 μm) in water. At the channel inlet (x = 0 mm) in water, all three particle sizes showed an *M*-value close to 0.2, indicating that the particles were evenly distributed after velocity gradient correction and that there was no margination. The *M*-value at x = 10 mm in water was also calculated for each of the particle sizes studied. Interestingly, both the 0.84-μm and 2.11-μm particles showed an M-value lower than 0.2. This may be explained by sedimentation, where settling velocities are dependent on particle size to the second power. Using the Stokes-Einstein equation (Einstein 1905) (Re = 0.018 << 1), settling velocities were estimated to be 0.459 μm/min, 1.15 μm/min, and 7.27 μm/min, for the 0.53-μm, 0.84-μm, and 2.11-μm particles. Given the parabolic velocity profile, particles close to the wall are traveling at a significantly slower speed relative to particles near the centerline and,

thus, particles closer to the wall have a longer residence time and are more prone to sedimentation. As only the middle-plane ($z \approx 0$) was imaged, settling particles would become out-of-focus and were therefore not recorded by the particle tracking code. While the density of the medium may be matched with that of the particle to mitigate sedimentation and thus negate these effects, this approach has not been pursued in this study because such density differences may also exist for actual drug carriers and possible sedimentation effects should not be neglected.

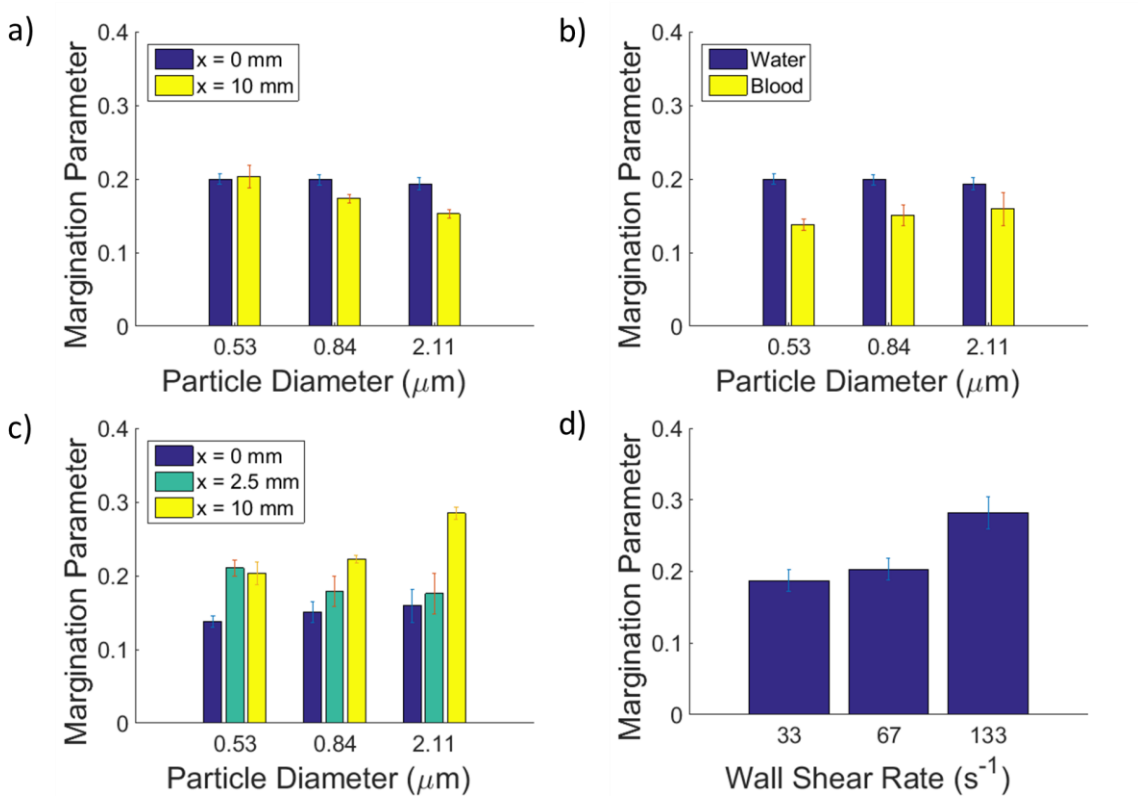

*Figure 2-7: Margination parameter (*M*) for different sizes of particles: (a) suspended in water at the inlet (x = 0) and at outlet (x = 10 mm); (b) suspended in water and blood, respectively, at x = 0. (c) suspended in blood at different channel positions (x). For (a-c), apparent wall shear rate = 61 s^{-1}; (d) Margination parameter (*M*) of 0.53-μm particles suspended in blood at varying flow rates at the outlet (x = 10 mm).*

The distance required to establish a fully developed flow in a microfluidic device is estimated to be 52.2 μm for water using the following equation and a calculated Reynolds number of 0.018 for the current experiment (Ahmad and Hassan 2010):

$$\frac{x_e}{L} = \frac{0.55}{0.13\,\mathrm{Re}+1} + 0.065\,\mathrm{Re} \qquad (2\text{-}5)$$

where x_e is the entrance length from the inlet that is required in order for flow to be considered fully developed and *L* is the characteristic length, or, in this case, the width of the channel (95 μm). Equation 2-5 assumes the fluid is a homogeneous Newtonian fluid, which is valid for water but not for blood. Figure 2-7(b) compares the *M*-value of three different sizes of particles at the inlet (i.e., x = 0) where the particles are suspended in water and blood. For all of the particle sizes studied, the *M*-value in the blood case is lower than that for water, suggesting that fewer particles were found close to the channel wall at the entrance in blood. However, as shown in Figure 2-7(c), the *M*-values downstream at x = 2.5 mm have returned to those observed in water (~0.2). We hypothesize that the reduction in *M*-value at the entrance is associated with an entrance flow effect as the blood-particle suspension is perfused through the tubing into the 3-mm diameter inlet and the microfluidic channel (Figure 2-1(b)). Blood is a non-Newtonian fluid and the flow is heterogeneous so the distance for establishing a fully developed flow is likely to be larger for blood than for water. Indeed, as predicted by simulations by Katanov, Gompper and Fedosov, the distance required in order for the CFL to fully develop is on the order of 2.4 mm for our microchannel, further supporting the experimental observations of this study (Katanov, Gompper *et al.* 2015). Furthermore, this experimental observation has two important implications. First, it implies the usual, implicit assumption of a uniform dispersion of particles at the entrance of a microfluidic device or other experimental system may not be true. Second, the presence of a flow constriction, while not a requirement for margination to occur, may have a non-negligible effect on particle margination. Since most microfluidic devices feature a constriction where fluid enters the channel from a larger inlet punch, results could be affected. It is therefore important to collect data at not only a downstream

channel location but also near the inlet to ensure an accurate interpretation of the results. The exact effect of flow constrictions is beyond the original scope of this paper. This experimental observation has important implications on drug delivery in vascular networks, where many different geometries and constriction shapes are possible. The potential effects of constriction geometry on margination may be significant and warrant further investigation in a future study.

2.3.2 Margination Velocity and Effective Diffusivity

Direct tracking of particles enables the analysis of velocity in not only the flow-direction (x) but also across the channel width (y-direction), which is of direct relevance to margination. In fact, margination velocity and the corresponding standard deviation have been reported in simulation studies by Kumar and Graham where the exact particle positions were known (Kumar and Graham 2011, Kumar and Graham 2012). None of the existing experimental studies have reported these values. Figures 2-8(a) – (f) show the y-velocity (u_y), or margination velocity, of individual particles as calculated from direct particle tracking in water and blood, respectively. It should be noted that these u_y values are averaged per particle and that a positive u_y corresponds to the movement of a particle towards either wall of the channel whereas a negative u_y indicates that a particle is moving towards the center of the channel. The u_y is calculated from the center of mass of the particle based on the brightness of the pixels. Briefly, we first weight each pixel by its relative brightness and then find the center of mass by finding the center of brightness. This gives us the center of the particle with a subpixel resolution and we can then calculate the y-velocity of the particle from frame to frame. In fact, the relatively large size of any blurred

particle image gives more pixels to calculate the center of the particle and increases the precision on calculating the position.

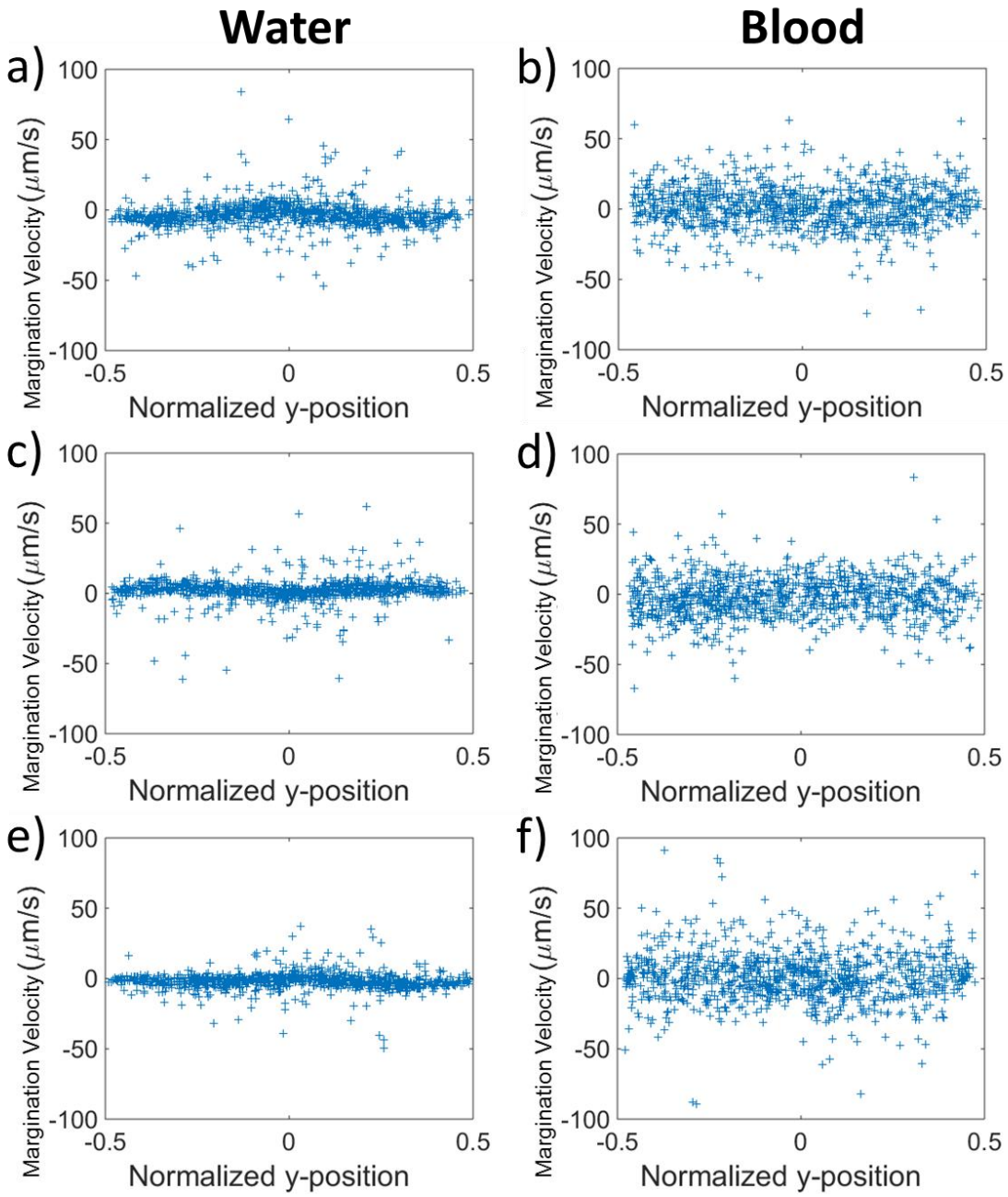

Figure 2-8: (a–f) Representative plots of average y-velocities for individual particles in water or blood: (a and b) 0.53 mm, (c and d) 0.84-mm, and (e and f) 2.11-mm particles.

For all particle sizes studied, there is a larger spread in u_y in blood compared to water as the suspending medium. The standard deviation in u_y, denoted as u_y', was calculated to be on the order of 9 μm/s for water (averaged over all three particle sizes) versus ~16 μm/s for blood, as shown in Table 2-2. The larger u_y'-value in the blood case is attributed to the collisions between particles and blood cells, which are absent in the water case. However, no noticeable difference in the u_y' values were observed among different particle sizes, probably because of the relatively short travel distance in y-direction, as limited by the field of view (205 by 205 μm). Further, the translational diffusivities of particles in water and blood cases were estimated by plotting the mean-square displacement as a function of time, as shown in Figures 2-9(a) and 2-9(b), and calculating the slope (s), where $D_y = s/2$. A relatively large error arises from the spatial and temporal limitations of our imaging system. Also, red blood cells can obscure some of the fluorescent signal of the particles. Despite the relatively large error in determining the particle position at short time scales, the calculated values for the water cases are of the same order of magnitude as the Brownian diffusivities calculated using the Stokes-Einstein-Sutherland equation (Sutherland 1905). As expected, the smaller the particle size, the higher the diffusivity in water. The higher experimental values may be caused by shear-induced diffusion (Lopez and Graham 2007). In the blood cases, the effective diffusivities are all on the order of 15 $\mu m^2/s$, much higher than those measured for the water cases (on the order of 2-5 $\mu m^2/s$), as shown in Table 2-2. Like u_y', this is probably caused by the collisions between particles and blood cells. Interestingly, in blood, the larger the particle

size, the higher the effective diffusivity, suggesting collisions, instead of thermal motions, are a predominant factor for margination.

Table 2-2: Experimental diffusivities and standard deviations of u_y versus particle size

	u_y' (μm/s)		Experimental Diffusivity (μm^2/s)	
Size (μm)	Water	Blood	Water	Blood
0.53	9.30 ±0.23	15.44 ±1.45	4.91 ±0.78	14.20 ±1.96
0.84	9.34 ±0.70	16.16 ±0.80	4.40 ±0.17	14.87 ±2.34
2.11	7.10 ±1.44	17.48 ±0.74	1.88 ±0.14	15.42 ±1.15

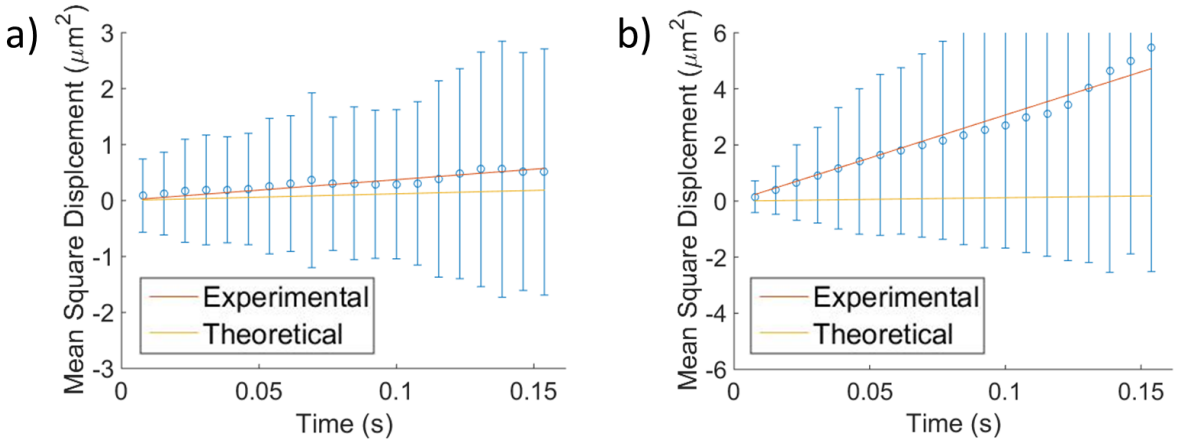

Figure 2-9: Mean square displacement as a function of time for 2.11 μm particles in: (a) water and (b) blood. Theoretical lines (yellow) on both plots have a slope equal to two times the Brownian diffusivity, which is calculated to be ~0.6 μm^2/s using the Stokes-Einstein-Sutherland equation. From data fitting, the effective diffusivities were estimated to be ~1.9 μm^2/s and ~15.4 μm^2/s for water and blood, respectively.

2.3.3 Effect of Particle Size

Using the *M*-values at x = 2.5 mm as benchmarks, the 2.11-μm particles showed the largest change in *M*-value and thus the highest margination propensity, with a 45% increase

relative to the case of an even distribution of particles, followed by the 0.84-μm particles and the 0.53-μm particles. Therefore, larger particle sizes were found to result in a higher margination propensity. The 0.53-μm particles showed similar *M*-values close to 0.2 at x = 2.5 mm and 10 mm, suggesting there is no margination for this particle size once the flow is fully established. This is in agreement with the findings from adhesion studies (Decuzzi, Gentile et al. 2007, Gentile, Chiappini et al. 2008, Gentile, Curcio et al. 2008, Charoenphol, Huang et al. 2010, Doshi, Prabhakarpandian et al. 2010, Namdee, Thompson et al. 2013, Tan, Shah et al. 2013) as well as a recent direct particle tracking study by D'Apolito *et al*. (D'Apolito, Tomaiuolo et al. 2015), where two spherical particle sizes (1 μm and 3 μm) were investigated. It is conjectured that larger particles interact more readily with RBCs and, as a result of their frequent collisions with RBCs, are propelled toward the walls of a blood vessel sooner than smaller particles, which have less frequent interactions. Zhao et al. put forward an equation to calculate the distance required for a particle to reach the CFL, or the "margination distance" (Zhao, Shaqfeh et al. 2012):

$$X = \frac{\langle u \rangle \left(\frac{W}{4} \right)^2}{D_y} \tag{2-6}$$

where $\langle u \rangle$ is the average flow-direction velocity, w is the channel width and D_y is the diffusivity in the y-direction. Using effective diffusivities estimated experimentally (Chapter 2.3.2), the margination distance is calculated from Equation 2-4 to be on the order of 7.5 mm. Since the *M* values are close to 0.2 at x = 2.5 mm, the *M* values at x = 10 mm likely reflect completed margination.

2.3.4 Effect of Flow Rate

As discussed in Section 1, two opposite trends have been reported for the effect of flow rates using particle adhesion to assess margination (Charoenphol, Huang et al. 2010, Namdee, Thompson et al. 2013). While adhesion and margination are related, evaluating margination based on the number of adhered particles could be further complicated by factors such as hydrodynamic drag, densities of ligands and receptors grafted onto both the particle surface and the wall channel, particle shape and contact orientation, and particle size relative to the CFL (Carboni, Tschudi et al. 2014, Müller, Fedosov et al. 2014, Vahidkhah and Bagchi 2015). Particles may have detached from the wall due to collisions with blood cells or increasing wall shear rate. This may explain why the margination propensity decreases as a function of increasing flow rate (Namdee, Thompson et al. 2013). Further, only particles that come into direct contact with the wall are being measured. This method does not account for particles that marginate to the CFL but do not adhere to the wall. As a result, larger particles may be predisposed to adhere more readily due to their larger size relative to the CFL. In this study, the margination parameter (M) was calculated based on the actual velocity profile and normalized by the total particles perfused through the microchannel for a given time. This analysis method is less susceptible to any variation in the actual particle number concentration. It also offers a fairer comparison between different flow rates because the total number of particles perfused through the device increases as a function of increasing flow rates (for a given number concentration and perfusion time). As shown in Figure 2-7(d), the higher the flow rate, the higher the M-value. This is probably caused by higher collision frequencies between particles at higher flow rates. This explanation is consistent with the observation that the standard deviation

of particle velocity in the y-direction (u_y) increases as a function of increasing flow rates, as shown in Table 2-3.

Table 2-3: Standard deviation of u_y (u_y') for varying flow rates in blood

Wall shear rate (s^{-1})	u_y' (μm/s)
33	10.27
67	14.22
133	23.68

2.4 Conclusions

To summarize, the margination of particles in blood was characterized by directly tracking the spatial distribution of particles passing through a microfluidic channel at different physiologically relevant flow rates. A margination parameter, *M*, was defined to quantify margination propensity after correcting for the velocity gradient in the flow direction (x). A benchmark value of 0.2 was established through a control experiment, where the particles were suspended in water with no margination. When suspended in water, particles close to the channel wall with longer residence time tended to settle, leading to relatively fewer particles found near the wall at the outlet (x = 10 mm) and consequently an *M*-value smaller than 0.2 for the 0.84-μm and 2.11-μm particles. When suspended in blood, the *M*-values for all particle sizes at the entrance (x = 0) were smaller than those in water. This is probably due to non-fully developed flow and constriction as the blood-particle mixture entered from the tubing and inlet into the microfluidic channel. The largest particles (2.11-μm) showed highest margination propensity, followed by the 0.84-μm particles, whereas the 0.53-μm particles showed no margination. While the results

cannot be compared directly to other studies because of differences in experimental conditions, the observed trend is qualitatively consistent with results reported by earlier experimental and simulation studies.

In addition to M, the particle velocity in the margination direction (u_y) was characterized experimentally for the first time. Compared to the case of water, all particle sizes showed a larger fluctuation in u_y when suspended in blood. Likewise, a higher effective diffusivity, on the order of 15 $\mu m^2/s$, was also observed in all the blood cases relative to the water cases, which vary from 2 – 5 $\mu m^2/s$. The larger fluctuations in v_y and higher effective diffusivity in blood are probably caused by the collisions between particles and blood cells, consistent with arguments put forward by earlier simulation studies (Kumar and Graham 2012, Kumar and Graham 2012, Kumar, Henríquez Rivera et al. 2014, Vahidkhah and Bagchi 2015). Further, the calculation of M accounts for the actual velocity gradient and the absolute total number of particles passed through the channel, offering a more robust way to compare data collected at different flow rates. An increase in flow rate led to both a larger M-value at the exit and a higher effective diffusivity, confirming experimental results by Charoenphol *et al.* (Charoenphol, Huang et al. 2010). However, limitations of this study do exist. Particle tracking is limited by the spatial and temporal resolution of the imaging system, the relatively small field of view, and the presence of RBCs, which, at higher hematocrits, can absorb/scatter light and make the direct tracking of fluorescent particles challenging. No significant difference in terms of the margination velocity and diffusivity was observed among different particle sizes when suspended in blood. Second, this study focuses on the distribution of particles within the channel and does not account for the transport of particles through the spacing between endothelial

cells, which typically varies from 0.3 to 4.7 μm (Hashizume, Baluk *et al.* 2000). Large particles may exhibit more margination propensity but may not be small enough to pass through the spacing to reach the tumor site. Finally, according to Wiedeman (Wiedeman 1963), the length of an arteriole in-vivo is only approximately 1 mm, with branches of other arteries every 0.2 mm so the length scale is not as close to in-vivo as it could be. All in all, this paper investigated the effect of particle size and shear rate on margination propensity based on the particle distribution, velocity (both along and transverse to the flow direction) and effective diffusivity. The findings suggested that margination is primarily caused by the collisions between particles and blood cells, instead of Brownian motion.

3 The Margination of Particles in Areas of Constricted Blood Flow

3.1 Introduction

Since 1997, stroke has been a leading cause of death globally (Murray and Lopez 1997, Wang 2016). While stroke in the gray matter of the brain is well-known, approximately 30% of all strokes occur in the white matter (Rosenzweig and Carmichael 2013). However, unlike the rest of the brain where the diameters of blood vessels can range from 15 to 140 μm, with an average diameter of 30 μm, blood vessels in the white matter of the brain are arterioles and have diameters of approximately 100 to 200 μm (Alexander and Putnam 1938, Rowbotham and Little 1965, Harnarine-Singh, Geddes *et al.* 1972). The narrowing of arterioles from the development of a stenosis is termed arteriolosclerosis and can cause strokes in the white matter, which can lead to dementia and motor function impairment amongst other complications (Rosenzweig and Carmichael 2013). Furthermore, lacunes are cavities that result from ruptured arteries of around 100 μm as a result of arteriosclerosis and can lead to death (Fisher 1965, Fujiwara, Ishikawa *et al.* 2009) and arteriolosclerosis can also be responsible for hypertension, chronic kidney disease and left ventricular hypertrophy (Kanbay, Snchez-Lozada *et al.* 2011). Arterioles are a very important part of the vasculature but have major differences from both tiny and large arteries.

While blood behaves as a nearly Newtonian fluid in large blood vessels, in vessels with smaller diameters, such as the aforementioned arterioles, blood rheology becomes more complex and a phenomenon known as margination can occur (Fedosov, Caswell et al. 2010). In these smaller blood vessels, typically having diameters less than about 300

μm (Pries, Secomb et al. 1996, Lim, Ober et al. 2012, Carugo, Capretto et al. 2013), interactions with red blood cells (RBCs) in the center of the vessel can cause particles to migrate to the periphery of the blood vessel, or marginate (Kumar and Graham 2012). While white blood cells (WBCs) were the first to be observed to marginate, drug-carrying microparticles were subsequently found to be able to also marginate (Dutrochet 1824, Segré and Silberberg 1962). Margination of drug-carrying particles is important because marginated particles are near the wall and will be more effective in delivering their drug cargo. For all particles, the extent of this margination depends upon particle size, among many other characteristics of the particles and also the blood (Kumar and Graham 2012, Carboni, Tschudi et al. 2014). However, while factors such as size, shape, and hematocrit and their effects on margination propensity have been investigated, the effects of stenoses on margination are largely unknown.

A number of studies have investigated drug delivery to a site of stenosis using specific attributes of the stenosis, such as the enhanced local shear (Holme, Fedotenko *et al.* 2012, Korin 2012, Korin, Kanapathipillai *et al.* 2013, Saxer, Zumbuehl *et al.* 2013). In this case, the margination of particles becomes even more important because shear is at a maximum for marginated particles. However, stenoses can have various geometries and there is a lack of understanding of the effects of stenosis geometry on the margination of drug particles, especially in the smaller arterioles. Additionally, while many studies have investigated the effects of various geometries of flow constrictions and expansions on red blood cell motion (Li, Fang *et al.* 2004, Zhao, Marhefka *et al.* 2008, Fujiwara, Ishikawa et al. 2009, Srivastava, Rastogi *et al.* 2010, Sousa, Pinho *et al.* 2011, Yaginuma, Oliveira *et al.* 2011, Ha and Lee 2013, Faustino, Pinho *et al.* 2014, Hall and Calt 2014, Monteiro,

Taboada *et al.* 2014, Pinho, Rodrigues *et al.* 2014, Xiao, Chen *et al.* 2014, Dimakopoulos, Kelesidis *et al.* 2015, Akbar 2016, Kim, Antaki *et al.* 2016, Taboada, Monteiro *et al.* 2016, Vahidkhah, Balogh *et al.* 2016, Zaman, Ali *et al.* 2017) and on platelet motion (Zhao, Marhefka et al. 2008, Kamada, Tsubota *et al.* 2011, Li, Ku *et al.* 2012, Bark Jr and Ku 2013, Ha and Lee 2013, Tovar-Lopez, Rosengarten *et al.* 2013), the effect of stenosis geometry on the margination of drug-carrying particles remains largely unexplored. It was previously observed that in regions of flow constriction the margination propensity of microparticles may be affected (Carboni, Bognet *et al.* 2016). Despite these findings, it is unclear as to how exactly the geometry of a stenosis, which includes both an area of constriction and of expansion, affects microparticle margination. This is also particularly relevant for in-vitro margination studies, all of which tend to include flow constrictions and expansions in their experimental apparatus as a result of constrictions that are present in tubing-to-tubing or tubing-to-inlet-port connections.

In this study, multiple channel geometries were investigated in-vitro via the use of microfluidic devices. The effects of occlusion percentage, constriction length, and degree of eccentricity of the entrance and exit of the stenosis were investigated and their effects on particle margination were quantified using direct particle tracking.

3.2 Methodology

3.2.1 Materials

Defibrinated bovine blood (Lampire Biological Laboratories, Inc., Pipersville, PA) was adjusted to 35% hematocrit using the previously established washing procedure. Fluorescent polystyrene spheres of 2.11 μm diameter were suspended in the blood and used

as model particles (Spherotech Inc., Lake Forest, IL). This particle size was chosen because it displayed the most margination in a previous study and, thus, would be the most affected by subtle changes in the constriction and expansion geometry (Carboni, Bognet et al. 2016). For microfluidic device fabrication, polydimethylsiloxane (PDMS) pre-polymer and curing agent were used (Silgard 184 Silicone Elastomer Kit, Krayden Inc., Denver, CO).

3.2.2 Microfluidic Device Design

Microfluidic device designs were produced using AutoCAD software. Three geometric parameters, namely percent occlusion, constriction length, and eccentricity, were explored and varied one at a time. Percent occlusion is defined the as the ratio of the channel width at the constricted area compared to the non-constricted area. Three different percent occlusions (25%, 50%, and 75%) as illustrated in Figure 3-1(a) were studied. The second parameter is constriction length and is defined as the distance between the end of constriction and the beginning of the expansion. Four constriction lengths, ranging from 50 μm to 10 mm were investigated (Figure 3-1(b)). The third parameter is eccentricity, which describes the gradualness of channel constriction and expansion, as illustrated in Figure 3-1(c). Mathematically, eccentricity at the constriction and expansion was calculated according to the formula for the eccentricity of an ellipse:

$$\varepsilon = \sqrt{1 - \frac{b^2}{a^2}} \tag{3-1}$$

where ε is the eccentricity and a and b are the length of the semi-major and semi-minor axis of the ellipse, respectively. A maximum eccentricity of 0.99 was selected to limit the transition length required to establish full constriction. All devices used in this study have

a channel depth of 100 μm and a channel width of 100 μm in the non-constricted area. As shown in Figure 3-2(a), the channel is 10 mm long both before and after the constricted area, while the constriction length varies. The distance required for a particle to fully marginate, or the margination distance, was calculated to be 7.5 mm, using a formula proposed by Zhao et al. (Zhao, Shaqfeh et al. 2012) and experimentally determined particle diffusivity (Carboni, Bognet et al. 2016). A 10-mm length was therefore chosen to ensure that margination reached completion before the introduction of a constricted area.

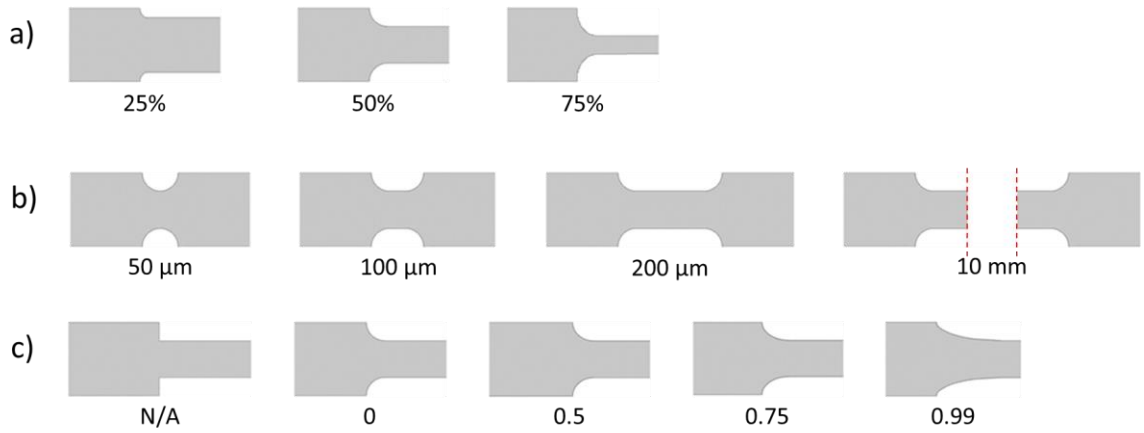

Figure 3-1: Device designs at the constriction, with the later expansion 10 mm downstream mirroring these geometries (a) Variable occlusion percentage (b) Variable constriction length with mirrored expansion after the given distance and (c) Variable eccentricity.

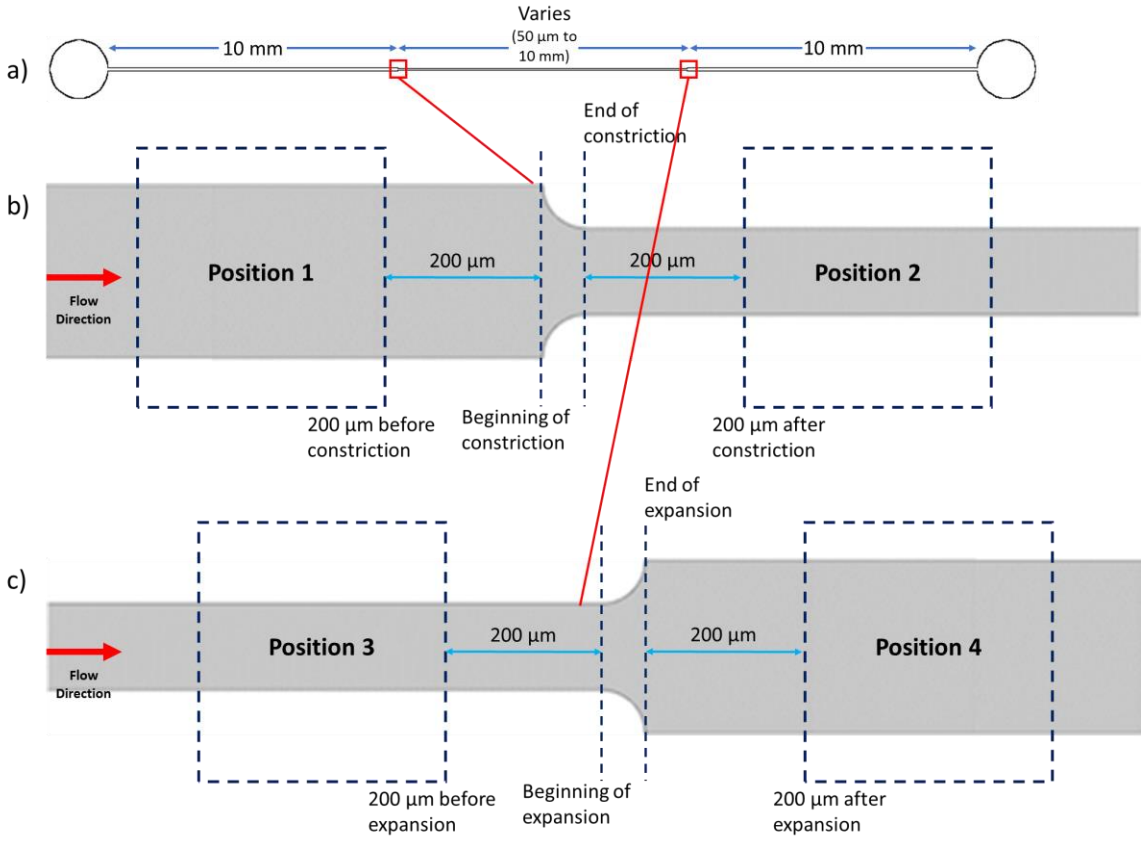

Figure 3-2: (a) Design of a typical device with 10 mm segments before and after a 10 mm constricted, middle segment (devices with constriction length variations had shorter constricted segments) (b) Close-up of the first red box, showing imaging positions 1 and 2 (c) Close-up of the second red box, showing imaging positions 3 and 4.

3.2.3 Device Fabrication

Microfluidic devices were fabricated from a commercially-obtained silicon wafer master (FlowJEM, Toronto, Canada) using PDMS and following established procedures. Briefly, elastomer base and curing agent were mixed in a 10:1 ratio. The resultant mixture was degassed for 10 minutes to remove air bubbles and placed in an oven and allowed to cure. The devices were cut out and punched to form an inlet and an outlet and then plasma

bonded (Basic Plasma Cleaner PDC-32G, Harrick Plasma, Ithaca, NY) to a glass coverslip slide (#1.5, Thermo Fisher Scientific Inc., Waltham, MA) using the custom procedure developed in Chapter 2.

3.2.4 Experimental Apparatus and Considerations

Blood containing the fluorescent 2.11-µm spherical particles was pumped through microfluidic devices using a pressure-driven pump system equipped with a flow controller (Fluigent Inc., Villejuif, France). This pump system, instead of a syringe pump, was used for better flow rate control (Carboni, Bognet et al. 2016). The fluid was pumped through the microfluidic device at a physiologically relevant average velocity of 1 mm/s in the non-constricted regions which corresponds to a volumetric flow rate of 0.60 µL/min and an apparent wall shear rate of 70.9 s^{-1} (Klug, Lessin *et al.* 1974, Pries, Secomb et al. 1995, Kubota, Tamura et al. 1996, Cai, Fan et al. 2012). The Reynolds number (Re) is defined as:

$$\mathrm{Re} = \frac{\rho W \bar{u}}{\mu} = \frac{\rho Q}{\mu W H} \tag{3-2}$$

where ρ is the density, W is the channel width, $\bar{u}$ is the mean fluid velocity, µ is the (dynamic) viscosity of the fluid, Q is the volumetric flow rate, and H is the depth (or height) of the channel. The Reynolds number compares inertial to viscous forces and was calculated to be approximately 0.030, suggesting that viscous forces dominate inertial forces and that the flow is laminar for all device geometries. Alternatively, Equation 3-2 can be written in terms of volumetric flow rate (Q) and channel depth (H). The volumetric flow rates and channel depth are kept constant in all experiments and the *Re* number therefore remains constant if a Newtonian fluid is assumed. However, this simplified Re

calculation does not take into account the shear-thinning nature of blood. A generalized Reynolds number for a power law fluid was defined by several authors (Metzner and Reed 1955, Madlener, Frey et al. 2009) as:

$$\mathrm{Re}_{genPL} = \frac{\rho w^n \bar{u}^{(2-n)}}{K((3n+1)/(4n))^n 8^{(n-1)}} \tag{3-3}$$

where n is the power law index of the fluid and K is the flow consistency index of the fluid. Equation 3-3 reduces to Equation 3-2 for a Newtonian fluid with $n = 1$ and $K = \mu$. Using literature values for blood *(*n = 0.716 *and* K = 0.0171 Pa*s*)* (Elblbesy and Hereba 2016), Re_{genPL} was calculated to be ca. 0.020 and ranges between 0.024 to 0.044 for 75% to 25% occlusion, respectively. Small Reynolds numbers like these imply that viscous forces are dominant in the current experimental system.

For each device, a 60,000-frame (~7.5 minutes) time-lapse video was acquired using a dry objective lens (40x) with a high-speed camera (Andor iXon Ultra 897 iX0897 EMCCD, 130 frames/s, Andor Technology Ltd., Belfast, UK) and an inverted fluorescence microscope (Nikon Eclipse Ti-E, Nikon Instruments Inc., Melville, NY) with an Epifluorescence source (Intensilight C-HGFIE, Nikon Instruments Inc., Melville, NY). These time lapse videos were collected at four positions: (1) before the constriction, (2) after the constriction, (3) before the expansion and (4) after the expansion. In each case, the time lapses were collected 200 µm away from the respective geometric change to allow for flow reestablishment. Figure 3-2(a) and Figure 3-2(b-c) show the areas of imaging for each full-length (10 mm) constriction device, with Positions 3 and 4 located downstream mirroring Positions 2 and 1, respectively. It should be noted that, for the case of variable constriction length, videos at Positions 2 and 3 were not collected because the lengths

studied were shorter than the viewing window and, as a result, videos at these positions were impossible to obtain. As such, only the results at Position 1 and Position 4 were recorded for these devices. After each time-lapse video was collected, the reservoir of blood was gently shaken to keep the solution well mixed and the device was perfused at a high flow rate (~8 μL/min) for approximately 2 minutes. After every 2-3 time lapses, the entire system was flushed for 10 minutes before collection of the next time lapse.

3.2.5 Image Analysis: Particle Tracking

MATLAB® was used to analyze the time-lapse videos. The fluorescent particles were tracked using code developed in-house. Similar to a previous study, the tracking code consists of three steps: first, a background correction was performed to remove any bright pixels associated with particles adhered to the bottom of the channel. Second, the position and size of all particles were then calculated using a gradient-based method. The calculated particle size was used to eliminate out-of-focus particles based on their apparent larger size. Lastly, the positions of all remaining particles were tracked as a function of time to calculate velocities.

Different from last time, some near-wall particles were found to be tracked, lost and tracked again, and sometimes again afterward as well. This was termed "double-tracking" or "triple-tracking" and new MATLAB® code was developed to correct for these phenomena. In the code, particle frame numbers and y-positions were compared – particles that shared a very close frame number and y-position were removed as they were highly likely to be double- or triple-tracked. The code removed the first track from particles that were detected to have been doubled-tracked and the first and second tracks from particles

that were detected to have been triple-tracked. The last track was kept for these particles since it was the longest and thus most accurate track.

Since this code had an impact on results, the results from Chapter 2 were rerun using this new code. However, no differences in the margination parameters were found. As a result, the double- and triple-tracking phenomena were concluded to only have occurred starting in this Chapter's experiments and were likely a result of using new software (Andor SOLIS was used in Chapters 3 and 4 whereas Andor IQ was used in Chapter 2) to track the particles or the use of a slightly higher microscope gain in this Chapter.

3.2.6 Quantifying Margination

The methodology for the quantification of margination propensity is detailed in a previous study by the authors (Carboni, Bognet et al. 2016). Briefly, the channel in each time-lapse video was first split into 10 equally-spaced segments and particles were tracked and counted in each of the 10 segments. The weighting by velocity was done to account for the naturally higher particle count near the center of the channel due to the higher velocity of the fluid and, therefore, throughput of particles. Since more particles will be seen nearer to the center of the channel where the velocity is at a maximum and more particles will be observed over a given time for a uniform dispersion, weighting the particles based on their velocities allows for velocity profile normalization. This weighting is given by the following equation (Carboni, Bognet et al. 2016):

$$P_{i^{th}segment \in [1,10]} = \sum_{j \in [1,n]} \frac{v_{x,\max}}{v_{x,j}} \tag{3-4}$$

where $P_{i^{th}\text{-}segment}$ is the total weighted particle count for the ith segment, $v_{x,\max}$ is the maximum particle velocity across the channel, $v_{x,j}$ is the velocity of the jth particle within the ith segment, and n is the total number of particles within the ith segment. From Equation 3-4, each particle in a segment is assigned a weighted value and slower particles will be weighted more heavily. We next define the margination parameter, M, as:

$$M = \frac{P_{1^{st}\ segment} + P_{10^{th}\ segment}}{\sum_{i^{th}\ segment\ \in [1,10]} P_i} \tag{3-5}$$

Equation 3-5 allows for results that are easily interpretable and comparable. Assuming an even distribution of particles in a fluid where no margination occurs, such as water, M should be equal to 0.20 because the weighting would result in each segment having 10% of the total particle weight and two of the segments are adjacent to the channel wall. As expected, an M of approximately 0.20 was found for a control experiment that was conducted using water, as shown in Figure 3-3(a). Larger values of M are indicative of marginating behavior and the magnitude of M can be compared between experiments to quantify the effects of each of the geometrical changes studied on particle margination. For each experiment, an average M was calculated after tracking and analyzing thousands of particles and a one-way ANOVA with a Tukey comparison was run on the results to ensure statistical significance.

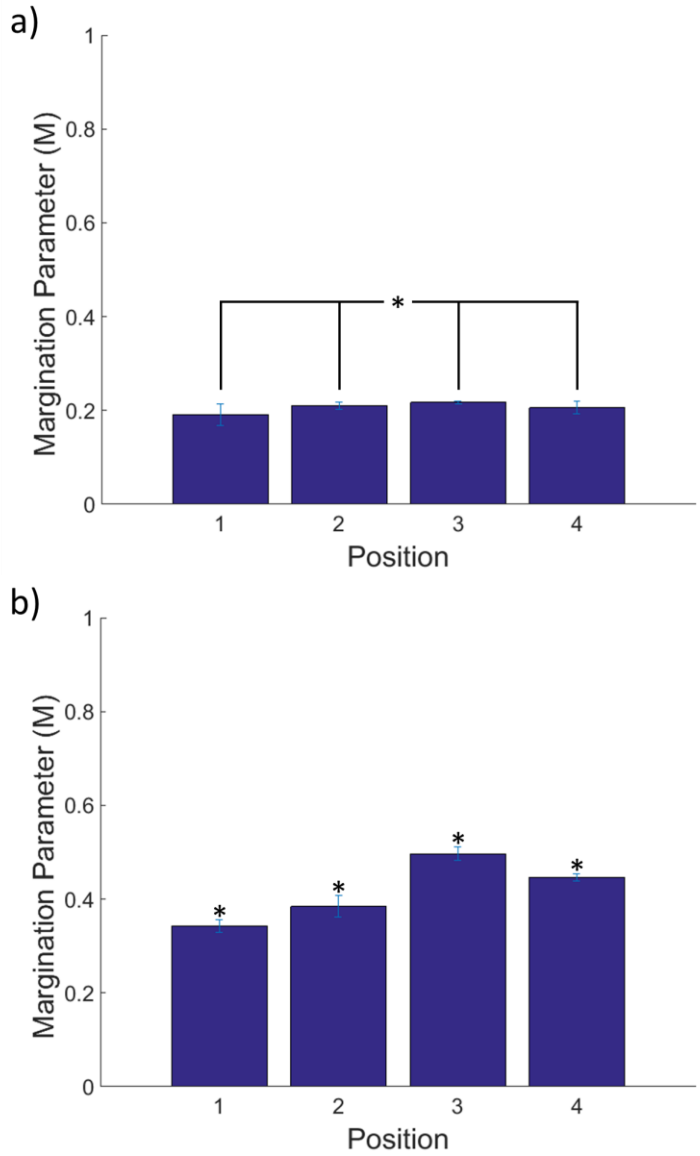

Figure 3-3: Margination Parameters at different positions for (a) water and (b) blood. Percent occlusion: 50%; constriction length: 10 mm; eccentricity: 0. Asterisks denote significance of a value from all others, asterisks with lines denote nonsignificance of the grouped values from one another but significance from non-grouped values.

3.3 Results

3.3.1 Effect of Position

For particles suspended in water, minimal changes in the margination parameter were observed with varying position, as shown in Figure 3-3(a). A one-way ANOVA has shown that none of these margination parameters are statistically significant from one another ($p > 0.05$ in all cases). This is as expected since there are no particle-RBC interactions in water and these values are all very close to the expected value of 0.20 for a fluid with an even distribution of particles after velocity normalization. Figure 3-3(b) shows the results for blood in the same device at various positions. A one-way ANOVA shows that all of these values are statistically significant from one another ($p < 0.05$). The margination parameter increases from Position 1 to Position 2 and from Position 2 to Position 3. However, a decrease in M is observed from Position 3 to Position 4.

This trend was observed for all device geometries with the exception of the shorter length devices (50, 100 and 200 μm) where Positions 2 and 3 are undefined. It was considered that particles in the constriction are more difficult to track due to their faster velocity and that this could in turn artificially inflate the margination parameter at Positions 2 and 3, leading to the observed increase from Position 1 to Position 2 and decrease from Position 3 to Position 4. However, since the water results show no significant difference in the margination parameter between positions it is likely that the blood results are not a result of tracking difficulties and that, instead, the geometry is the cause of the change in margination parameter from location to location. We hypothesize that particle-RBC interactions - the driving force for margination (Kumar and Graham 2012, Kumar and Graham 2012, Kumar, Henríquez Rivera et al. 2014, Vahidkhah and Bagchi 2015) - are

significantly altered by the constriction and also by the expansion geometries. Effect of Variable Occlusion Percentage

As shown in Figure 3-4, the *M* value increases with an increasing occlusion percentage. These results were confirmed to be significant via the use of a one-way ANOVA ($p < 0.05$). The degree of occlusion appears to have a large effect on the *M* value. For instance, increasing percent occlusion from 25% to 75% results in a 41.6% increase in the *M* value. Blood is considered to be an incompressible fluid and the mean velocity in the constricted region will change due to the reduction in the cross-sectional area of the channel, as given by the continuity equation:

$$Q = \bar{u}A \tag{3-6}$$

where Q is the volumetric flow rate, $\bar{u}$ is the mean velocity of the fluid and A is the cross-sectional area of the channel. For the same volumetric flow rate, a reduction in the cross-sectional area of the channel results in a proportional increase in the velocity of the fluid. An occlusion of 25%, 50% and 75% yield an increase in velocity by a factor of 1.33, 2 and 4, respectively. Other studies have linked higher shear rates to increased margination (Charoenphol, Huang et al. 2010, Namdee, Thompson et al. 2013, Carboni, Bognet et al. 2016). This may be a result of enhanced RBC-particle interactions. These interactions, which are between elastic and stiff particles and termed heterogeneous collisions, are identified as a driving force for margination (Kumar and Graham 2011, Kumar and Graham 2012, Kumar, Henríquez Rivera et al. 2014). In atherosclerosis, for example, myocardial infarctions are known to occur at percent occlusions above 70% (Pijls 2009, Holme,

Fedotenko et al. 2012). However, the cutoff value for a stenosis to become life-threatening is largely unknown for arterioles.

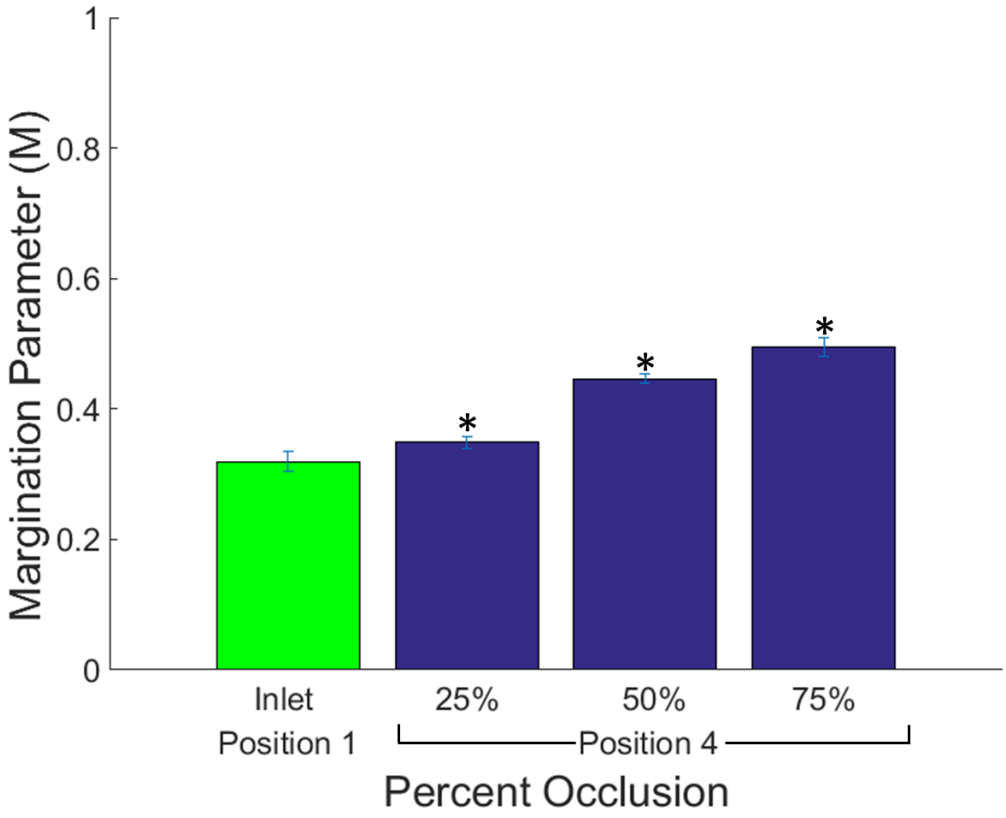

Figure 3-4: Variable percent occlusion device results. Length: 10 mm; eccentricity: 0. Asterisks denote significance of a value from all others, asterisks with lines denote nonsignificance of the grouped values from one another but significance from non-grouped values.

3.3.2 Effect of Variable Constriction Length

As shown in Figure 3-5, the *M* value increases with increasing constriction length. A one-way ANOVA showed that 50 and 200 μm lengths were significantly different but that 50 and 100 and 100 and 200 μm lengths were not. This demonstrates that, while length

does have an effect on the *M* value, the effect is difficult to see in 50 to 100 μm intervals. While longer constrictions do allow more time for further particle margination to occur, even a short length of 200 μm results in 14% enhanced margination compared to a length of 50 μm. As such, it is possible that there are other interactions, such as between particles and RBCs as the constriction and/or expansion occurs, that could result in such enhanced margination despite such a small difference in constriction length. This hypothesis is further supported by experimental results showing the effects of just the constriction on the M-value, where the M-value was found to increase in each case. In each experiment where a video within the constriction was acquired and analyzed, just after the constriction the M-value was found to increase. These results, combined with the results for variable constriction length, suggest that margination may be slightly enhanced by the presence of even a short constriction. While the lengths of cerebral arterioles in humans are known to be on the order of 3 mm (Aydin, Rosenblum *et al.* 1991), the length of a typical arteriolosclerotic region is not documented in the literature. Should it be on the order of the length of a cerebral arteriole, however, then margination would be significant and would fall somewhere between the values of the 200 μm length channel and the 10,000 μm length channel.

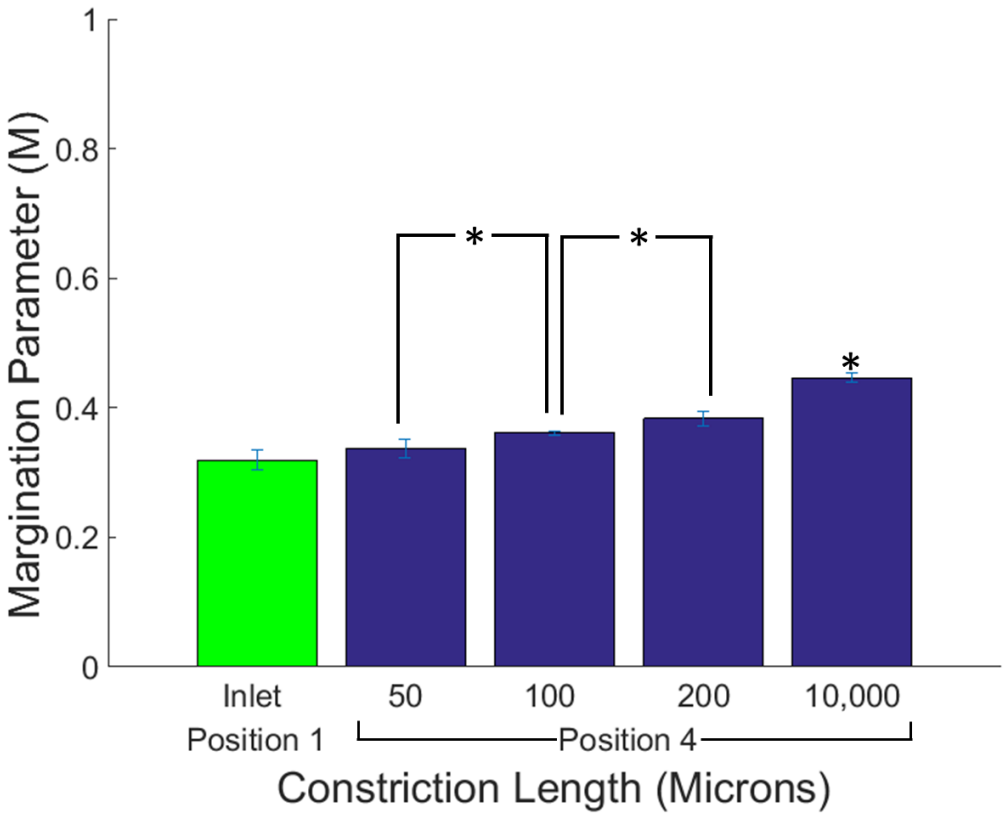

Figure 3-5: Variable constriction length device results. Percent occlusion: 50%; eccentricity: 0. Asterisks denote significance of a value from all others, asterisks with lines denote nonsignificance of the grouped values from one another but significance from non-grouped values.

3.3.3 Effect of Variable Eccentricity

The eccentricity of the occlusion was varied between a sudden constriction/expansion (N/A), a quarter-circle (0 eccentricity) entrance and an increasing eccentricity (0.5, 0.75 and 0.99) to explore the effects that the shape of the entrance had on particle margination. The results are shown in Figure 3-6. A one-way ANOVA showed significance ($p < 0.05$) of the results for the 0 and 0.5 eccentricity, while the other values

were insignificant from one another but significant in comparison to the 0 and 0.5 eccentricities. From these results, as the entrance and exit to and from the constricted area become more and more gradual (eccentricity increases), margination was found to decrease. However, interestingly, the sudden constriction/expansion device showed significantly lower margination than the 0-eccentricity device. Indeed, the M-value for the N/A eccentricity device was comparable to (and insignificant from) the M-values for the 0.75 and 0.99 eccentricity devices. These results for the N/A device, though puzzling, were confirmed through multiple experiments.

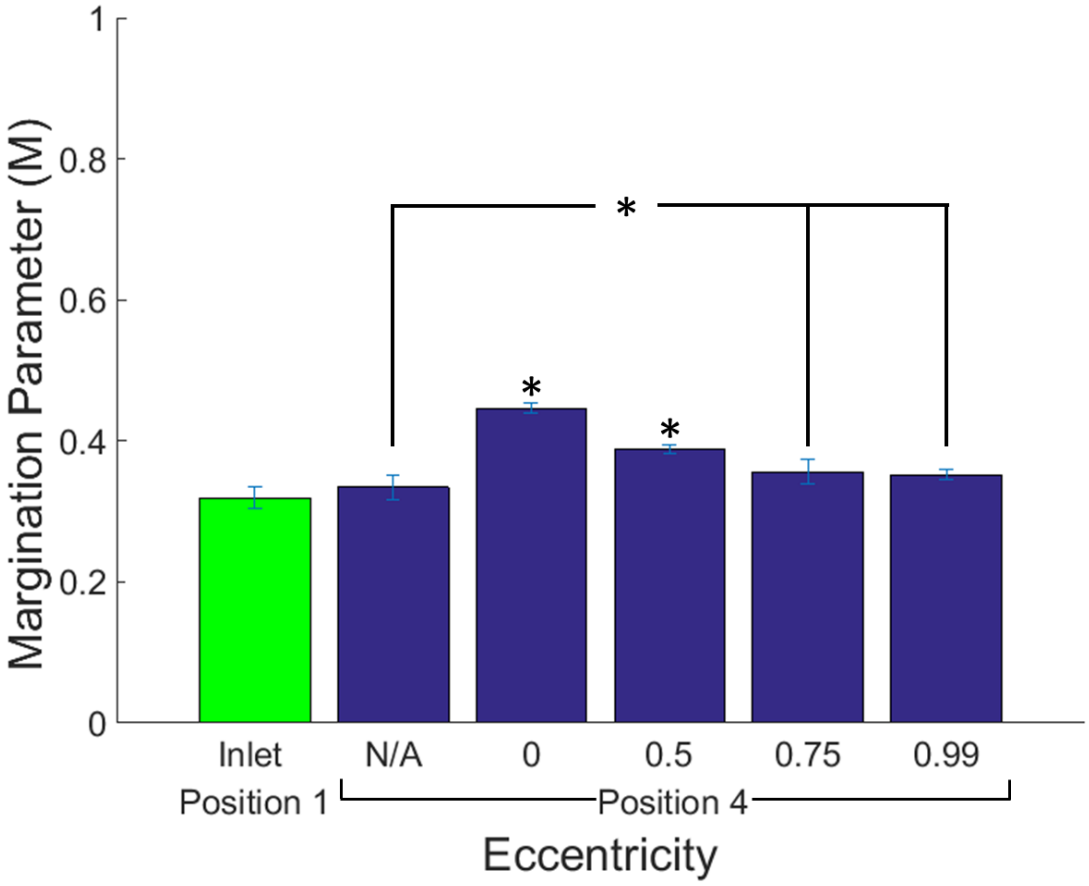

Figure 3-6: Variable eccentricity device results. Length: 10 mm; percent occlusion: 50%. Asterisks denote significance of a value from all others, asterisks with lines denote nonsignificance of the grouped values from one another but significance from non-grouped values.

It is observed that the lower M-value at position 4 could be a result of the expansion directly before it. The N/A eccentricity device had a much higher M-value at position 3, of 0.4157. However, at position 4, the M-value dropped to the outlet value of 0.3342 depicted in Figure 3-5. Recalling that position 1 is 200 µm before the constriction, that position 2 is 200 µm after the constriction, position 3 is 200 µm before the expansion and position 4 is

200 µm after the expansion, the M-values for positions 1 and 2 and for positions 3 and 4 should be the same if the geometry has no effect on particle margination since the distance between these two sets of positions is very small. It was found that the N/A eccentricity device had the largest increase in M-value from position 1 to position 2 and also the largest decrease in M-value from position 3 to position 4 out of all of the variable eccentricity devices. This suggests that the constriction and expansion areas had the largest effect on margination in the N/A eccentricity device out of all other variable eccentricity geometries and supports the hypothesis that the straight walls had a major albeit unexpected and largely negative impact on the margination of particles in this geometry.

In literature, some studies observed a recirculating flow after a sudden expansion (Sollier, Go *et al.* 2014, Dhar, Pao *et al.* 2016). This recirculating flow was investigated for the N/A eccentricity device as a potential explanation for the unexpectedly low M-values observed. Recirculating flow was found to occur as a result of two competing lift forces arising from inertia: a shear-gradient lift force and a wall-effect lift force for particle Reynold's numbers (Re_p) greater than one, as given by the following equation:

$$\mathrm{Re}_p = \mathrm{Re}\left(\frac{a}{W}\right)^2 \tag{3-7}$$

where a is the particle diameter and W is the width of the channel. For this study, Re_p was approximately 4.45×10^{-5}, which is well outside of the range for recirculating flow. Furthermore, no flow perturbations, such as a recirculating flow, were observed experimentally in the N/A eccentricity geometry after reviewing time-lapse videos taken at the constriction and expansion regions.

To better understand the flow profile of the N/A eccentricity device, blood was modeled as a power-law fluid in COMSOL software and the results are shown in Fig. 3-7. Stagnant zones with no flow were clearly observed near the corners at the entrance and exit of the constricted channel. Further, no recirculation was observed at the exit of the constricted channel, consistent with the experimental observation. However, it should be noted that blood is treated as a homogeneous fluid in the simulations. Such approach is inadequate in capturing margination which originates from the interactions between RBCs and particles. For future work, numerical models may be extended to offer insights into experimental observations reported in this paper for varying stenosis geometries, especially in the case of sudden constriction and expansion.

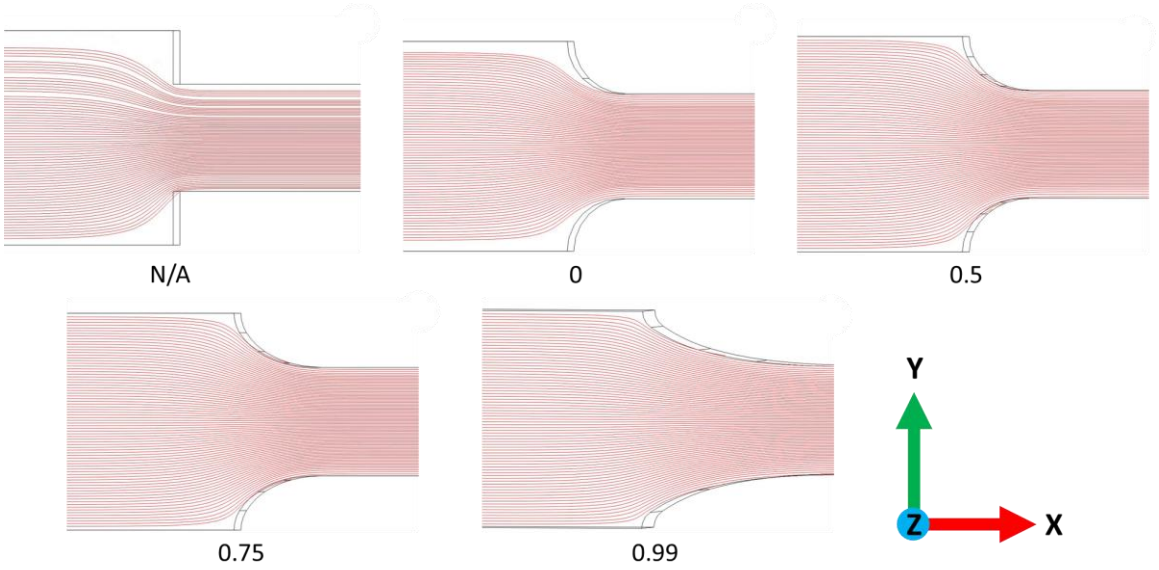

Figure 3-7: COMSOL model of the flow for various eccentricities.

3.4 Conclusions

To summarize, particle margination was quantified via the direct tracking of fluorescent model particles in microfluidic devices having different constriction and

expansion geometries. A margination parameter, or *M* value, was calculated at different locations as the particles enter and exit the constricted areas mimicking a stenosed blood vessel. The higher the *M*-value, the larger the degree of margination. As a control experiment, particles were suspended in water and pumped through the devices. No signs of margination were recorded at all the positions imaged. In the case of blood, the *M*-value increased after a constriction but decreased after an expansion, suggesting that channel geometry has an important effect on particle margination. The effects of the degree of occlusion (or percent occlusion), constriction length, and the gradualness of constriction/expansion were further investigated. Increasing percent occlusion and increasing constriction length increased particle margination. As the percent occlusion increases, a higher shear rate will be present in the constricted region, which has previously been shown to lead to enhanced margination (Charoenphol, Huang et al. 2010, Carboni, Bognet et al. 2016).

As for the positive effect of constriction length on margination, it is attributed to: (i) a longer residence time for longer constriction lengths and/or (ii) enhanced particle-RBC interactions, which have shown to be the root cause of margination (Kumar and Graham 2012, Kumar, Henríquez Rivera et al. 2014, Vahidkhah and Bagchi 2015). In terms of the channel shape, a more gradual constriction/expansion region (with increasing eccentricity) resulted in a lesser degree of margination, with the exception of a sudden constriction/expansion geometry. No recirculating flows were observed experimentally or COMSOL simulations. The exact reason is unclear and requires further numerical modeling, such as particle dynamics simulations, which consider the discrete interactions between particles and RBCs. All in all, this study reveals that the channel geometry has

non-negligible effects on particle margination. However, percent occlusion, constriction length and eccentricity are not well-defined and are not fully characterized in existing in-vivo studies. The findings of this paper call for a more detailed geometric characterization of the stenosed areas in order to better understand the underlying physics.

4 Effects of Pulsatile Blood Flow Patterns on Particle Margination

4.1 Introduction

It is well-known that blood flow is generally pulsatile in nature, characterized by time-dependent variations in both pressure and flow rate (Pan, Wang *et al.* 2014). Existing in-vitro experimental studies of particle margination utilize either pulsatile flow or a single constant, steady flow rate when running experiments. While these studies commonly do not cite their reasoning as to why they chose a particular flow rate, a study by Phibbs (Phibbs 1966) and also a separate study by Goldsmith and Spain (Goldsmith and Spain 1984) found that there existed an enhanced concentration of WBCs near the periphery of blood vessels in pulsatile flow when compared to the concentration in steady flow. Furthermore, a later study by Xu and Wootton investigated the margination of platelets in both pulsatile and steady blood flow and found increased platelet margination in pulsatile vs steady blood flow, especially (Xu and Wootton 2004). They also concluded that margination may develop more rapidly near the vessel wall in pulsatile vs steady flow conditions (Xu and Wootton 2004).

However, this study utilized 3 mm diameter tubes as the experimental system. In blood vessel or channel diameters above approximately 300 μm, the effects of individual RBCs are negligible (Pries, Secomb et al. 1996, Lim, Ober et al. 2012, Carugo, Capretto et al. 2013). Below this diameter, mechanical interactions between RBCs and walls cause the RBCs to tend to focus towards the center of the channel, termed axial migration, and causes significant non-Newtonian behavior (Bayliss 1959, Goldsmith and Mason 1961, Pries, Secomb et al. 1996, Sankar, Nagar *et al.* 2015). The experimental system employed by Xu and Wootton characterized a large blood vessel and does not take into account the axial

migration of RBCs that is present in a smaller blood vessel. This focusing of RBCs towards the center of the blood vessel has been observed by several modeling studies to lead to heterogeneous interactions between RBCs and WBCs, which are thought to be a major driving force for margination (Kumar and Graham 2011, Kumar and Graham 2012). Further, the study in Chapter 2 produced results that experimentally supported the existence of these particle-RBC interactions and their importance to margination (Carboni, Bognet et al. 2016). Despite these unique mechanics and the importance of arterioles, especially cerebral arterioles in white-matter stroke as described in Chapter 3 (Alexander and Putnam 1938, Fisher 1965, Rowbotham and Little 1965, Harnarine-Singh, Geddes et al. 1972, Fujiwara, Ishikawa et al. 2009, Kanbay, Snchez-Lozada et al. 2011, Rosenzweig and Carmichael 2013), almost no studies look at the effects of pulsatile flow in smaller arteries and arterioles (Kanaris, Anastasiou *et al.* 2012).

As such, an experimental study of the effects of pulsatile vs steady flow in a smaller blood vessel such as the current arteriolar geometry with a width of 100 μm was conducted. The goal was to illuminate the effects on margination of pulsatile vs steady flow in smaller arterioles and arteries. Furthermore, the effects of varying the frequency and amplitude of the pulses were investigated. Exploring these variables and observing the degree of margination produced by variations in each could lead to an isolation and better understanding of the mechanisms by which pulsatile flow may cause enhanced margination. This, in turn, could shed light on the degree of necessity in using pulsatile flow in experiments that seek to employ the most accurate system possible for the purposes of quantifying or investigating margination.

4.1.1 Modeling Physiological Pulsatile Flow

Physiological pulsatile flow is modeled in a number of studies, with information on the physiologically relevant range and shape of the pulsations (Chaturani and Palanisamy 1989). The simplest model for pulsatile flow was developed by Womersley in 1955 but was for large arteries, not smaller arterioles (Womersley 1955, Elad and Einav 2009). While some of the smallest arteries do not exhibit pulsatile flow because it is damped out by the time it reaches them (Burton 1965, Charm and Kurland 1974), it is still present in arterioles (Elad and Einav 2009).

The shape of physiological pulsatile flow can be modeled as a sine wave (Ku, Giddens *et al.* 1985, Chaturani and Palanisamy 1989, Ojha, Ethier *et al.* 1990, Walker, Johnston *et al.* 2014). The amplitude or flow rate of such a function can be taken as the typical flow rate in the relevant blood vessel, in this case an arteriole. As for the frequency, a number of studies mention different numbers, many even for the same or similar flow conditions. A near-1 hz pulse frequency appears to be dominant but the only studies available that mention frequency are the studies of larger channels. Bok et al. and Kahveci and Becker, for example, utilized a pulse frequency of 60 pulses/minute, or 1 hz in their experiments (Lee, Assadi *et al.* 1978, Kahveci and Becker 2015). However, a frequency of approximately 0.27 hz was also used in a different large-channel experiment (Walker, Johnston et al. 2014) as was a frequency of 2.9 hz (Ojha, Ethier et al. 1990). Finally, the experiment by Xu and Wootton found a frequency of 1.04 hz (Xu and Wootton 2004). Knowing these physiologically relevant values, an experiment was designed.

4.2 Methodology

4.2.1 Materials

Defibrinated bovine blood (Lampire Biological Laboratories, Inc., Pipersville, PA) was adjusted to 35% hematocrit using a washing procedure detailed in a previous study (Carboni, Bognet et al. 2016). Fluorescent polystyrene spheres of 2.11 μm diameter were suspended in the blood and used as model particles (Spherotech Inc., Lake Forest, IL). This particle size was chosen because it displayed the most margination in a previous study and, thus, would be the most affected by subtle changes in the blood flow patterns (Carboni, Bognet et al. 2016). For microfluidic device fabrication, polydimethylsiloxane (PDMS) pre-polymer and curing agent were used (Silgard 184 Silicone Elastomer Kit, Krayden Inc., Denver, CO).

4.2.2 Device Fabrication

Microfluidic devices were fabricated from a commercially-obtained silicon wafer master (FlowJEM, Toronto, Canada), as in a previous study. PDMS was used and established procedures were followed. Briefly, elastomer base and curing agent were mixed in a 10:1 ratio. The resultant mixture was degassed for 10 minutes to remove air bubbles and placed in an oven and allowed to cure. The devices were cut out and punched to form an inlet and an outlet and then plasma bonded (Basic Plasma Cleaner PDC-32G, Harrick Plasma, Ithaca, NY) to a glass coverslip slide (#1.5, Thermo Fisher Scientific Inc., Waltham, MA) using the custom procedure developed in Chapter 2.

4.2.3 Experimental Setup

Blood containing the fluorescent 2.11-μm spherical particles was pumped through microfluidic devices via the use of a pressure-driven pump system that included a flow

controller (Fluigent Inc., Villejuif, France). This pump system also included limited scripting software that was utilized to create a pulsatile flow. While the software was not capable of directly following a sine wave, scripts were written that set the flow rate to a value, waited for a length of time and then set the flow rate to 0. The pump was incapable of instantaneously adjusting the flow rate and required time to fully adjust the flow rate to the desired value. However, the resultant shape of the flow rate vs time plot over the course of a given experiment resembled a sine curve naturally, simply by setting the flow rate to 0 or the desired value. Due to the nature of the scripts employed, the pulse flow rate (PFR) was defined as the flow rate that was set as the maximum, or peak. Similarly, the pulse wait time (PWT) was defined as the wait time between setting the flow rate to 0 or to the maximum value. For example, for an experiment employing pulsatile flow ranging between 0 and 0.6 µL/min, the PFR would be 0.6 µL/min and the PWT might be set to 1 second. In this case, the pump would set the flow rate to 0.6 µL/min from 0, wait 1 second, set the flow rate to 0, wait 1 second, set the flow rate to 0.6 µL/min, etc.

In order to confirm the fit to a sine wave, the flow rate over time was recorded from the flow controller. A backbone MATLAB® code for the fitting of sine waves was obtained from MATLAB® Mathworks® and edited in-house for application to the current study. It was found that a sine wave was a good fit for the resultant flow rate curves, as can be seen in Figure 4-1. In this way, a pulsatile flow, similar to that observed physiologically (Ku, Giddens et al. 1985, Chaturani and Palanisamy 1989, Ojha, Ethier et al. 1990, Walker, Johnston et al. 2014), was achieved. However, due to the pump requiring a minimum amount of time to adjust the flow rate to the entered value, the minimum time between pulses was limited. It was found that PWTs of lower than 1 second could not be

confidently employed, resulting in curves that were very noisy with very questionable accuracy and reproducibility (Figure 4-2).

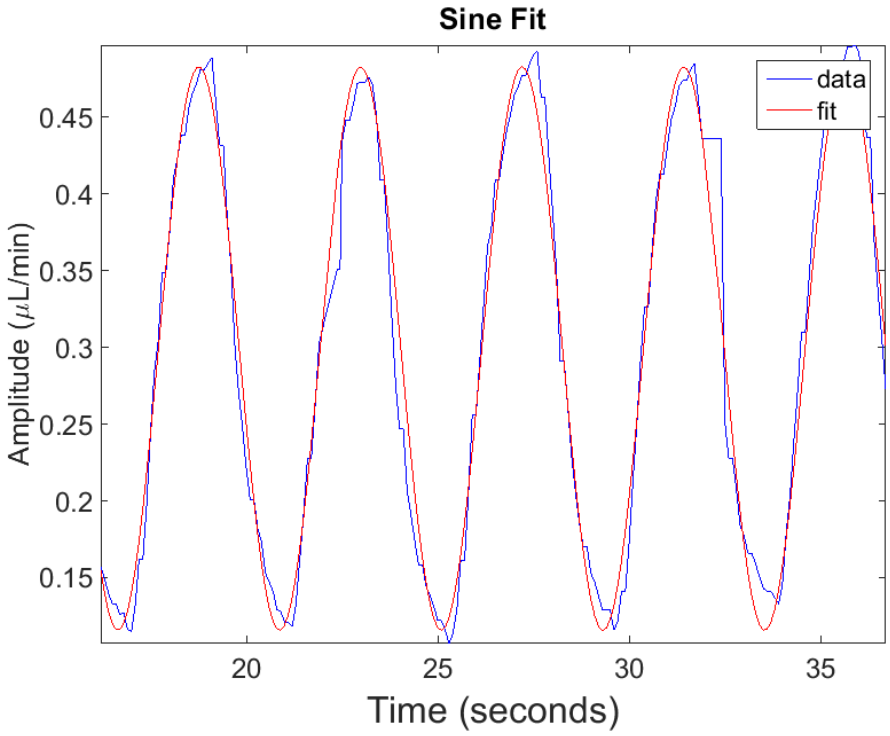

Figure 4-1: Sample sine-wave fit to experimental flow data.

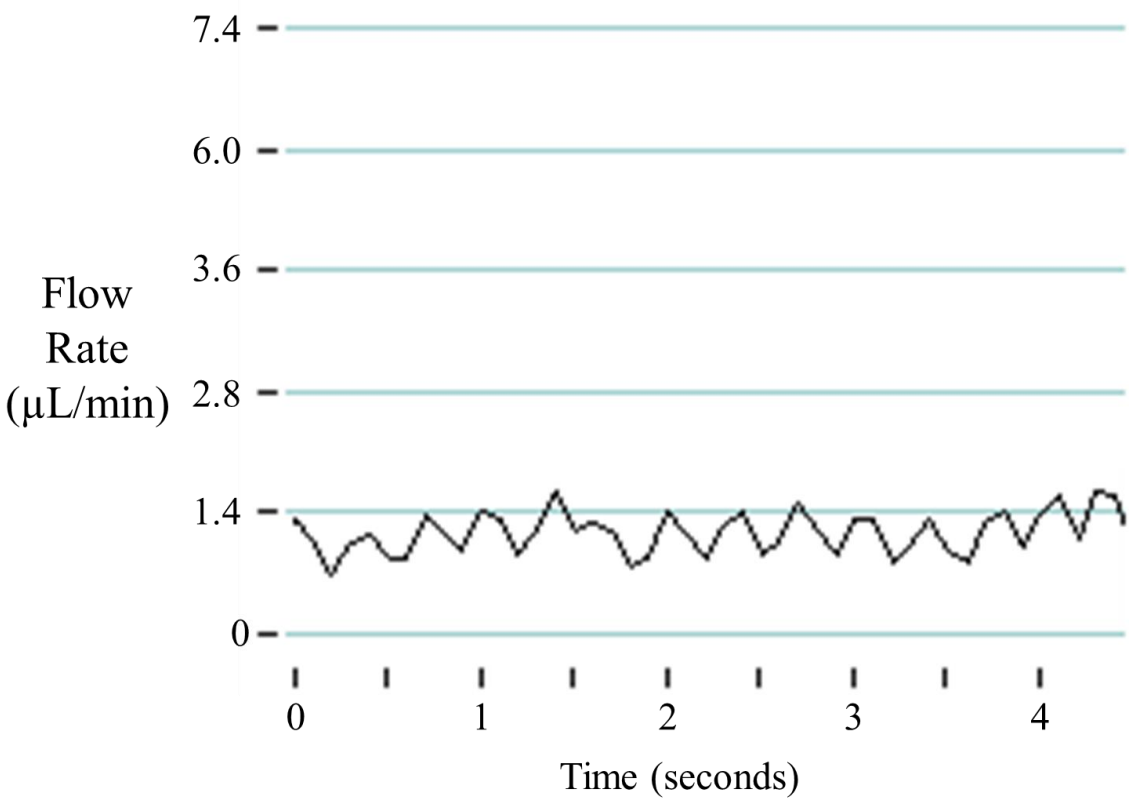

Figure 4-2: Variation of flow rate while employing a 0.5 second pulse wait time.

Having confirmed the resemblance to a sine wave, fluid was pumped through the microfluidic device at various PFRs (0.3, 0.6, 1.2 and 2.4 µL/min) and using various PWTs (1, 1.5, 2, 2.5 and 3 seconds) to explore the effects of variations of the two, both individually and together. Furthermore, a steady-flow scenario was also investigated. For each device, a 60,000-frame (~7.5 minutes) time-lapse video was acquired using a dry objective lens (40x) with a high-speed camera (Andor iXon Ultra 897 iX0897 EMCCD, 130 frames/s, Andor Technology Ltd., Belfast, UK) and an inverted fluorescence microscope (Nikon Eclipse Ti-E, Nikon Instruments Inc., Melville, NY) with an Epifluorescence source (Intensilight C-HGFIE, Nikon Instruments Inc., Melville, NY). After each time-lapse video was collected, the reservoir of blood was gently shaken to keep

the solution well mixed and the device was perfused at a high flow rate (~8 μL/min) for approximately 2 minutes. After every 2-3 time lapses, the entire system was flushed for 10 minutes before collection of the next time lapse. These time lapses were all acquired at the same location and during the same experiment, using the same prepared blood sample.

4.2.4 Analysis

MATLAB® was used to analyze the time-lapse videos. The fluorescent particles were tracked using code developed in-house. Similar to previous chapters, the tracking code consists of three steps: first, a background correction was performed to remove any bright pixels associated with particles adhered to the bottom of the channel. Second, the position and size of all particles were then calculated using a gradient-based method. The calculated particle size was used to eliminate out-of-focus particles based on their apparent larger size. Lastly, the positions of all remaining particles were tracked as a function of time. However, due to the dependence of velocity on time with pulsatile flow, velocities were not calculated as they would be extremely variable and wholly dependent upon the part of the pulsation that the particle was tracked.

4.2.5 Quantifying Margination

In Chapters 2 and 3, the velocity of each particle was calculated and subsequently used to normalize the particle distributions observed during an experiment. As a result, a margination parameter with a value of 0.2 indicated a random distribution, displaying no margination, and values higher than 0.2 were indicative of margination. However, since the velocity in pulsatile flow is variable and dependent upon when during the pulsation the particles were tracked, an alternative to the margination parameter is required for experiments with pulsatile flow. Since the main objectives of this study are internally

comparative in nature, a simplified, non-normalized margination parameter was defined as the ratio of the number of particles in the near-wall segments to the total number of particles as follows:

$$M_{non} = \frac{p_{1^{st}\,segment} + p_{10^{th}\,segment}}{\sum_{i^{th}\,segment \in [1,10]} p_i} \tag{4-1}$$

Each p in Equation 4-1 is the non-normalized count of particles in a given segment as opposed to the previous definition where it symbolized the total particle weight for that segment. Effectively, the non-normalized margination parameter for this chapter is the percentage of particles that were found to marginate and will be termed M_{non}. These values mean little alone, unlike those in previous chapters, but can still be easily compared to see the differences in margination between the various experimental conditions in this study.

4.3 Results and Discussion

4.3.1 Steady vs Pulsatile Flow

Figure 4-3 shows M_{non} for both a steady flow and pulsatile flow (PFR = 0.6 µL/min, PWT = 1 second). A significant difference between margination in steady and in pulsatile flow was not observed. While other studies discovered enhanced degrees of margination in larger arteries in pulsatile vs steady flow (Phibbs 1966, Goldsmith and Spain 1984, Xu and Wootton 2004), this phenomenon was not observed in the current experimental arteriolar system. This could be because of the extremely laminar nature of the flow at a channel width of 100 µm which may have resulted in a dampening of interactions that led to the observed enhanced margination in the larger channels or this result could be due to larger inertial forces that are prevalent with larger Reynolds number flows.

There was a large degree of error in the pulsatile experiment. To ensure validity of the results, this experiment and the steady flow experiment were each repeated once and the initial findings were confirmed – no significant difference between the steady and pulsatile flow was found in this second repetition either. As a result, the use of a steady or a pulsatile flow is observed to be largely interchangeable for the flow parameters used in this Chapter and likely, by extension, for the flow parameters used in Chapter 2 and Chapter 3.

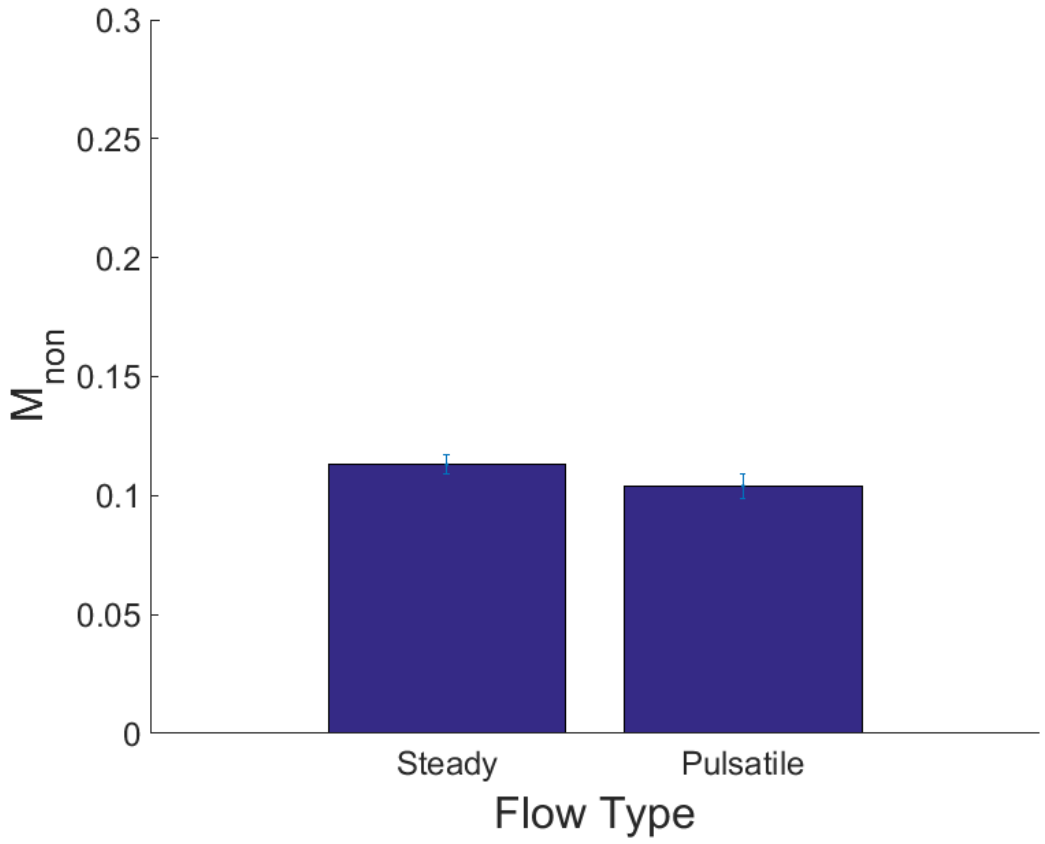

Figure 4-3: Non-normalized margination parameter for steady vs pulsatile flow.

4.3.2 Effect of Varying Pulse Wait Time

Varying PWT from 1 second to 3 seconds does not have an effect on the margination parameter. As can be seen in Figure 4-4, despite variations in the wait time between pulses, M_{non} did not vary significantly. Indeed, a one-way ANOVA with a Tukey comparison test showed that there were no significant differences in the margination parameter between each of the varying PWT experiments.

To further confirm these results, a variation in PWT from 1 to 2 seconds was carried out for a PFR of 1.2 µL/min (Figure 4-5). It was hypothesized that in an area of faster flow where margination would naturally be enhanced (based on the findings in Chapter 2), a more significant variation may occur between different PWTs. However, these results also did not show a significant difference when compared to one another. As a result, varying PWT was found to have no effect on the margination propensity of particles in the current system. This is likely because inertial effects for the experimental system are negligible and PWT may have a largely inertial effect on margination, though no studies have investigated or confirmed this.

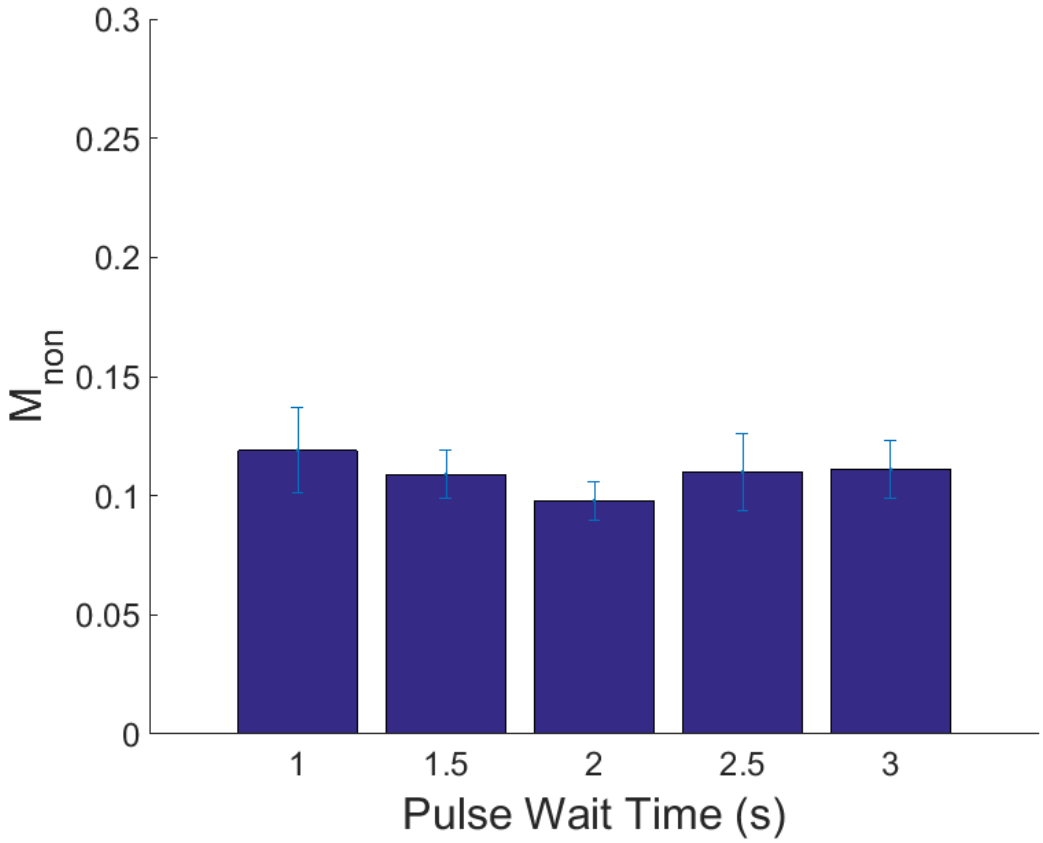

Figure 4-4: Non-normalized margination parameter with a varying pulse wait time. Flow rate = 0.6 µL/min.

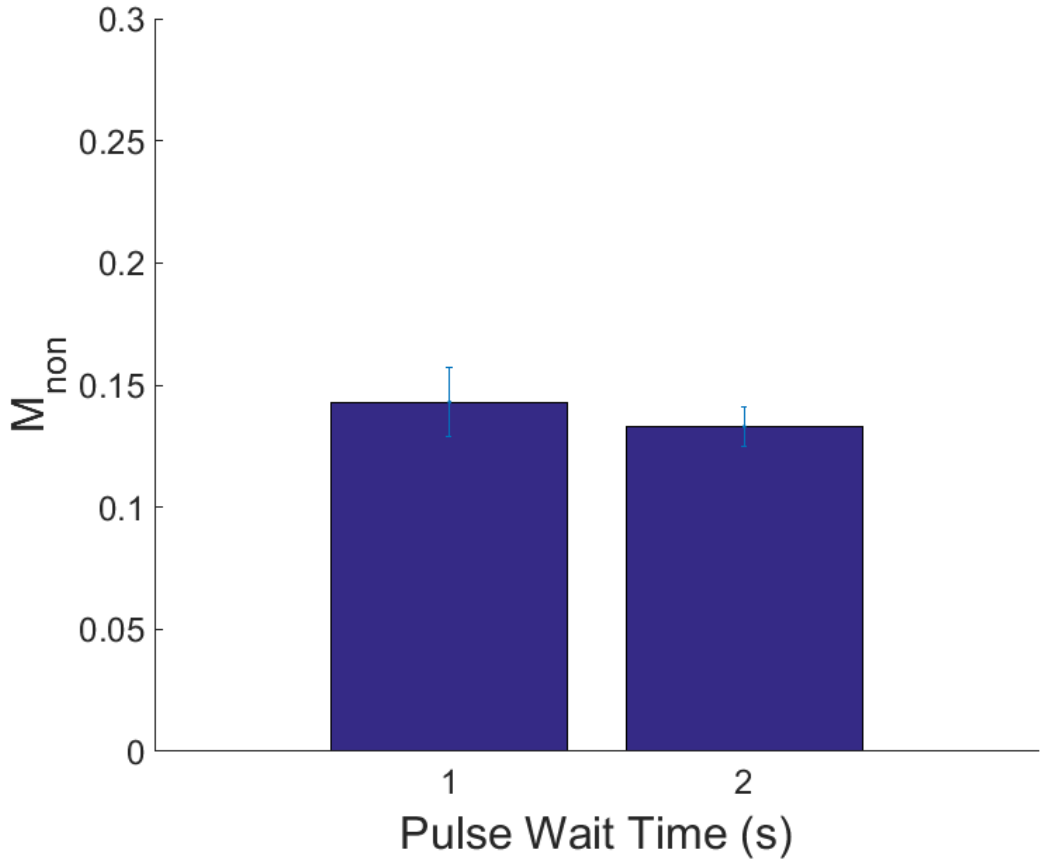

Figure 4-5: Non-normalized margination parameter with a varying pulse wait time. Flow rate = 1.2 µL/min.

4.3.3 Effect of Varying Pulse Flow Rate

Figure 4-6 shows the results from varying PFR. A one-way ANOVA was carried out and all results were found to be significant except for the 0.3 and 0.6 µL/min results, which were not significant from one another. The trend observed shows higher margination with a higher PFR which, similar to the findings in Chapter 2, is likely a result of enhanced particle-RBC interactions with larger flow rates. While this is not a particularly novel result, the variation of the PFR was effectively a variation of the amplitude of the sine curves and, thus, the final variable quality of a sine curve.

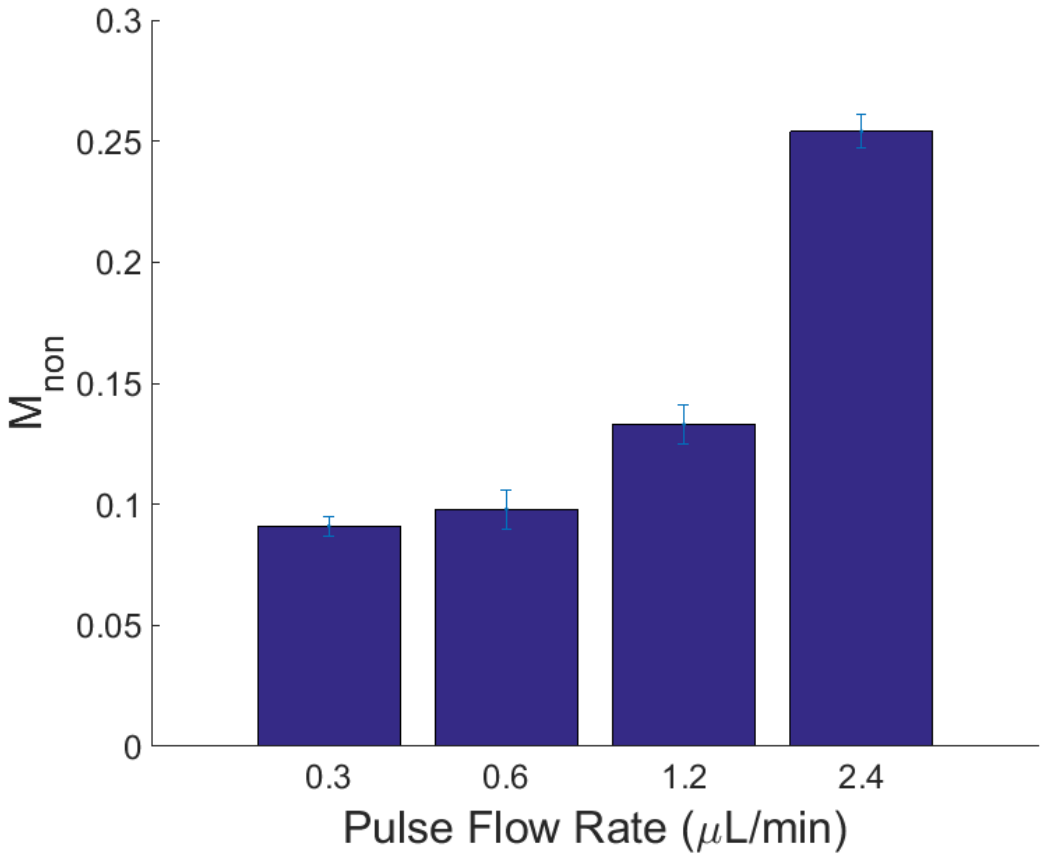

Figure 4-6: Non-normalized margination parameter with a varying pulse flow rate. Pulse wait time = 2 seconds.

4.4 Conclusions

No significant differences were observed between pulsatile and steady flow and also between varying PWTs. It is possible that the observed increased WBC margination in other studies between steady and pulsatile flow was dependent on effects that were only present within the larger channel size (Phibbs 1966, Goldsmith and Spain 1984, Xu and Wootton 2004). These effects could have been inertial in nature since the channel size and, therefore, the magnitude of the Reynolds Number is a major difference between those studies and this one. Unfortunately, this conclusion is difficult to support with the results

of this study due to the absence of significantly enhanced margination in either case causing them to be null results. Increasing PFRs were found to lead to increasing margination, as was expected and following the findings of Chapter 2 for variable shear-rate flow.

Overall, this study did not find major differences between steady and pulsatile flow for an arteriolar geometry of approximately 100 μm width. The use of steady or pulsatile flow for this geometry of blood vessel appear to be interchangeable without adverse effects on experimental data. Furthermore, the results of this study should be applicable to any geometry wherein the vessel or channel diameter is less than approximately 500 μm, which is the cutoff for the effects of individual blood cells to become significant (Pries, Secomb et al. 1996, Lim, Ober et al. 2012, Carugo, Capretto et al. 2013). These results are valuable for future margination or other experimental studies since steady flow is generally much more easily employed and replicated as opposed to pulsatile flow which may have variations depending on the quality of the pumping system, as seen in this study.

5 Conclusions

5.1 Dissertation Overview

In this dissertation, novel findings related to particle margination were obtained. A wide variety of particle, flow and geometrical characteristics were investigated and the effects of each on the margination propensity of particles was quantified and evaluated. Practically, the findings of this work can be used in the design of drug-carrying particles in order to maximize drug delivery. Furthermore, a number of these findings can be applied to in-vitro experiments that seek to further investigate the phenomenon of margination, simplifying the experiments and providing insight as to the effects that could be observed from various device designs or experimental apparatuses.

While the main focus of this dissertation was on margination and how each parameter affects it, a number of other contributions were also made. First, the limitations of a syringe pump for very low flow rates were realized. Next, a standardized and normalized definition for margination was developed. Third, the limitations of manual-tracking studies and their potential for large error was highlighted.

5.2 Summary of Major Findings and Contributions

Chapter One motivated the research and provided background knowledge combined with objectives for each portion of this work. Chapter One introduced blood and detailed the complications of biological fluids. Further, it went on to explain the phenomenon of margination and how various particle and other properties can affect particle margination while also highlighting the current experimental understanding of the phenomenon. A lack of direct tracking studies exists and some adhesion studies are known to produce results that are questionable thanks to the very nature of adhesion as a

measurement mechanism. This effectively displays the need for direct tracking studies and the value of results that look at the entirety of the particle distribution and not just the marginating particles.

Chapter Two introduced one of the first direct tracking studies of particle margination and the first automated direct-particle-tracking study. The main original contributions and scientific findings of Chapter Two are as follows:

1) Discovery of the limitations of a syringe pump; for extremely low flow rates, the syringe pump creates a chaotic and vaguely pulsatile flow over time as opposed to the smooth, constant flow rate of a pressure-driven pump
2) Velocity-normalized definition of margination, which allows for an easy comparison and interpretation of results between experiments and even potentially between studies
3) Suspending media control experiments highlighted that sedimentation can have a pronounced effect in this experimental system
4) Large amounts of error were found when analyzing particle counts of 100 whereas particle counts of 1000 had much lower standard deviations; this highlights a weakness of manual direct tracking studies in that their particle counts are extremely limited compared to the developed automated direct tracking methodology
5) The presence of a flow constriction may have non-negligible effects on the margination of particles and the implicit assumption regarding a uniform distribution of particles near the inlet of a device cannot be assumed; baseline

values of margination near the beginning of a device's length are very important to measure and consider and may vary with different particle qualities

6) Margination velocity was higher for all particle sizes in blood than in water; this supports the concept of particle-RBC interactions being a major driving force for margination, especially since the blood was washed
7) Margination propensity of particles tends to increase with particle size, with a 45% increase upon changing particle size from 0.53 μm diameter to 2.11 μm diameter
8) Larger particles require more time/device length before they reach their full margination potential
9) Higher flow rate leads to a higher particle margination

Chapter Three followed from contribution #4 from Chapter Two and worked to achieve a deeper understanding as to how constriction and expansion regions affect margination, modelling various geometrical differences in stenosis geometry for not only in-vitro experimental applications but also for clinical applications in the treatment of arteriolosclerosis and white-matter stroke. The contributions and findings are as follows:

1) Control results with water and blood as the suspending media showed that the existence of a region of constriction and/or expansion does have an effect on particle margination; constrictions appear to have a positive effect and enhance margination whereas expansions appear to have a negative effect and result in a reduction in margination
2) Increasing percent occlusion was found to lead to an increasing amount of particle margination

3) Increasing constriction length was found to lead to an increasing amount of particle margination
4) Particle margination decreases as eccentricity increases from 0 to 0.99 and the constriction becomes more gradual and less sudden; this trend does not hold when including the N/A eccentricity device, however
5) Particle margination in the case of N/A eccentricity (straight, sudden constriction/expansion) was found to be most similar to the 0.75 and 0.99 eccentricity devices and much lower than the 0 eccentricity, breaking the observed trend of particle margination decreasing with an increasing "gradualness" of a constriction or expansion

Chapter Four investigated the effects of pulsatile flow, dissecting a sine wave pulsation and comparing the effects on margination of each component as well as the effects of using a steady flow vs a pulsatile flow experimentally. The contributions and findings are as follows:

1) No significant difference in the margination of particles between steady, constant flow and pulsatile flow was observed, implying that the two are interchangeable for the current experimental system and also possibly for experimental systems with similar flow patterns, such as for systems with channel diameters below 500 μm
2) Variation of the wait time between pulses and, thus, the cycle duration did not result in any significant variations in particle margination
3) Increasing the pulse flow rate and thus the amplitude was observed to lead to an increase in particle margination

5.3 Significance and Applications

This work highlights major factors that affect the margination of particles and has a wide variety of pharmaceutical applications. This research is useful for the general design of drug-carrying particles in that larger particle sizes were found to marginate the most effectively over time and, therefore, to deliver their drug payload the most effectively. However, this assumes that these larger particle sizes are practical for drug delivery which may not always be the case. However, in some situations it may be possible to utilize an aggregate of nanoparticles, thus attaining the benefits of enhanced margination as a result of larger particle size while also retaining the benefit of a small particle for drug delivery to the targeted site. Relatedly, these results can be applied to the treatment of arteriolosclerosis since shear-activated nanoparticle clusters have recently become a drug delivery technique of interest (Holme, Fedotenko et al. 2012, Saxer, Zumbuehl et al. 2013). Lastly, the discovery that large particles take a longer time to reach their maximum margination potential shows that, in some cases, smaller particles may actually be desirable over larger particles, especially when combined with the lower settling velocity of these smaller particles.

5.4 Future Directions

While a large number of various factors and their effects on margination were elucidated in this work, there still remains an enormous amount to investigate before margination is fully understood, especially experimentally. While particle properties such as size and shape and their effects on margination are now fairly clear, particle density and stiffness and their effects on margination are not well understood experimentally due to the inherent difficulty in varying just one of these properties without affecting the other.

Likewise, little work has been done to study the effects of particle charge on particle-RBC interactions and, thus, on particle margination except for one study involving charged liposomes (D'Apolito, Bochicchio *et al.* 2017). For now, it is important to simply continue investigating the variations of one property to achieve a better understanding of how that property can affect margination. Especially in the case of properties such as particle shape, where the orientation of a particle can cause enormous variations in the adhesion strength, direct-tracking studies of these particle properties under a standardized experimental protocol is desirable for a full and general understanding of each property. Once each property is well understood between studies, each of which employs similar experimental systems and practices, an ideal later or capstone study would vary each of these properties with the others and find the overall ideal particle for drug delivery. Taking into account and varying particle size, shape, stiffness, density and charge within a single study would be challenging but could lead to a "master" particle design for maximum margination. The physiological and realistic limitations on drug-carrier properties and the drug delivery mechanism should also be considered as well as the channel size/hematocrit, allowing for the design of a particle that not only marginates extremely well but also delivers its payload effectively despite the blood vessel size and local hematocrit variations that are naturally present in the body.

The effects of hematocrit variations on margination are still not well-understood either. Although it can be hypothesized based on current simulation work that an increasing hematocrit leads to enhanced particle-RBC interactions and, in turn, higher particle margination, this extrapolation does not take into account effects like the potential disappearance of the CFL with higher hematocrits and the effects that this could have on

particle margination. The absence of a CFL would mean that particles would not cease interacting with RBCs once they have marginated and could actually lead to a decrease in margination if the RBCs then push these particles back towards the centerline with them. The extrapolation of the effects of parameters such as the hematocrit on margination may not always be accurate due to variations near the extremes or even in middle-ranges. The amount of interactions and flow properties that are changed by varying a parameter like hematocrit means that the effects on particle behavior is not as predictable as modeling studies may indicate and these studies are limited in the amount of RBCs and, thus, the channel size that can be simulated as well. Lastly, hematocrit can also vary with channel or blood vessel size and this introduces an entire new level of complexity when exploring its effects. As such, further experimental work exploring the effects of varying hematocrit, especially involving different channel sizes, is necessary in order to fully understand it.

The study of margination is undoubtedly important but it is also important to consider the delivery of the drug to the targeted site as well, after margination has occurred. During the course of this work, preliminary experiments with a flow chamber (RC-50 Imaging Chamber, Warner Instruments, LLC, Hamden, CT) were performed. This flow chamber is comprised of two separate channels and a membrane that is sandwiched between them and is shown in Figure 5-1. The ultimate goal of this work was to mimic a blood vessel and tumor system using a thin membrane, with a designated pore size, inside of the flow chamber which could eventually be replaced with a cultured membrane of endothelial or perhaps even cancer-affected endothelial cells, which would have enhanced spacing.

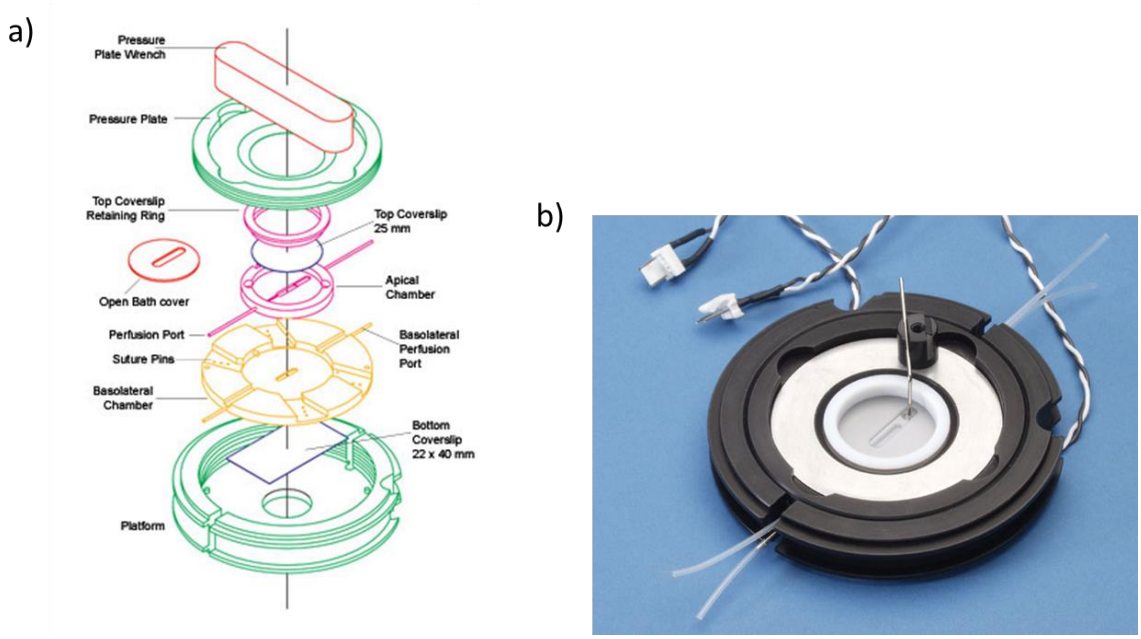

Figure 5-1: (a) Diagram of the exploded flow chamber, with each individual component labeled and (b) the assembled flow chamber with some inlet/outlet tubing attached.

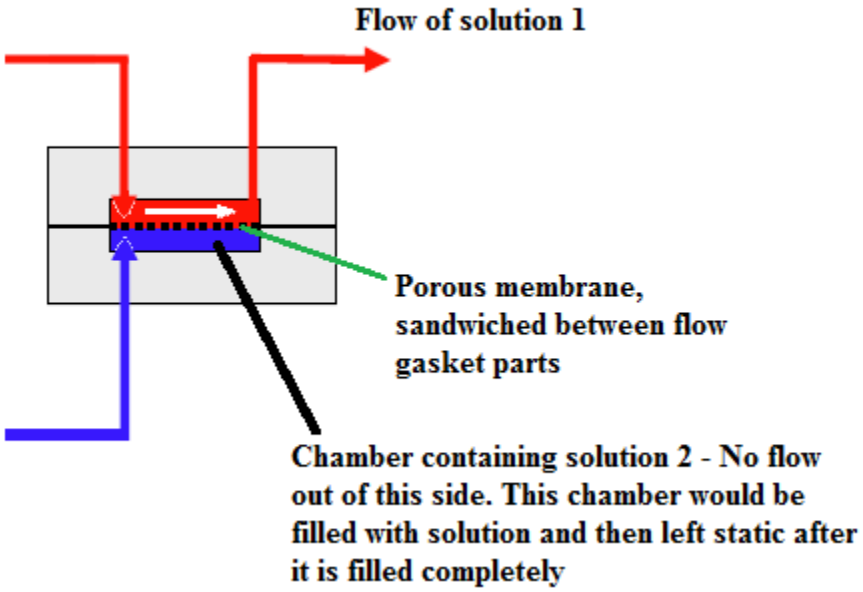

Figure 5-2: Diagram of eventual experimental setup.

As shown in Figure 5-2, the bottom chamber would be held static, without flow. Sandwiched between this channel and the upper channel would be a porous membrane, which would serve to mimic the area near a targeted site for drug delivery. Initially, this was planned to have a pore size of ~2 µm, representing the largest endothelial cell spacing that has been observed near a tumor site. However, this membrane would ideally consist of live cells for a more realistic system. Finally, the top channel would be perfused with blood, containing fluorescent particles that will serve to represent drug-carrying particles. Some preliminary results were obtained with this membrane, as shown in Figure 5-3, where 0.53 µm diameter particles were observed to successfully move through the pores and to the other side of the membrane from the flow-side.

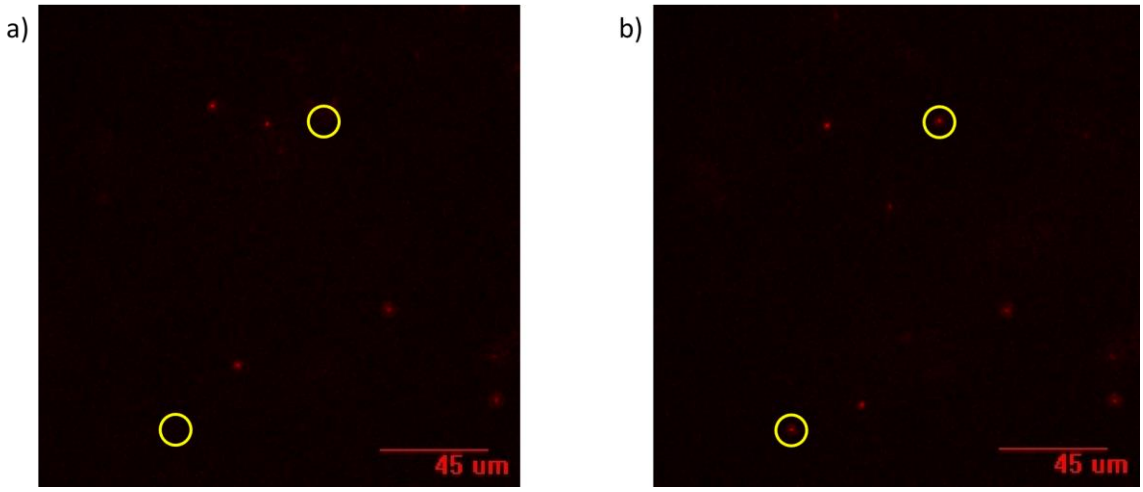

Figure 5-3: Example images showing the appearance of two 0.53 µm diameter particles after they traveled through an opaque, porous membrane with a pore diameter of 2 µm.

Margination and drug delivery could be simultaneously quantified by examination of the particle concentration in the bottom, static chamber at the end of an experiment with this setup. Overall, this would be a rigorous experiment involving not only margination but

also the actual drug delivery itself, something which margination studies tend to gloss over in favor of an in-depth look at only the margination of a particle. On the other hand, many studies have, for example, examined the transport of drug-carrying particles into a tumor but have not examined the margination involved (Kyle, Huxham *et al.* 2004, Dreher, Liu *et al.* 2006, Prabhakarpandian, Pant *et al.* 2008, Hsiao, Torisawa *et al.* 2009, Rosano, Tousi *et al.* 2009, Fukumura, Duda *et al.* 2010, Prabhakarpandian, Shen *et al.* 2011, Zervantonakis, Kothapalli *et al.* 2011, LaBarbera, Reid *et al.* 2012, Zervantonakis, Hughes-Alford *et al.* 2012, Breslin and O'Driscoll 2013, Moya, Tran *et al.* 2013, Verbridge, Chakrabarti *et al.* 2013, Vidi, Maleki *et al.* 2014, Prabhakarpandian, Shen *et al.* 2015). The combination of margination and drug delivery into one study could provide valuable knowledge regarding the interplay between the two. Further, the membrane could be varied easily in order to mimic different disease sites or tumor sites and how different receptors or other factors could impact drug delivery when combined with particle margination.

Other future directions of this research may also involve an investigation of how margination is related to channel size. No studies currently explore the effects of blood vessel size on margination beyond stating that the cutoff blood vessel diameter for the formation of a CFL is approximately 300 or 500 μm (Pries, Secomb et al. 1996, Lim, Ober et al. 2012, Carugo, Capretto et al. 2013). The effect of channel size on margination is not only relevant for in-vitro studies but also has physiological relevance as particles must navigate through a wide variety of differently-sized blood vessels. In particular, almost all current experimental in-vitro margination studies use an arbitrary channel size that is rarely the same as that used in another study. As such, comparison of results between studies can be difficult if channel size varies a lot, since hematocrit also varies with channel size.

Indeed, as mentioned before, a study on the variations of hematocrit and channel size and their effects on margination would be extremely useful to bridge the gap, so to speak, between all current experimental margination literature where differing hematocrits and channel sizes were selected. There exists the implicit assumption in current experimental margination literature that the results of one in-vitro study are comparable to those of another, even if both studies used only similar channel size, hematocrit and other experimental parameters instead of values that were exactly the same. This assumption, while not unreasonable, is not supported by any current study of margination and so a study that confirms or denies the validity of such study-to-study comparisons that operate with different channel sizes or slightly different hematocrits etc. would be valuable.

Lastly, the current experimental studies of margination that employ microfluidics involve a channel with a square or rectangular cross-section. The applicability of this as a representation of a blood vessel is questionable given that blood vessel cross-sections are well-known to be circular. While it was not extremely important for the current work by nature of imaging margination only on one place of the device, an investigation into the effects of different cross-sectional geometries on margination could prove interesting if the square or rectangular cross-section is found to alter the flow behavior or RBC-RBC or RBC-particle interactions in some unexpected way. Indeed, a study of WBC margination in a bifurcating microfluidic device found that switching from a rectangular cross-section to a circular cross-section resulted in a complete reversal of the distribution of marginated leukocytes among the branches of a bifurcation (Yang, Forouzan et al. 2011).

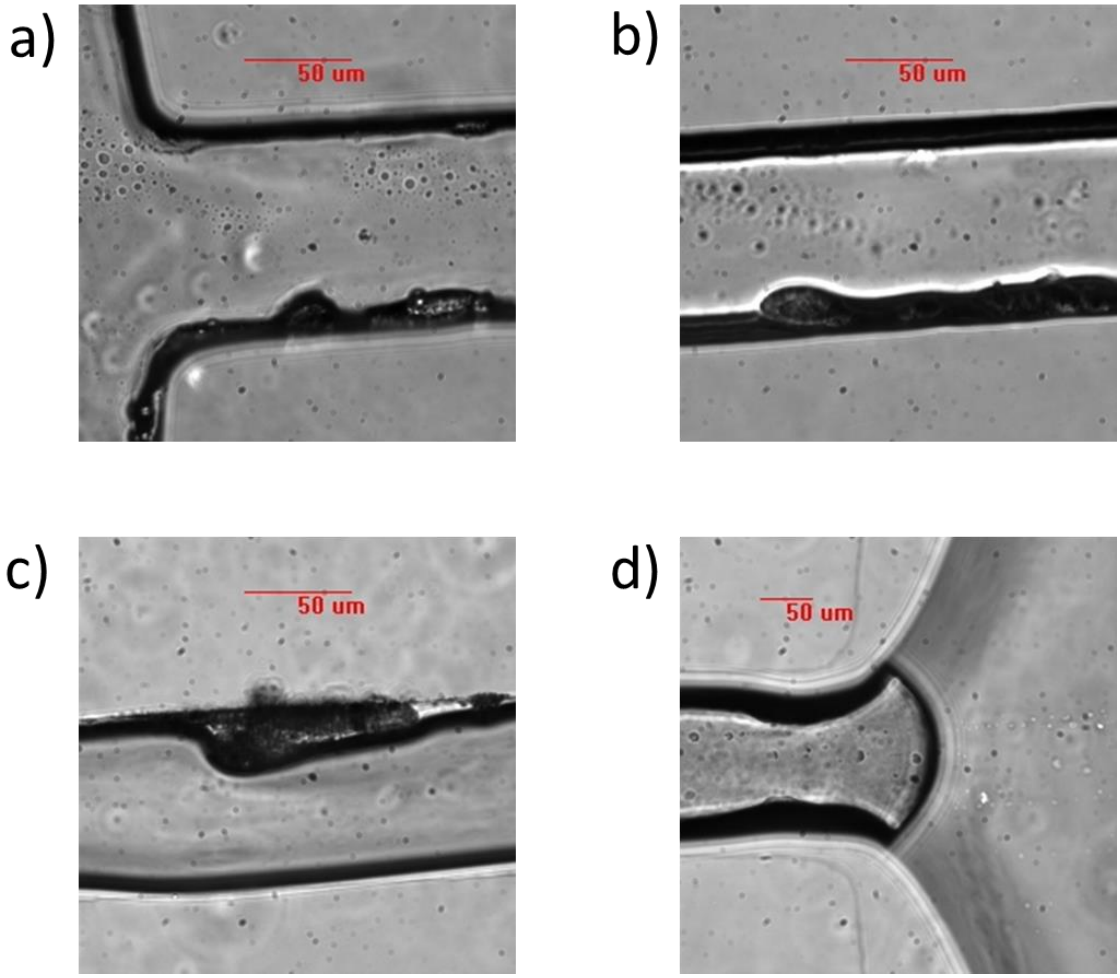

Figure 5-4: Images of device channels after attempting to use uncured PDMS to make a circular (or ovular) cross-section device (a) Just after the inlet landing pad, which can be seen to the right, some bumpiness on the lower wall (b) Slightly up-channel, another bump at the lower wall (c) Majorly misshapen part of the channel (d) Outlet of the device, the uncured PDMS was unable to be completely expelled and ended up sealing the outlet so that flow could not be perfused through the device.

There exist techniques for forming a circular cross-section in a microfluidic device from a square cross-section (Yang, Forouzan et al. 2011) and a preliminary attempt during the course of this work yielded partial success. Briefly, uncured PDMS is injected into a fully-cured and plasma bonded device. Next, air is injected so as to push out the uncured PDMS. The device is then placed onto a hot plate to cure and the resultant geometry is approximately circular. However, multiple issues with this procedure were encountered during an initial attempt. First, some of this PDMS clings to the walls and was not completely removed, resulting in a number of irregularities in the channel, with random variations in width throughout it without a discernible pattern. These variations can be seen in Figure 5-4, with Figure 5-4(c) showing a particularly large misshapen device portion. Figure 5(d) also showcases another major problem – not all of the PDMS was able to be pushed out of the device, likely due to the landing pad outlet region. The residual PDMS cured and sealed the outlet, preventing flow from perfusing throughout the device and leaving the device. With a more controlled and precise air flow while pushing out the PDMS, a circular cross-section device may be achievable. A study such as this would be feasible but the ability to precisely control the shape and smoothness of the final product for reproducibility purposes and consistency between experiments would be a major challenge. Furthermore, the outlet issue may not be solved by simply removing the landing pad region, which would also be a major challenge if the outlet were to keep sealing itself as a result of the injected PDMS. It is possible that faster airflow may solve this issue, but the residual PDMS is the issue and may relax and end up sealing the outlet anyway. This study would be dependent upon the solution of these two major issues.

6 References

Abbitt, K. B. and G. B. Nash (2001). "Characteristics of leucocyte adhesion directly observed in flowing whole blood in vitro." British Journal of Haematology **112**(1): 55-63.

Abkarian, M., C. Lartigue and A. Viallat (2002). "Tank treading and unbinding of deformable vesicles in shear flow: Determination of the lift force." Physical Review Letters **88**(6): 068103.

Abkarian, M., C. Lartigue and A. Viallat (2002). "Tank treading and unbinding of deformable vesicles in shear flow: Determination of the lift force." Physical Review Letters **88**(6): 068103-068101-068103-068104.

Abkarian, M. and A. Viallat (2005). "Dynamics of vesicles in a wall-bounded shear flow." Biophysical Journal **89**(2): 1055-1066.

Ahmad, T. and I. Hassan (2010). "Experimental analysis of microchannel entrance length characteristics using microparticle image velocimetry." Journal of Fluids Engineering, Transactions of the ASME **132**(4): 041102-041101-041102-041113.

Akbar, N. S. (2016). "Non-Newtonian model study for blood flow through a tapered artery with a stenosis." Alexandria Engineering Journal **55**(1): 321-329.

Alexander, L. and T. J. Putnam (1938). "Pathological alterations of cerebral vascular patterns." Research Publications of the Association for Research in Nervous and Mental Disease **18**: 471-543.

AlMomani, T., H. S. Udaykumar, J. S. Marshall and K. B. Chandran (2008). "Micro-scale dynamic simulation of erythrocyte-platelet interaction in blood flow." Ann Biomed Eng **36**(6): 905-920.

Amin, T. M. and J. A. Sirs (1985). "The blood rheology of man and various animal species." Quarterly Journal of Experimental Physiology **70**(1): 37-49.

Aydin, F., W. I. Rosenblum and J. T. Povlishock (1991). "Myoendothelial junctions in human brain arterioles." Stroke **22**(12): 1592-1597.

Baele, P. L. (2010). Plasma and Albumin. Alternatives to Blood Transfusion in Transfusion Medicine, Wiley-Blackwell**:** 83-108.

Barbee, J. H. and G. R. Cokelet (1971). "The Fahraeus effect." Microvascular Research **3**(1): 6-16.

Bark Jr, D. L. and D. N. Ku (2013). "Platelet transport rates and binding kinetics at high shear over a thrombus." Biophysical Journal **105**(2): 502-511.

Bayliss, L. E. (1959). "The axial drift of the red cells when blood flows in a narrow tube." The Journal of Physiology **149**(3): 593-613.

Bishop, J. J., A. S. Popel, M. Intaglietta and P. C. Johnson (2001). "Effects of erythrocyte aggregation and venous network geometry on red blood cell axial migration." American Journal of Physiology-Heart and Circulatory Physiology **281**(2): H939-H950.

Breslin, S. and L. O'Driscoll (2013). "Three-dimensional cell culture: The missing link in drug discovery." Drug Discovery Today **18**(5-6): 240-249.

Brizel, D. M., B. Klitzman, J. M. Cook, J. Edwards, G. Rosner and M. W. Dewhirst (1993). "A comparison of tumor and normal tissue microvascular hematocrits and red cell fluxes in a rat window chamber model." International Journal of Radiation Oncology, Biology, Physics **25**(2): 269-276.

Burton, A. C. (1965). Physiology and biophysics of the circulation. Chicago, Year Book, Medical Publishers.
Cai, B., J. Fan, M. Zeng, L. Zhang and B. M. Fu (2012). "Adhesion of malignant mammary tumor cells MDA-MB-231 to microvessel wall increases microvascular permeability via degradation of endothelial surface glycocalyx." Journal of Applied Physiology **113**(7): 1141-1153.
Carboni, E., K. Tschudi, J. Nam, X. Lu and A. K. Ma (2014). "Particle Margination and Its Implications on Intravenous Anticancer Drug Delivery." AAPS PharmSciTech **15**(3): 762-771.
Carboni, E. J., B. H. Bognet, G. M. Bouchillon, A. L. Kadilak, L. M. Shor, M. D. Ward and A. W. K. Ma (2016). "Direct Tracking of Particles and Quantification of Margination in Blood Flow." Biophysical Journal **111**(7): 1487-1495.
Carugo, D., L. Capretto, E. Nehru, M. Mansour, N. Smyth, N. Bressloff and X. L. Zhang (2013). "A Microfluidic-Based Arteriolar Network Model for Biophysical and Bioanalytical Investigations." Current Analytical Chemistry **9**(1): 47-59.
Charm, S. E. and G. S. Kurland (1974). Blood Flow and Microcirculation. New York, John Wiley & Sons.
Charoenphol, P., R. B. Huang and O. Eniola-Adefeso (2010). "Potential role of size and hemodynamics in the efficacy of vascular-targeted spherical drug carriers." Biomaterials **31**(6): 1392-1402.
Charoenphol, P., P. J. Onyskiw, M. Carrasco-Teja and O. Eniola-Adefeso (2012). "Particle-cell dynamics in human blood flow: Implications for vascular-targeted drug delivery." Journal of Biomechanics **45**(16): 2822-2828.
Chaturani, P. and V. Palanisamy (1989). "Microcontinuum model for pulsatile blood flow through a stenosed tube." Biorheology **26**(4): 835-846.
D'Apolito, R., G. Tomaiuolo, F. Taraballi, S. Minardi, D. Kirui, X. Liu, A. Cevenini, R. Palomba, M. Ferrari, F. Salvatore, E. Tasciotti and S. Guido (2015). "Red blood cells affect the margination of microparticles in synthetic microcapillaries and intravital microcirculation as a function of their size and shape." Journal of Controlled Release **217**: 263-272.
D'Apolito, R., S. Bochicchio, A. Dalmoro, A. A. Barba, S. Guido and G. Tomaiuolo (2017). "Microfluidic investigation of the effect of liposome surface charge on drug delivery in microcirculation." Current Drug Delivery **14**(2): 231-238.
Decuzzi, P., F. Gentile, A. Granaldi, A. Curcio, F. Causa, C. Indolfi, P. Netti and M. Ferrari (2007). "Flow chamber analysis of size effects in the adhesion of spherical particles." International Journal of Nanomedicine **2**(4): 689-696.
Decuzzi, P., S. Lee, B. Bhushan and M. Ferrari (2005). "A theoretical model for the margination of particles within blood vessels." Annals of Biomedical Engineering **33**(2): 179-190.
Decuzzi, P., R. Pasqualini, W. Arap and M. Ferrari (2009). "Intravascular Delivery of Particulate Systems: Does Geometry Really Matter?" Pharmaceutical Research **26**(1): 235-243.
Dhar, M., E. Pao, C. Renier, D. E. Go, J. Che, R. Montoya, R. Conrad, M. Matsumoto, K. Heirich, M. Triboulet, J. Rao, S. S. Jeffrey, E. B. Garon, J. Goldman, N. P. Rao, R. Kulkarni, E. Sollier-Christen and D. Di Carlo (2016). "Label-free enumeration, collection

and downstream cytological and cytogenetic analysis of circulating tumor cells." Scientific Reports **6**.
Dimakopoulos, Y., G. Kelesidis, S. Tsouka, G. C. Georgiou and J. Tsamopoulos (2015). "Hemodynamics in stenotic vessels of small diameter under steady state conditions: Effect of viscoelasticity and migration of red blood cells." Biorheology **52**(3): 183-210.
Doshi, N., B. Prabhakarpandian, A. Rea-Ramsey, K. Pant, S. Sundaram and S. Mitragotri (2010). "Flow and adhesion of drug carriers in blood vessels depend on their shape: A study using model synthetic microvascular networks." Journal of Controlled Release **146**(2): 196-200.
Dreher, M. R., W. Liu, C. R. Michelich, M. W. Dewhirst, F. Yuan and A. Chilkoti (2006). "Tumor vascular permeability, accumulation, and penetration of macromolecular drug carriers." Journal of the National Cancer Institute **98**(5): 335-344.
Dutrochet, H. (1824). Recherches anatomiques et physiologiques sur la structure intime des animaux et des végétaux, et sur leur motilité, J. B. Baillière.
Einstein, A. (1905). "Über die von der molekularkinetischen Theorie der Wärme geforderte Bewegung von in ruhenden Flüssigkeiten suspendierten Teilchen." Annalen der Physik **322**(8): 549-560.
Einstein, A. and R. Fürth (1956). Investigations on the Theory of the Brownian Movement, Dover Publications.
Elad, D. and S. Einav (2009). Physical and Flow Properties of Blood. Biomedical Engineering and Design Handbook, Volume 1. M. Kutz, McGraw Hill Professional.
Elblbesy, M. A. and A. T. Hereba (2016). "Computation of the Coefficients of the Power law model for Whole Blood and Their Correlation with Blood Parameters." Applied Physics Research **8**(2): 1.
Fåhraeus, R. (1929). "THE SUSPENSION STABILITY OF THE BLOOD." Physiological Reviews **9**(2): 241-274.
Faustino, V., D. Pinho, T. Yaginuma, R. C. Calhelha, G. M. Kim, S. Arana, I. C. F. R. Ferreira, M. S. N. Oliveira and R. Lima (2014). Flow of red blood cells suspensions through hyperbolic microcontractions. Lecture Notes in Computational Vision and Biomechanics. **12:** 151-163.
Fedosov, D. A., B. Caswell, A. S. Popel and G. E. Karniadakis (2010). "Blood Flow and Cell-Free Layer in Microvessels." Microcirculation **17**(8): 615-628.
Fedosov, D. A., J. Fornleitner and G. Gompper (2012). "Margination of White Blood Cells in Microcapillary Flow." Physical Review Letters **108**(2): 028104.
Ferri, M., S. Lombardini and C. Pallotti (1994). Leukocyte classifications by size functions. Applications of Computer Vision, 1994., Proceedings of the Second IEEE Workshop on.
Firrell, J. C. and H. H. Lipowsky (1989). "Leukocyte margination and deformation in mesenteric venules of rat." American Journal of Physiology **256**(6): H1667-H1674.
Fisher, C. M. (1965). "Lacunes: Small, deep cerebral infarcts." Neurology **15**(8): 774-784.
Fitzgibbon, S., A. P. Spann, Q. M. Qi and E. S. G. Shaqfeh (2015). "In vitro measurement of particle margination in the microchannel flow: Effect of varying hematocrit." Biophysical Journal **108**(10): 2601-2608.
Freund, J. B. (2007). "Leukocyte margination in a model microvessel." Physics of Fluids **19**(2): 13.

Fujiwara, H., T. Ishikawa, R. Lima, N. Matsuki, Y. Imai, H. Kaji, M. Nishizawa and T. Yamaguchi (2009). "Red blood cell motions in high-hematocrit blood flowing through a stenosed microchannel." Journal of Biomechanics **42**(7): 838-843.
Fukumura, D., D. G. Duda, L. L. Munn and R. K. Jain (2010). "Tumor microvasculature and microenvironment: Novel insights through intravital imaging in pre-clinical models." Microcirculation **17**(3): 206-225.
Gentile, F., C. Chiappini, D. Fine, R. C. Bhavane, M. S. Peluccio, M. M. C. Cheng, X. Liu, M. Ferrari and P. Decuzzi (2008). "The effect of shape on the margination dynamics of non-neutrally buoyant particles in two-dimensional shear flows." Journal of Biomechanics **41**(10): 2312-2318.
Gentile, F., A. Curcio, C. Indolfi, M. Ferrari and P. Decuzzi (2008). "The margination propensity of spherical particles for vascular targeting in the microcirculation." Journal of nanobiotechnology **6**: 9.
Gentile, F., A. Curcio, C. Indolfi, M. Ferrari and P. Decuzzi (2008). "The margination propensity of spherical particles for vascular targeting in the microcirculation." Journal of nanobiotechnology **6**: 1-9.
Godin, B., R. E. Serda, J. Sakamoto, P. Decuzzi and M. Ferrari (2010). Nanoparticles for Cancer Detection and Therapy. Nanotechnology, Wiley-VCH Verlag GmbH & Co. KGaA.
Goldsmith, H. L. and S. G. Mason (1961). "Axial migration of particles in poiseuille flow." Nature **190**(4781): 1095-1096.
Goldsmith, H. L. and S. Spain (1984). "Margination of leukocytes in blood-flow through small tubes." Microvascular Research **27**(2): 204-222.
Gulan, U., B. Luthi, M. Holzner, A. Liberzon, A. Tsinober and W. Kinzelbach (2012). "Experimental study of aortic flow in the ascending aorta via Particle Tracking Velocimetry." Experiments in Fluids **53**(5): 1469-1485.
Ha, H. and S. J. Lee (2013). "Hemodynamic features and platelet aggregation in a stenosed microchannel." Microvascular Research **90**: 96-105.
Hall, C. L. and M. Calt (2014). "Computational modeling of thrombotic microparticle deposition in nonparallel flow regimes." Journal of Biomechanical Engineering **136**(11).
Harnarine-Singh, D., G. Geddes and J. B. Hyde (1972). "Sizes and numbers of arteries and veins in normal human neopallium." Journal of Anatomy **111**(1): 171-179.
Hashizume, H., P. Baluk, S. Morikawa, J. W. McLean, G. Thurston, S. Roberge, R. K. Jain and D. M. McDonald (2000). "Openings between Defective Endothelial Cells Explain Tumor Vessel Leakiness." The American Journal of Pathology **156**(4): 1363-1380.
Henríquez Rivera, R. G., K. Sinha and M. D. Graham (2015). "Margination regimes and drainage transition in confined multicomponent suspensions." Physical Review Letters **114**(18): 188101-188101-188101-188105.
Holme, M. N., I. A. Fedotenko, D. Abegg, J. Althaus, L. Babel, F. Favarger, R. Reiter, R. Tanasescu, P. L. Zaffalon, A. Ziegler, B. Müller, T. Saxer and A. Zumbuehl (2012). "Shear-stress sensitive lenticular vesicles for targeted drug delivery." Nature Nanotechnology **7**(8): 536-543.
Hou, H. W., A. A. S. Bhagat, A. G. L. Chong, P. Mao, K. S. W. Tan, J. Y. Han and C. T. Lim (2010). "Deformability based cell margination-A simple microfluidic design for malaria-infected erythrocyte separation." Lab on a Chip **10**(19): 2605-2613.

Hou, H. W., H. Y. Gan, A. A. S. Bhagat, L. D. Li, C. T. Lim and J. Han (2012). "A microfluidics approach towards high-throughput pathogen removal from blood using margination." Biomicrofluidics **6**(2): 13.
Hsiao, A. Y., Y. s. Torisawa, Y. C. Tung, S. Sud, R. S. Taichman, K. J. Pienta and S. Takayama (2009). "Microfluidic system for formation of PC-3 prostate cancer co-culture spheroids." Biomaterials **30**(16): 3020-3027.
Jain, A. and L. L. Munn (2009). "Determinants of Leukocyte Margination in Rectangular Microchannels." Plos One **4**(9): 8.
Jain, A. and L. L. Munn (2011). "Biomimetic postcapillary expansions for enhancing rare blood cell separation on a microfluidic chip." Lab on a Chip **11**(17): 2941-2947.
Kahveci, K. and B. R. Becker (2015). "A numerical model of pulsatile blood flow in compliant arteries of a truncated vascular system." International Communications in Heat and Mass Transfer **67**: 51-58.
Kamada, H., K. I. Tsubota, M. Nakamura, S. Wada, T. Ishikawa and T. Yamaguchi (2011). "Computational study on effect of stenosis on primary thrombus formation." Biorheology **48**(2): 99-114.
Kanaris, A. G., A. D. Anastasiou and S. V. Paras (2012). "Modeling the effect of blood viscosity on hemodynamic factors in a small bifurcated artery." Chemical Engineering Science **71**: 202-211.
Kanbay, M., L. G. Snchez-Lozada, M. Franco, M. Madero, Y. Solak, B. Rodriguez-Iturbe, A. Covic and R. J. Johnson (2011). "Microvascular disease and its role in the brain and cardiovascular system: A potential role for uric acid as a cardiorenal toxin." Nephrology Dialysis Transplantation **26**(2): 430-437.
Katanov, D., G. Gompper and D. A. Fedosov (2015). "Microvascular blood flow resistance: Role of red blood cell migration and dispersion." Microvascular Research **99**: 57-66.
Kim, J., J. F. Antaki and M. Massoudi (2016). "Computational study of blood flow in microchannels." Journal of Computational and Applied Mathematics **292**: 174-187.
Kirby, B. (2010). Micro- and Nanoscale Fluid Mechanics: Transport in Microfluidic Devices, Cambridge University Press.
Klug, P. P., L. S. Lessin and P. Radice (1974). "Rheological Aspects of Sickle Cell Disease." Archives of Internal Medicine. **133**(4): 577-590.
Korin, N. (2012). "Shear-activated nanotherapeutics for drug targeting to obstructed blood vessels (Science (2012) (738))." Science **337**(6101): 1453.
Korin, N., M. Kanapathipillai and D. E. Ingber (2013). "Shear-responsive platelet mimetics for targeted drug delivery." Israel Journal of Chemistry **53**(9-10): 610-615.
Kratz , A., M. Ferraro , P. M. Sluss and K. B. Lewandrowski (2004). "Normal Reference Laboratory Values." New England Journal of Medicine **351**(15): 1548-1563.
Ku, D. N., D. P. Giddens, C. K. Zarins and S. Glagov (1985). "Pulsatile flow and atherosclerosis in the human carotid bifurcation. Positive correlation between plaque location and low and oscillating shear stress." Arteriosclerosis **5**(3): 293-302.
Kubota, K., J. Tamura, T. Shirakura, M. Kimura, K. Yamanaka, T. Isozaki and I. Nishio (1996). "The behaviour of red cells in narrow tubes in vitro as a model of the microcirculation." British Journal of Haematology **94**(2): 266-272.

Kumar, A. and M. D. Graham (2011). "Segregation by membrane rigidity in flowing binary suspensions of elastic capsules." Physical Review E **84**(6): 066316-066311-066316-066317.
Kumar, A. and M. D. Graham (2011). "Segregation by membrane rigidity in flowing binary suspensions of elastic capsules." Physical Review E **84**(6): 17.
Kumar, A. and M. D. Graham (2012). "Margination and segregation in confined flows of blood and other multicomponent suspensions." Soft Matter **8**(41): 10536-10548.
Kumar, A. and M. D. Graham (2012). "Mechanism of Margination in Confined Flows of Blood and Other Multicomponent Suspensions." Physical Review Letters **109**(10): 108102-108101-108102-108105.
Kumar, A., R. G. Henríquez Rivera and M. D. Graham (2014). "Flow-induced segregation in confined multicomponent suspensions: Effects of particle size and rigidity." Journal of Fluid Mechanics **738**: 423-462.
Kyle, A. H., L. A. Huxham, A. S. J. Chiam, D. H. Sim and A. I. Minchinton (2004). "Direct assessment of drug penetration into tissue using a novel application of three-dimensional cell culture." Cancer Research **64**(17): 6304-6309.
LaBarbera, D. V., B. G. Reid and B. H. Yoo (2012). "The multicellular tumor spheroid model for high-throughput cancer drug discovery." Expert Opinion on Drug Discovery **7**(9): 819-830.
Langer, H. F. and T. Chavakis (2009). "Leukocyte-endothelial interactions in inflammation." Journal of Cellular and Molecular Medicine **13**(7): 1211-1220.
Lee, B. Y., C. Assadi, J. L. Madden, D. Kavner, F. S. Trainor and W. J. McCann (1978). "Hemodynamics of arterial stenosis." World Journal of Surgery **2**(5): 621-627.
Lee, S. Y., M. Ferrari and P. Decuzzi (2009). "Design of bio-mimetic particles with enhanced vascular interaction." Journal of Biomechanics **42**(12): 1885-1890.
Lee, S. Y., M. Ferrari and P. Decuzzi (2009). "Shaping nano-/micro-particles for enhanced vascular interaction in laminar flows." Nanotechnology **20**(49): 11.
Lee, S. Y., M. Ferrari and P. Decuzzi (2009). "Shaping nano-/micro-particles for enhanced vascular interaction in laminar flows." Nanotechnology **20**(49): 1-11.
Lee, T. R., M. Choi, A. M. Kopacz, S. H. Yun, W. K. Liu and P. Decuzzi (2013). "On the near-wall accumulation of injectable particles in the microcirculation: smaller is not better." Scientific Reports **3**: 1-8.
Lee, T. R., M. Choi, A. M. Kopacz, S. H. Yun, W. K. Liu and P. Decuzzi (2013). "On the near-wall accumulation of injectable particles in the microcirculation: smaller is not better." Scientific Reports **3**: 8.
Li, H., H. Fang, Z. Lin, S. Xu and S. Chen (2004). "Lattice boltzmann simulation on particle suspensions in a two-dimensional symmetric stenotic artery." Physical Review E - Statistical, Nonlinear, and Soft Matter Physics **69**(3 1): 031919-031911-031919-031919.
Li, M., D. N. Ku and C. R. Forest (2012). "Microfluidic system for simultaneous optical measurement of platelet aggregation at multiple shear rates in whole blood." Lab on a Chip - Miniaturisation for Chemistry and Biology **12**(7): 1355-1362.
Lim, E. J., T. J. Ober, J. F. Edd, G. H. McKinley and M. Toner (2012). "Visualization of microscale particle focusing in diluted and whole blood using particle trajectory analysis." Lab on a Chip **12**(12): 2199-2210.

Liu, Y., J. Tan, A. Thomas, D. Ou-Yang and V. R. Muzykantov (2012). "The shape of things to come: importance of design in nanotechnology for drug delivery." Therapeutic delivery **3**(2): 181-194.
Lopez, M. and M. D. Graham (2007). "Shear-induced diffusion in dilute suspensions of spherical or nonspherical particles: Effects of irreversibility and symmetry breaking." Physics of Fluids **19**(7): 073602-073601-073602-073610.
MacEwan, S. R., D. J. Callahan and A. Chilkoti (2010). "Stimulus-responsive macromolecules and nanoparticles for cancer drug delivery." Nanomedicine **5**(5): 793-806.
Madlener, K., B. Frey and H. K. Ciezki (2009). "Generalized reynolds number for non-newtonian fluids." Progress in Propulsion Physics **1**(237): 237-250.
Metzner, A. B. and J. C. Reed (1955). "Flow of non-newtonian fluids—correlation of the laminar, transition, and turbulent-flow regions." AIChE Journal **1**(4): 434-440.
Mohandas, N. and J. A. Chasis (1993). "Red blood cell deformability, membrane material properties and shape: regulation by transmembrane, skeletal and cytosolic proteins and lipids." Seminars in Hematology **30**(3): 171-192.
Monteiro, F. C., B. Taboada and R. Lima (2014). Visualization of red blood cells flowing through a PDMS microchannel with a microstenosis: An image analysis assessment. Computational Vision and Medical Image Processing IV - Proceedings of Eccomas Thematic Conference on Computational Vision and Medical Image Processing, VIPIMAGE 2013.
Moya, M., D. Tran and S. C. George (2013). "An integrated in vitro model of perfused tumor and cardiac tissue." Stem Cell Research and Therapy **4**(SUPPL.1).
Müller, K., D. A. Fedosov and G. Gompper (2014). "Margination of micro- and nano-particles in blood flow and its effect on drug delivery." Scientific Reports **4**: 1-8.
Müller, K., D. A. Fedosov and G. Gompper (2015). "Understanding particle margination in blood flow - A step toward optimized drug delivery systems." Medical Engineering and Physics **38**(1): 2-10.
Munn, L. and M. Dupin (2008). "Blood Cell Interactions and Segregation in Flow." Ann. Biomed. Eng. **36**(4): 534-544.
Murray, C. J. L. and A. D. Lopez (1997). "Mortality by cause for eight regions of the world: Global Burden of Disease Study." Lancet **349**(9061): 1269-1276.
Namdee, K., A. J. Thompson, P. Charoenphol and O. Eniola-Adefeso (2013). "Margination Propensity of Vascular-Targeted Spheres from Blood Flow in a Microfluidic Model of Human Microvessels." Langmuir **29**(8): 2530-2535.
Narsimhan, V., H. Zhao and E. S. G. Shaqfeh (2013). "Coarse-grained theory to predict the concentration distribution of red blood cells in wall-bounded Couette flow at zero Reynolds number." Physics of Fluids **25**(6): 061901-061901-061901-061921.
Nobis, U., A. R. Pries, G. R. Cokelet and P. Gaehtgens (1985). "Radial distribution of white cells during blood flow in small tubes." Microvascular Research **29**(3): 295-304.
Ojha, M., C. R. Ethier, K. W. Johnston and R. S. C. Cobbold (1990). "Steady and pulsatile flow fields in an end-to-side arterial anastomosis model." Journal of Vascular Surgery **12**(6): 747-753.
Pan, Q., R. Wang, B. Reglin, G. Cai, J. Yan, A. R. Pries and G. Ning (2014). "A one-dimensional mathematical model for studying the pulsatile flow in microvascular networks." Journal of Biomechanical Engineering **136**(1).

Pearson, M. J. and H. H. Lipowsky (2000). "Influence of erythrocyte aggregation on leukocyte margination in postcapillary venules of rat mesentery." American Journal of Physiology-Heart and Circulatory Physiology **279**(4): H1460-H1471.
Phibbs, R. H. (1966). "Distribution of leukocytes in blood flowing through arteries." The American journal of physiology **210**(5): 919-925.
Pijls, N. H. J. (2009). "Acute Myocardial Infarction and Underlying Stenosis Severity." American Journal of Cardiology **103**(9): 1204-1205.
Pinho, D., R. O. Rodrigues, T. Yaginuma, V. Faustino, D. Bento, C. S. Fernandes, V. Garcia, A. I. Pereira and R. Lima (2014). Motion of rigid particles flowing in a microfluidic device with a pronounced stenosis: Trajectories and deformation index. 11th World Congress on Computational Mechanics, WCCM 2014, 5th European Conference on Computational Mechanics, ECCM 2014 and 6th European Conference on Computational Fluid Dynamics, ECFD 2014.
Prabhakarpandian, B., K. Pant, R. C. Scott, C. B. Patillo, D. Irimia, M. F. Kiani and S. Sundaram (2008). "Synthetic microvascular networks for quantitative analysis of particle adhesion." Biomedical Microdevices **10**(4): 585-595.
Prabhakarpandian, B., M. C. Shen, J. B. Nichols, C. J. Garson, I. R. Mills, M. M. Matar, J. G. Fewell and K. Pant (2015). "Synthetic tumor networks for screening drug delivery systems." Journal of Controlled Release **201**: 49-55.
Prabhakarpandian, B., M. C. Shen, K. Pant and M. F. Kiani (2011). "Microfluidic devices for modeling cell-cell and particle-cell interactions in the microvasculature." Microvascular Research **82**(3): 210-220.
Pries, A. R., T. W. Secomb and P. Gaehtgens (1995). "Structure and hemodynamics of microvascular networks: Heterogeneity and correlations." American Journal of Physiology - Heart and Circulatory Physiology **269**(5 38-5): H1713-H1722.
Pries, A. R., T. W. Secomb and P. Gaehtgens (1996). "Biophysical aspects of blood flow in the microvasculature." Cardiovascular Research **32**(4): 654-667.
Reasor, D. A., M. Mehrabadi, D. N. Ku and C. K. Aidun (2012). "Determination of Critical Parameters in Platelet Margination." Annals of Biomedical Engineering **41**(2): 238-249.
Rosano, J. M., N. Tousi, R. C. Scott, B. Krynska, V. Rizzo, B. Prabhakarpandian, K. Pant, S. Sundaram and M. F. Kiani (2009). "A physiologically realistic in vitro model of microvascular networks." Biomedical Microdevices **11**(5): 1051-1057.
Rosenzweig, S. and S. T. Carmichael (2013). "Age-dependent exacerbation of white matter stroke outcomes: A role for oxidative damage and inflammatory mediators." Stroke **44**(9): 2579-2586.
Rowbotham, G. F. and E. Little (1965). "Circulations of the cerebral hemispheres." British Journal of Surgery **52**(1): 8-21.
Sankar, D. S., A. K. Nagar and A. V. Kumar (2015). "Mathematical analysis of single and two-phase flow of blood in narrow arteries with multiple contrictions." Journal of Applied Fluid Mechanics **8**(4): 871-883.
Saxer, T., A. Zumbuehl and B. Müller (2013). "The use of shear stress for targeted drug delivery." Cardiovascular Research **99**(2): 328-333.
Schmid-Schonbein, G. W., K. L. P. Sung, H. Tozeren, R. Skalak and S. Chien (1981). "Passive mechanical properties of human leukocytes." Biophysical Journal **36**(1): 243-256.

Schmid-Schönbein, G. W., S. Usami, R. Skalak and S. Chien (1980). "The interaction of leukocytes and erythrocytes in capillary and postcapillary vessels." Microvascular Research **19**(1): 45-70.
Segré, G. and A. Silberberg (1962). "Behaviour of macroscopic rigid spheres in Poiseuille flow Part 2. Experimental results and interpretation." Journal of Fluid Mechanics **14**(01): 136-157.
Sollier, E., D. E. Go, J. Che, D. R. Gossett, S. O'Byrne, W. M. Weaver, N. Kummer, M. Rettig, J. Goldman, N. Nickols, S. McCloskey, R. P. Kulkarni and D. Di Carlo (2014). "Size-selective collection of circulating tumor cells using Vortex technology." Lab on a Chip - Miniaturisation for Chemistry and Biology **14**(1): 63-77.
Son, Y. (2007). "Determination of shear viscosity and shear rate from pressure drop and flow rate relationship in a rectangular channel." Polymer **48**(2): 632-637.
Sousa, P. C., F. T. Pinho, M. S. N. Oliveira and M. A. Alves (2011). "Extensional flow of blood analog solutions in microfluidic devices." Biomicrofluidics **5**(1).
Srivastava, V. P., R. Rastogi and R. Vishnoi (2010). "A two-layered suspension blood flow through an overlapping stenosis." Computers and Mathematics with Applications **60**(3): 432-441.
Sun, C. and L. L. Munn (2008). "Lattice-Boltzmann simulation of blood flow in digitized vessel networks." Computers and Mathematics with Applications **55**(7): 1594-1600.
Sutherland, W. (1905). "LXXV. A dynamical theory of diffusion for non-electrolytes and the molecular mass of albumin." Philosophical Magazine Series 6 **9**(54): 781-785.
Taboada, B., F. C. Monteiro and R. Lima (2016). "Automatic tracking and deformation measurements of red blood cells flowing through a microchannel with a microstenosis: the keyhole model." Computer Methods in Biomechanics and Biomedical Engineering: Imaging and Visualization **4**(3-4): 229-237.
Tan, J. F., S. Shah, A. Thomas, H. D. Ou-Yang and Y. L. Liu (2013). "The influence of size, shape and vessel geometry on nanoparticle distribution." Microfluidics and Nanofluidics **14**(1-2): 77-87.
Tan, J. F., A. Thomas and Y. L. Liu (2012). "Influence of red blood cells on nanoparticle targeted delivery in microcirculation." Soft Matter **8**(6): 1934-1946.
Tokarev, A. A., A. A. Butylin, E. A. Ermakova, E. E. Shnol, G. P. Panasenko and F. I. Ataullakhanov (2011). "Finite platelet size could be responsible for platelet margination effect." Biophysical Journal **101**(8): 1835-1843.
Tovar-Lopez, F. J., G. Rosengarten, M. Nasabi, V. Sivan, K. Khoshmanesh, S. P. Jackson, A. Mitchell and W. S. Nesbitt (2013). "An Investigation on Platelet Transport during Thrombus Formation at Micro-Scale Stenosis." PLoS ONE **8**(10).
Toy, R., E. Hayden, C. Shoup, H. Baskaran and E. Karathanasis (2011). "The effects of particle size, density and shape on margination of nanoparticles in microcirculation." Nanotechnology **22**(11): 9.
Toy, R., E. Hayden, C. Shoup, H. Baskaran and E. Karathanasis (2011). "The effects of particle size, density and shape on margination of nanoparticles in microcirculation." Nanotechnology **22**(11): 1-9.
Vahidkhah, K. and P. Bagchi (2015). "Microparticle shape effects on margination, near-wall dynamics and adhesion in a three-dimensional simulation of red blood cell suspension." Soft Matter **11**(11): 2097-2109.

Vahidkhah, K., P. Balogh and P. Bagchi (2016). "Flow of Red Blood Cells in Stenosed Microvessels." Scientific Reports **6**.
Vejlens, G. (1938). "The distribution of leukocytes in the vascular system." Acta Pathol Microbiol Scand (Suppl) **33**: 1-239.
Verbridge, S. S., A. Chakrabarti, P. Delnero, B. Kwee, J. D. Varner, A. D. Stroock and C. Fischbach (2013). "Physicochemical regulation of endothelial sprouting in a 3D microfluidic angiogenesis model." Journal of Biomedical Materials Research - Part A **101**(10): 2948-2956.
Vidi, P. A., T. Maleki, M. Ochoa, L. Wang, S. M. Clark, J. F. Leary and S. A. Lelièvre (2014). "Disease-on-a-chip: Mimicry of tumor growth in mammary ducts." Lab on a Chip - Miniaturisation for Chemistry and Biology **14**(1): 172-177.
Walker, A. M., C. R. Johnston and D. E. Rival (2014). "On the characterization of a non-newtonian blood analog and its response to pulsatile flow downstream of a simplified stenosis." Annals of Biomedical Engineering **42**(1): 97-109.
Wang, H. e. a. (2016). "Global, regional, and national life expectancy, all-cause mortality, and cause-specific mortality for 249 causes of death, 1980–2015: a systematic analysis for the Global Burden of Disease Study 2015." The Lancet **388**(10053): 1459-1544.
Wiedeman, M. P. (1963). "Dimensions of blood vessels from distributing artery to collecting vein." Circulation research **12**: 375-378.
Womersley, J. R. (1955). "Method for the calculation of velocity, rate of flow and viscous drag in arteries when the pressure gradient is known." The Journal of Physiology **127**(3): 553-563.
Xiao, L. L., S. Chen, C. S. Lin and Y. Liu (2014). "Simulation of a single red blood cell flowing through a microvessel stenosis using dissipative particle dynamics." MCB Molecular and Cellular Biomechanics **11**(1): 67-85.
Xu, C. and D. M. Wootton (2004). "Platelet near-wall excess in porcine whole blood in artery-sized tubes under steady and pulsatile flow conditions." Biorheology **41**(2): 113-125.
Yaginuma, T., M. S. N. Oliveira, R. Lima, T. Ishikawa and T. Yamaguchi (2011). Red blood cell deformation in flows through a PDMS hyperbolic microchannel. Technical Proceedings of the 2011 NSTI Nanotechnology Conference and Expo, NSTI-Nanotech 2011.
Yang, X. X., O. Forouzan, J. M. Burns and S. S. Shevkoplyas (2011). "Traffic of leukocytes in microfluidic channels with rectangular and rounded cross-sections." Lab on a Chip **11**(19): 3231-3240.
Zaman, A., N. Ali and M. Sajid (2017). "Numerical simulation of pulsatile flow of blood in a porous-saturated overlapping stenosed artery." Mathematics and Computers in Simulation **134**: 1-16.
Zervantonakis, I. K., S. K. Hughes-Alford, J. L. Charest, J. S. Condeelis, F. B. Gertler and R. D. Kamm (2012). "Three-dimensional microfluidic model for tumor cell intravasation and endothelial barrier function." Proceedings of the National Academy of Sciences of the United States of America **109**(34): 13515-13520.
Zervantonakis, I. K., C. R. Kothapalli, S. Chung, R. Sudo and R. D. Kamm (2011). "Microfluidic devices for studying heterotypic cell-cell interactions and tissue specimen cultures under controlled microenvironments." Biomicrofluidics **5**(1).

Zhao, H., E. S. G. Shaqfeh and V. Narsimhan (2012). "Shear-induced particle migration and margination in a cellular suspension." Physics of Fluids **24**(1): 011902-011901-011902-011921.
Zhao, R., J. N. Marhefka, F. Shu, S. J. Hund, M. V. Kameneva and J. F. Antaki (2008). "Micro-flow visualization of red blood cell-enhanced platelet concentration at sudden expansion." Annals of Biomedical Engineering **36**(7): 1130-1141.